INVESTIGATING THE EFFECTS OF CLIMATE CHANGE ON THE SURFACE RUNOFF POTENTIAL OVER KIZILIRMAK BASIN

A THESIS SUBMITTED TO
THE GRADUATE SCHOOL OF NATURAL AND APPLIED SCIENCES
OF
MIDDLE EAST TECHNICAL UNIVERSITY

BY

NUMAN BURAK BARKIŞ

IN PARTIAL FULFILLMENT OF THE REQUIREMENTS
FOR
THE DEGREE OF MASTER OF SCIENCE
IN
CIVIL ENGINEERING

SEPTEMBER 2022

Approval of the thesis:

INVESTIGATING THE EFFECTS OF CLIMATE CHANGE ON THE SURFACE RUNOFF POTENTIAL OVER KIZILIRMAK BASIN

submitted by **NUMAN BURAK BARKIŞ** in partial fulfillment of the requirements for the degree of **Master of Science** i**n Civil Engineering, Middle East Technical University** by,

Prof. Dr. Halil Kalıpçılar
Dean, Graduate School of **Natural and Applied Sciences** _____

Prof. Dr. Erdem Canbay
Head of the Department, **Civil Engineering** _____

Assoc. Prof. Dr. M. Tuğrul Yılmaz
Supervisor, **Civil Engineering Dept., METU** _____

Examining Committee Members:

Prof. Dr. İsmail Yücel
Civil Engineering Dept., METU _____

Assoc. Prof. Dr. M. Tuğrul Yılmaz
Civil Engineering Dept., METU _____

Prof. Dr. Elçin Kentel Erdoğan
Civil Engineering Dept., METU _____

Assoc. Prof. Dr. Ali Arda Şorman
Civil Engineering Dept., ESTU _____

Assoc. Prof. Dr. Koray K. Yılmaz
Geological Engineering Dept., METU _____

Date: 02.09.2022

I hereby declare that all information in this document has been obtained and presented in accordance with academic rules and ethical conduct. I also declare that, as required by these rules and conduct, I have fully cited and referenced all material and results that are not original to this work.

Name Last name : Numan Burak Barkış

Signature :

ABSTRACT

INVESTIGATING THE EFFECTS OF CLIMATE CHANGE ON THE SURFACE RUNOFF POTENTIAL OVER KIZILIRMAK BASIN

Barkış, Numan Burak
Master of Science, Civil Engineering
Supervisor : Assoc. Prof. Dr. M. Tuğrul Yılmaz

September 2022, 124 pages

The aim of this study is to analyze the expected change in the surface runoff potential that will occur due to climate change in the Kızılırmak Basin until 2100. HBV hydrological model was run in this study to investigate the expected change in 3 sub-basins (SB 1535, SB 1541, and SB 1545) of Kızılırmak Basin. Total of 56 CMIP5-based GCM/RCM daily model datasets, downloaded from CORDEX EUR-11 at 0.11^0 spatial resolution and reflect RCP 8.5 emission scenario, were utilized. Among these model datasets, 10 of them were eliminated after a validation step performed using ERA5-Land precipitation and temperature dataset. Remaining 46 datasets are corrected for potential systematic biases in their mean values using ERA5-Land dataset-based historical temperature and precipitation simulations. Bias corrected datasets are utilized in all HBV model-based simulations. After the parameters of HBV were calibrated utilizing historical runoff observations, obtained parameter sets were used in future simulations to investigate the expected changes in the surface runoff potential of 3 sub-basins between the years of 2021 and 2099. The results show HBV model simulations have very high consistency with the past observations that NSE values for the daily simulations are 0.87, 0.66, and 0.81 for the three sub-basins listed above, respectively. Overall, the current surface runoff potential is

expected to decrease in all 3 sub-basins between 2061 and 2099, where the rate of the decrease will be between 34% and 57% of the current multi-decadal averages.

Keywords: Climate Change, Surface Runoff, Kızılırmak Basin, HBV, ERA5-Land, CORDEX, CMIP5

ÖZ

İKLİM DEĞİŞİKLİĞİNİN KIZILIRMAK HAVZASI YÜZEY SUYU POTANSİYELİ ÜZERİNE ETKİLERİNİN ARAŞTIRILMASI

Barkış, Numan Burak
Yüksek Lisans, İnşaat Mühendisliği
Tez Yöneticisi: Doç. Dr. M. Tuğrul Yılmaz

Eylül 2022, 124 sayfa

Bu çalışmanın amacı Kızılırmak Havzasında 2100 yılına kadar iklim değişikliği sebebiyle oluşacak yüzey suyu potansiyelindeki muhtemel değişimi elde etmektir. Kızılırmak havzasının 3 alt havzasında (SB 1535, SB 1541, ve SB 1545) beklenen değişimi araştırmak için HBV hidrolojik modeli kullanılmıştır. CORDEX EUR-11'den 0.110 çözünürlükte indirilen RCP 8.5 iklim senaryosu göz önünde bulundurularak toplamda 56 CMIP5 tabanlı GCM/RCM günlük model veri seti kullanılmıştır. Bu model veri setlerinden 10 tanesi ERA5-Land yağış ve sıcaklık veri seti kullanılarak gerçekleştirilen doğrulama adımı sonrası elenmiştir. Kalan 46 veri seti ERA5-Land veri setine tabanlı geçmiş yağış ve sıcaklık simülasyonları kullanılarak ortalama değerlerdeki olası sistematik hatalar için düzeltilmiştir. Hata düzeltmeleri yapılmış veri kümeleri tüm HBV model simülasyonlarında kullanılmıştır. Geçmiş akım gözlemleri kullanılarak HBV parametreleri kalibre edildikten sonra, 2021 ve 2099 yılları arasında 3 alt havzanın yüzey suyu potansiyelindeki olası değişiklikleri araştırmak için elde edilen parametre setleri gelecek simülasyonlarda kullanılmıştır. Sonuçlar, HBV model simülasyonlarının geçmiş gözlemlerle çok yüksek tutarlılığa sahip olduğunu göstermekte olup günlük

simülasyonlar için NSE değerleri yukarıda listelenen üç alt havza için sırasıyla 0.87, 0.66 ve 0.81 olmaktadır. Genel olarak, 2061 ve 2099 yılları arasında 3 alt havzanın tümünde mevcut yüzey suyu potansiyelinin azalması beklenmektedir; bu düşüş oranı, mevcut çoklu on yıllık ortalamaların %34 ila %57'si arasında olacaktır.

Anahtar Kelimeler: İlkim Değişikliği, Yüzey Suyu, Kızılırmak Havzası, HBV, ERA5-Land, CORDEX, CMIP5

To my family,

ACKNOWLEDGMENTS

First of all, I would like to express my gratitude to my advisor Assoc. Prof. Dr. M. Tuğrul Yılmaz for his guidance and support. During the preparation of this thesis, he always spared time for me whenever I wanted and advised me to do my best.

I would also like to thank the Examining Committee Members Prof. Dr. İsmail Yücel, Prof. Dr. Elçin Kentel Erdoğan, Assoc. Prof. Dr. Koray K. Yılmaz, Assoc. Prof. Dr. Ali Arda Şorman for accepting to be my thesis jury members and for their valuable comments and recommendations.

I would like to thank especially Asst. Prof. Mahdi Hesami Afşhar and Dr. Burak Bulut. They helped me a lot with their experience during the thesis process. I learned a lot from them. Thank you for your contributions. It was a proud point for me to work with you on such good projects.

I would like to thank my dear friends Nazlı Barçın Doğan, Tuğkan Tanır, Beyza Özel and Ecem Bahçelioğlu with whom I shared the B-07 study room, for funny room conversations and entertaining lunches.

Above all, I would like to express my deepest gratitude to my family, who have always supported me throughout my life. I would like to express my special thanks to my dear father Zülfikar Barkış, my dear mother Nadiye Barkış, my dear brother Özgür Barkış, my dear sister Merve Barkış and my uncle Feyzi Barkış for the unconditional and endless love.

TABLE OF CONTENTS

LIST OF TABLES

TABLES

LIST OF FIGURES

FIGURES

LIST OF ABBREVIATIONS

ABBREVIATIONS

AOGCM	Coupled Atmosphere Ocean Global Climate Model
CMIP	Coupled Model Intercomparison Project
CORDEX	Coordinated Regional Climate Downscaling Experiment
ECMWF	The European Centre for Medium-Range Weather Forecasts
ESM	Earth System Model
GAP	Genetic Algorithm and Powell optimization
GCM	General Circulation Model or Global Climate Model
HBV	Hydrologiska Byråns Vattenbalansavdelning
IPCC	Intergovernmental Panel on Climate Change
MGM	Turkish State Meteorological Service
Mtoe	Million Ton of Oil Equivalent
NOAA	National Oceanic and Atmospheric Administration
NSE	Nash-Sutcliffe Efficiency
OECD	The Organisation for Economic Co-operation and Development
PET	Potential Evapotranspiration
RCM	Regional Climate Model
RCP	Representative Concentration Pathways
RMSE	Root Mean Square Error
SB	Sub-basin
SYGM	General Directorate of Water Management

UNFCCC	United Nations Framework Convention on Climate Change
WCRP	World Climate Research Programme
WGI	Working Group I
WMO	World Meteorological Organization

CHAPTER 1

INTRODUCTION

It is expected that the drought characteristics (e.g., severity, length, area) over Turkey will be adversely affected as a result of climate change. As a result this will follow shortage in water potential, increase in the water demand, decrease in agricultural products, and a population movement for both humans and animals from where the water potential is scarce to abundant. In order to protect the ecological balance and to ensure the sustainable development of human communities, it is necessary to use and manage water resources in the most rational way that can meet the present and the future needs.

The Kızılırmak basin is one of the 25 river basins in Turkey, and it is the longest river basin in Turkey. It has the second largest drainage area after the Euphrates-Tigris basin. Since the Kızılırmak basin supplies water to Ankara (ASKİ, 2022), the capital of Turkey, its surface runoff potential, and expected changes in the surface runoff potential due to climate change are very important.

In the studies carried out so far, analysis of precipitation, rainfall-runoff, drought, and flood potential of the Kızılırmak basin have been examined using historical observations (Güner Bacanlı et al., 2012; Yüce & Ercan, 2015; Efe, 1996; Dadaser-Celik et al., 2012; Ercan et al., 2019; SYGM, 2019). On the other hand, a comprehensive analysis of the expected change in the surface runoff potential of the Kızılırmak basin under the pressure climate change has not been conducted yet.

Future surface runoff potential investigation immediately requires hydrological models, where temperature and precipitation are one of the primary inputs for many models. Accordingly, future projections of these two variables are required to

investigate the expected change in the water potential of basins. There are many General Circulation Model (GCM) and Regional Climate Model (RCM) simulations that are available over Turkey, that provide future projections of temperature and precipitation estimates over Turkey. Among them Turkish State Meteorological Service (MGM) and General Directorate of Water Management (SYGM) run their own simulations (three GCM and single RCM) over Turkey only, where CORDEX experiments are available over much larger domains and contains much higher number of GCM/RCM model datasets. So far, the studies investigating the impact of climate change utilized relatively lower number of ensembles, where the study by Ersoy (2022) for the first time utilized very high number of high-resolution projection datasets to investigate the variability of drought characteristics over 25 watersheds in Turkey. On the other hand, there is no study so far investigating the expected change of the future water potential of any basin using such a high number of climate projection datasets. Existing studies mostly used low number of projection datasets (one to three RCM datasets) mostly obtained from the simulations of SYGM (carried out by the Ministry of Forestry and Water Affairs, General Directorate of Water Management (SYGM, 2016)) while the use of large number (e.g., higher than 30) of ensembles obtained from CORDEX remained non-existent.

In this study, the impact of climate change on surface runoff potential over 3 sub-basins of Kızılırmak basin were investigated using the HBV hydrological model, where the future projections utilize very high number of GCM-RCM couple datasets (56 GCM-RCM) obtained from the simulations run over the EUR-11 domain of CORDEX. This thesis consists of five chapters. First chapter includes the aim of this study, brief information about the importance of surface runoff, and why it should be examined in detail. Second chapter gives information about the literature review. Third chapter gives information about the methodology of thesis and detailed information of data which is used and study area. The results and discussion of the study are in the fourth chapter. The last chapter includes conclusions and recommendations.

CHAPTER 2

LITERATURE REVIEW

2.1 Climate Change and Its Impacts

Long term shifts in temperatures and weather patterns can be expressed as climate change. These shifts might be natural, but since the 1800s human-made activities have become one of the main reasons of climate change (IPCC, 2014). In order to get energy, burnings of fossil fuels such as coal, oil, natural gas have increased, where large amount of greenhouse gases such as carbon dioxide (CO_2), methane (CH_4) are released into the atmosphere. These greenhouse gases trap the radiation/energy in the atmosphere, and it leads to an increase in the earth temperature which is called global warming (IPCC, 2014).

Accordingly, United Nations Framework Convention on Climate Change (UNFCCC) refers climate change attributable directly or indirectly to human activities that change the composition of the global atmosphere, and which add to the natural climate variability observed over comparable time periods (UNFCCC, 2011). This leads to changes in the weather patterns and an increase in the frequency and severity of extreme events over many locations. As a result, climate change has become one of the biggest problems that the humanity is facing during the past decades.

CO_2 is one of the most important greenhouse gases that released from both human activities and natural sources. The high level of greenhouse gases in the atmosphere resulting from the people activities has been one of the main causes of the climate change since middle of the 20^{th} century (WMO, 2021). According to National Oceanic and Atmospheric Administration (NOAA), 412.5 ppm (parts per million) was the global average atmospheric CO_2 value in 2020. When it is compared to 2019,

there was an increase of 2.6 ppm which was the 5th highest annual increase in recent years according to NOAA. The amount of CO_2 in the atmosphere has increased by 43.5 ppm with an increase of 12 percent compared to 2000. Figure 2-1 and Figure 2-2 show the amount of CO_2 in the atmosphere in ppm for the past 800,000 years and last decades, respectively (NOAA, 2022).

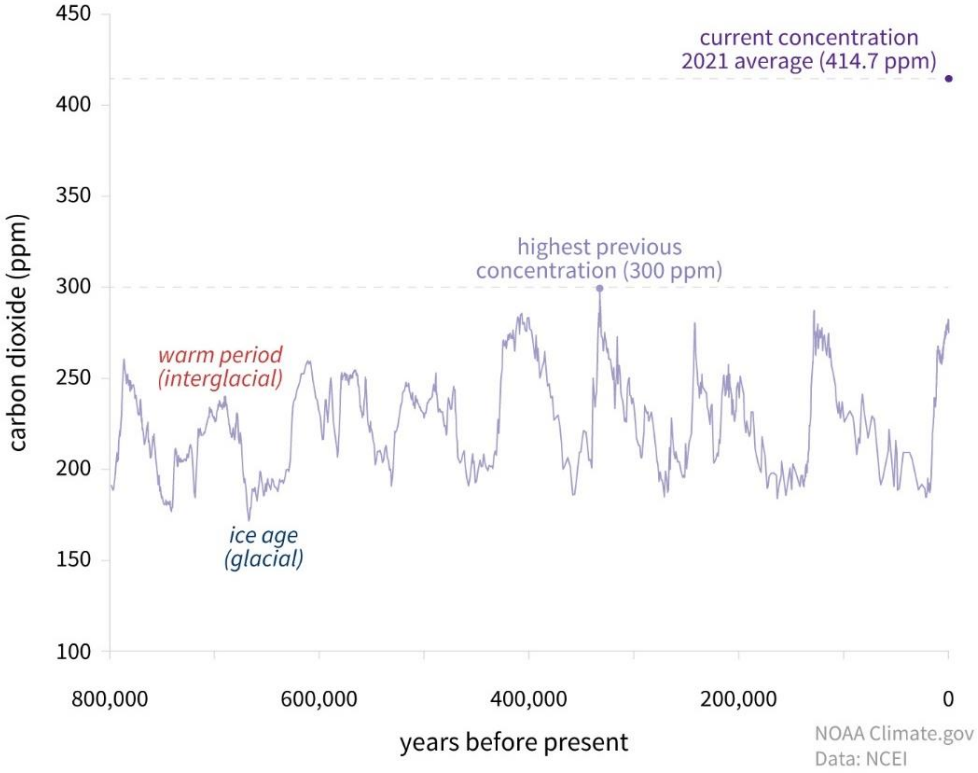

Figure 2-1 Global atmospheric CO_2 concentrations for the past 800,000 years (NOAA, 2022)

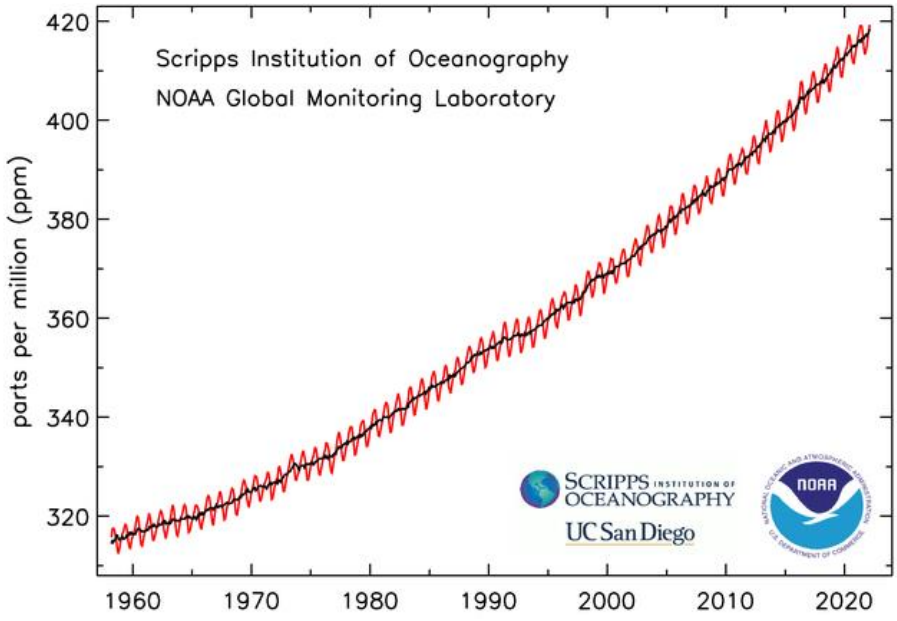

Figure 2-2 Atmospheric CO_2 concentrations at NOAA global monitoring laboratory (NOAA, 2022)

According to Höök et al. (2012), the use of fossil fuel in order to obtain energy dominates the Earth energy system and today more than 80% of world's produced energy is obtained from fossil fuels. The use of petroleum or gasoline for transportation purposes, the burning of coal for heating or use of natural gas for industrial activities are the examples. Figure 2-3 shows the world production of fossil energy from 1800 to 2010.

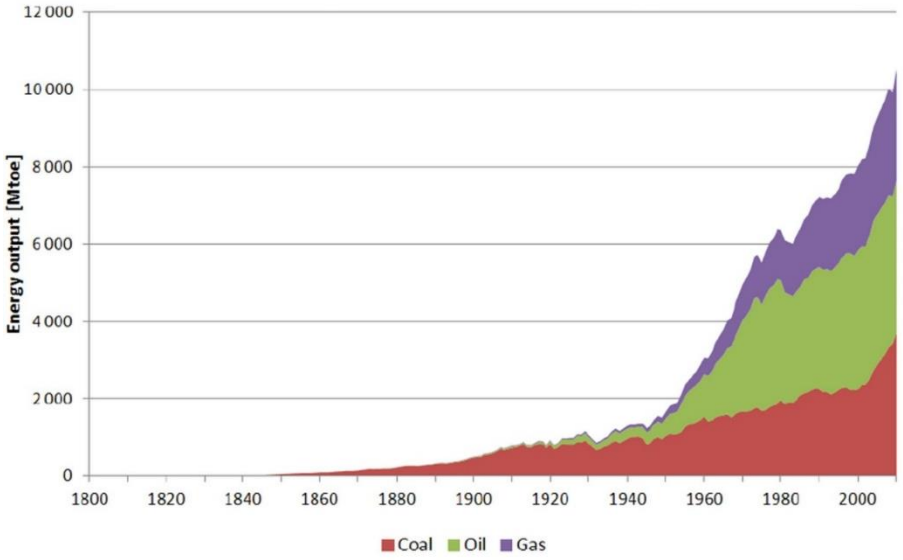

Figure 2-3 Historical world production of fossil energy from 1800 to 2010 (Höök et al., 2012)

Precipitation has great importance for water cycle. Increase in the global average temperature because of the climate change can give rise to change in the precipitation regimes. While changes in the precipitation regimes can cause drought with the help of the high evaporation and changes in the wind pattern in some regions, it can also cause flash floods in other regions because of the heavy rains (Hao et al., 2018). Changes in land use due to the climate change change the hydrological cycle and lead to temporal and regional differences in water resources (Yang et al., 2021).

Various studies have been conducted showing the impact of climate change on precipitation regimes and trends. It is widely accepted that the water cycle and precipitation patterns will be significantly affected by climate change (Oruç, 2018). In some regions, change in the precipitation regimes are expected due to impacts of the climate change. An increase in the frequency and intensity of extreme precipitation, lower number of rainy days, and more extreme precipitation are some examples. Changes in these precipitation regimes are expected to continue through the end of the 21st century under the climate change conditions (Oruç, 2018).

In addition to the use of fossil fuels, humans are adversely affecting the earth's climate by other activities as well, such as increased livestock farming, cutting down forests, etc. These activities add high amounts of greenhouse gases to the ones that are naturally emitted to the atmosphere, hence, exacerbating global warming. According to WMO (2021), mean temperature of the Earth for 2021 was approximately 1.1 ± 0.13°C higher than the average of between 1850 and 1900. Even though 2021 experienced La Niña event, it was the 7th warmest year ever (i.e., La Niña causes a temporary drop in global average temperature). Figure 2-4 shows the global average temperature difference from the pre-industrial levels for the 6 global datasets (WMO, 2021).

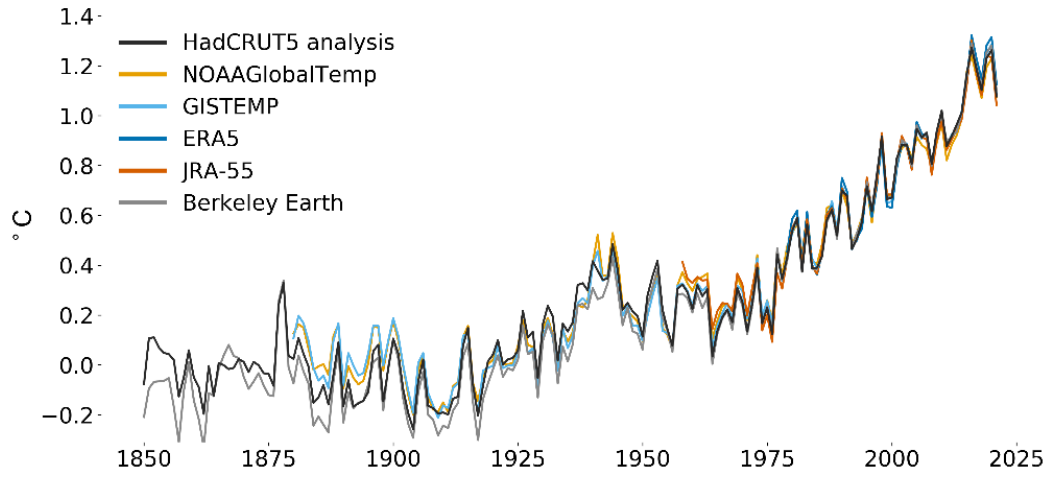

Figure 2-4 Global mean temperature difference from 1850 to 1900 for the 6 global datasets (WMO, 2021)

The increase in the global surface temperature assessed by WGI which is working group I in IPCC is approximately 1.09°C [0.95 to 1.20] for the period 2011-2020 compared to the period 1850-1900 (IPCC, 2022). The estimated increase in global surface temperature since the IPCC 5th assessment report is mainly due to further warming since 2003–2012 (0.19°C [0.16 to 0.22]) (IPCC, 2022). According to the five scenarios evaluated by WGI, even for the very low greenhouse gas emissions scenario, the probability of global warming reaching or exceeding 1.5°C in the near term (2021-2040) is at least more than 50% (IPCC, 2022).

According to NOAA, global land and ocean temperature has been increasing by about 0.10 °C for each decade (Figure 2-5) (NOAA, 2022). The year of 2021 has been characterized by record high annual temperatures over parts of southern Asia, northern Africa, southern South America, and some parts of the Pacific and Atlantic Oceans, and in most parts of the world (NOAA, 2022). Very small parts of the world were below than the average temperature, where no land or ocean areas had record low temperature for year of 2021 (Figure 2-6) (NOAA, 2022).

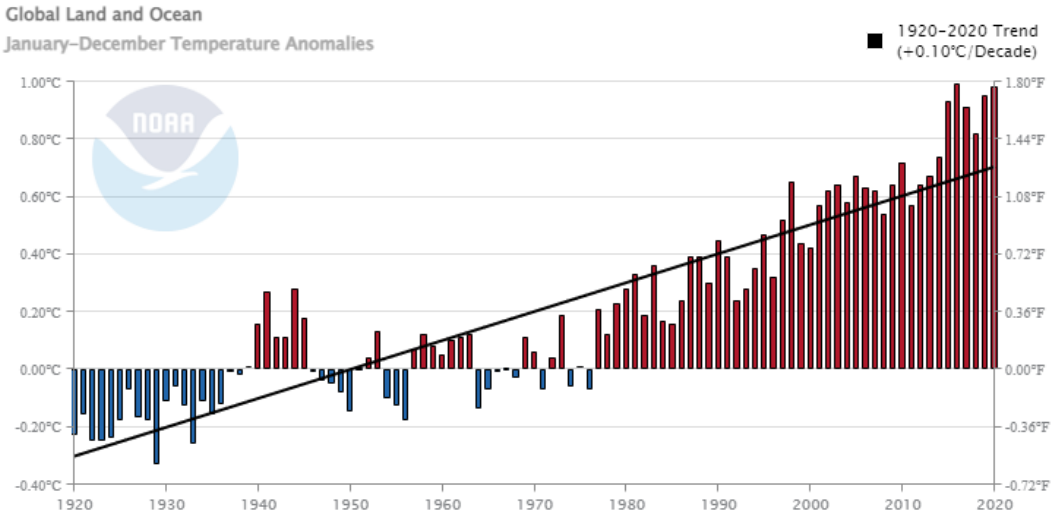

Figure 2-5 Global Land and Ocean Temperature (NOAA, 2022)

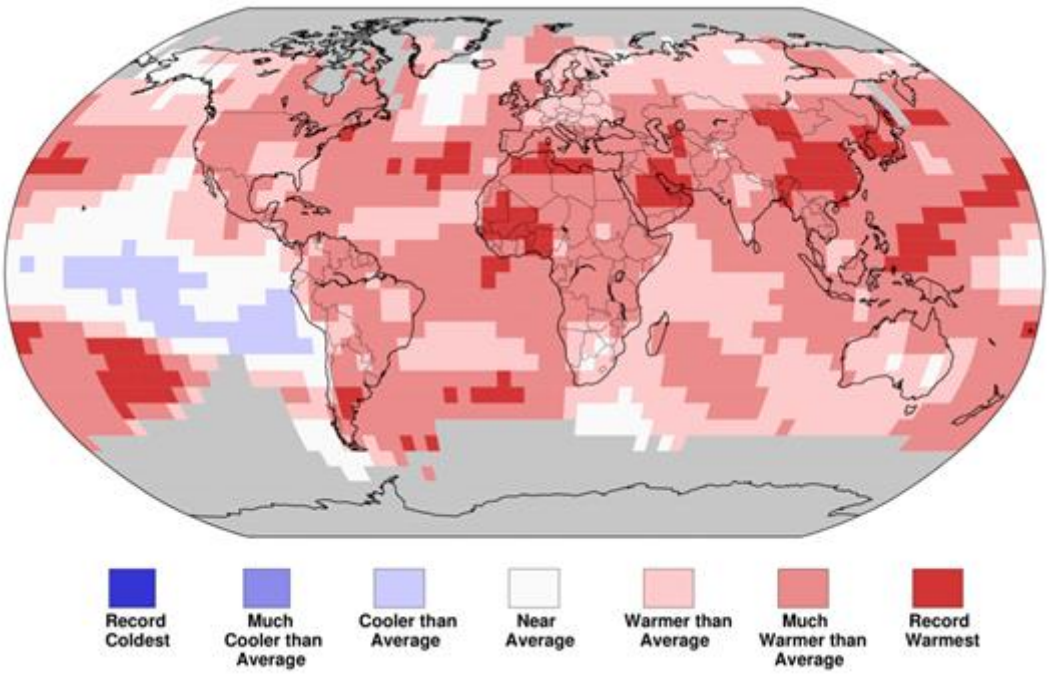

Figure 2-6 Land and Ocean Surface Temperature Percentiles in January-December 2021 (NOAA, 2022)

2.2 Climate Change Effects Over Surface Runoff

River discharge is affected by various factors such as variability of climate, water withdrawal, or changes of land use. Variability in the climate and the most important of these, variability in precipitation, play an important role in runoff variability. It is expected that global warming will affect the 2 most basic climate variables (i.e., precipitation and temperature), substantially changing the hydrological regimes in the future. Combined with increased demographic pressure and reduced adaptive capacity, it can have important effects on people and industries, depending upon the water availability (Roudier et al., 2014).

For a wide variety of animals and plant life, wetlands and waterbodies supply important habitats and allow them to migrate living organisms and resources throughout the landscape. Increase in the global surface temperature and changes in the pattern of precipitation may rise water temperature and change runoff flow that

can have harmful impacts on aquatic organisms. Along with the diminishing world's available water resources, more competition for the available resources is expected. This decreasing water availability will exert increasing pressure on the natural systems in favor of urban and agricultural uses.

Surface runoff is essential for many industries which include generation of electricity, agricultural and livestock activities, or fisheries. Even though agricultural activities are fed by rain, some agricultural lands are heavily dependent on surface runoff to carry out their agricultural activities. For example, approximately 50% of the rice production of Mali is met by a dam on the Niger river (Roudier et al., 2014). Fishing is largely based on river discharge and during the drought times of the 1970s and 1980s, there was a 50% loss in fisheries production in the Niger delta, and millions of dollars were lost (Roudier et al., 2014).

Climatic factors such as precipitation, temperature, and evaporation influence the trends of mean annual runoff over rivers. Analyzing 40 large rivers in the world between the years of 1960 and 2010, Shi et al. (2019) concludes climate change is the main driver of the streamflow changes and about 25% of streamflow changes are due to human activities.

Human activities and climate change directly or indirectly affect the magnitude and direction of change in streamflow and runoff. There is no clear trend of increasing or decreasing the streamflow at the global level. Trend occurs mostly at the regional level (IPCC, 2022). For example, there is a general increasing trend in the northern higher latitude regions, while there is a mixed trend (ascending, decreasing or stable) in the remaining regions of the world. Climatic factors contribute to the formation of these trends, and they have more influence than direct human activities in large global basins (IPCC, 2022).

According to UNFCCC (2011), some examples of impacts of climate change on water resources are listed below.

- Runoff and availability of water are estimated to increase in areas which are located at high latitudes and in some wet tropics and are also projected to decrease in most of mid latitudes and dry tropics, some of which are currently water stressed areas.
- Areas that are severely affected from drought will likely to experience more droughts. Additionally, extreme precipitation events are expected to have higher intensity and frequency, which will cause increased risk of flooding.
- It is estimated that hundreds of millions of people will experience increased water stress.

River runoff contains some of the precipitation that cannot be stored or does not evaporate. Changes in the seasonal flow regime due to climate change and the variability of flow between years are affiliated with the changes in precipitation amount and timing, evaporation demand, and precipitation as snow or rain (Stagl et al., 2014). According to Stagl et al. (2014), in general, it has been noticed that while there was a marginal increase in the annual river runoff in the northern and northeastern parts of Europe, there was a reduction in the southern and southeastern parts of Europe.

2.3 Climate Change in Turkey

The impacts of climate change perhaps could better be understood via comparisons of the temperature and the precipitation observations during recent years and long term averages. For example, average temperature over Turkey was 14.9 °C in 2020. This was the third warmest year in the last 50 years. There have been steady positive anomalies in the average temperature of Turkey since 1998 (except 2011) (Turkish State Meteorological Service, 2021). Figure 2-7 shows the temperature anomalies between 1971 and 2020 where average temperature is calculated between 1981 and 2010. Figure 2-8 show the spatial distribution of mean temperature differences of Turkey. (Turkish State Meteorological Service, 2021).

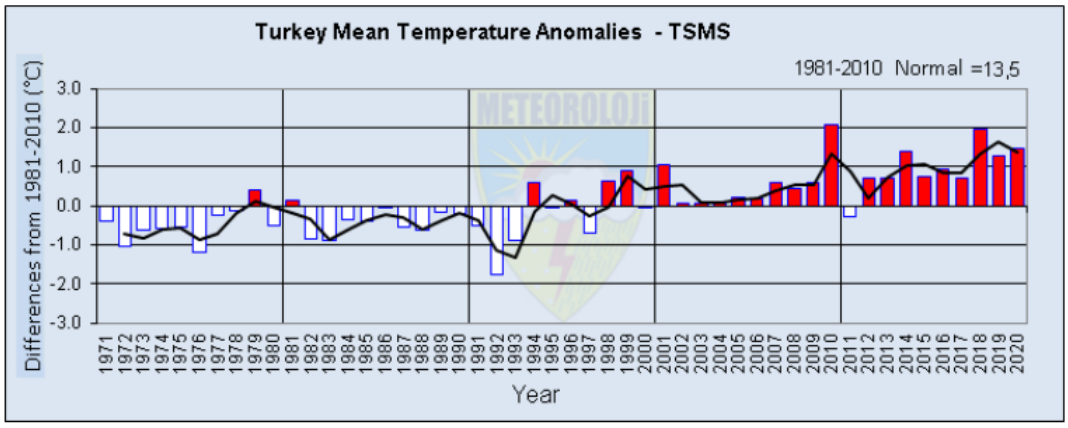

Figure 2-7 Mean Temperature Differences of Turkey (Turkish State Meteorological Service, 2021)

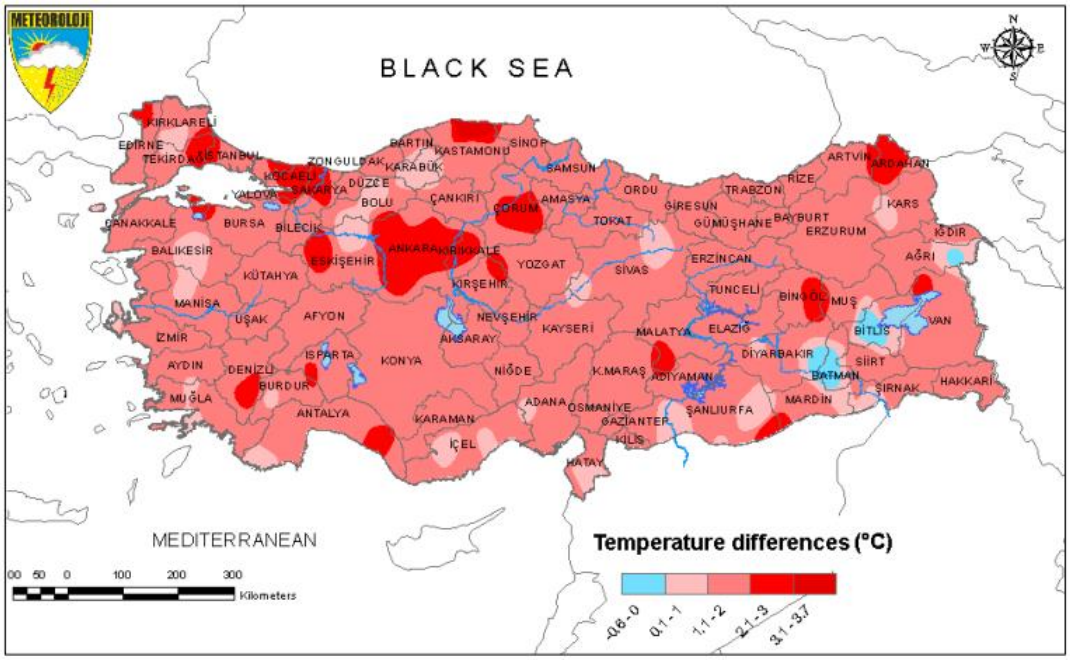

Figure 2-8 Spatial Distribution of Mean Temperature Differences of Turkey (Turkish State Meteorological Service, 2021)

Areal average rainfall over Turkey in 2020 was 500 mm, which is 74 mm lower than the average between 1981 and 2010. Figure 2-9 shows the mean areal rainfall differences of Turkey from 1981 to 2020 and Figure 2-10 show monthly areal rainfall differences of Turkey. These figures have been prepared by taking into consideration the average of 1981-2010 (Turkish State Meteorological Service, 2021).

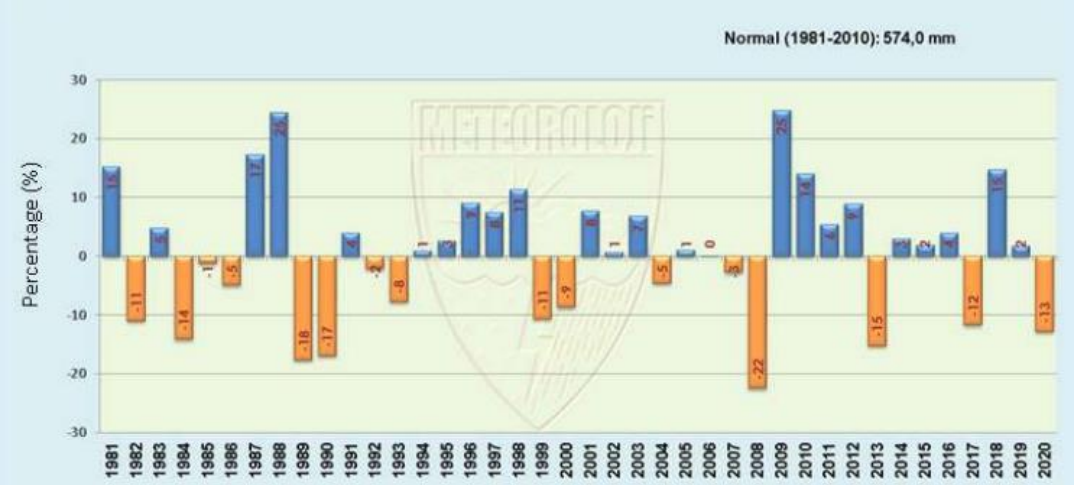

Figure 2-9 Mean Areal Rainfall Differences of Turkey (Turkish State Meteorological Service, 2021)

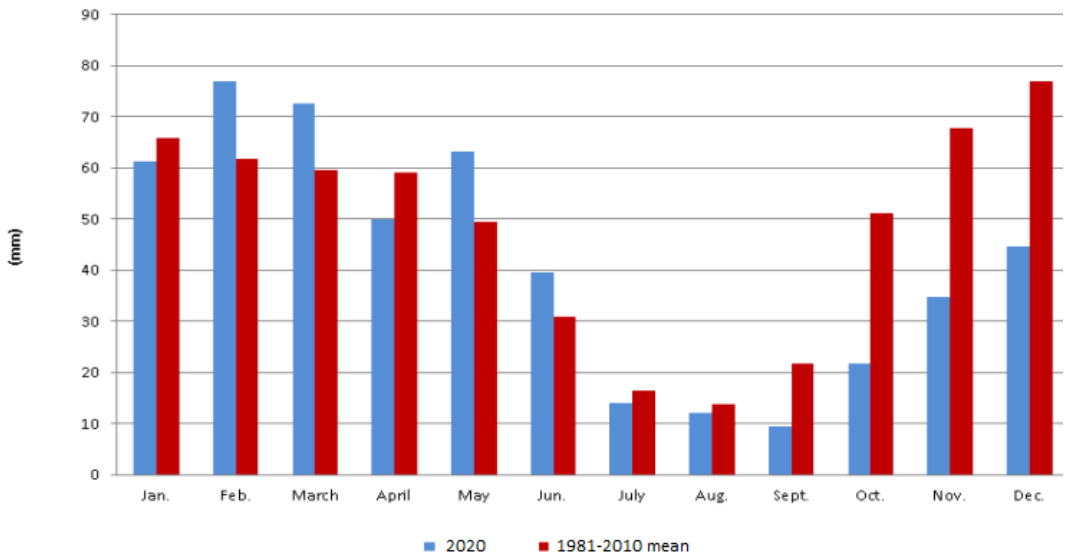

Figure 2-10 Monthly Areal Rainfall Differences of Turkey (Turkish State Meteorological Service, 2021)

Precipitation and temperature are the main climatic factors that affect the surface runoff in a river. Changes in surface runoff is expected due to increasing temperatures and changes in precipitation patterns. According to Aktaş (2014), there was a decreasing trend in the stream flow of Akçay and Çine river, especially between the years 1985 and 1998. He also stated that it is expected that there will be a further 15-20% decrease in the average surface flow in Turkey after 2040.

The study of Balov and Altunkaynak (2020), which was conducted over the basins Melen and Munzur rivers, shows the total water volume will decrease in both basins in the future following the decrease in precipitation and increase in temperature and, they stated that the average percentage of reduction in the volume of surface runoff at the end of the 21st century for Melen and Munzur rivers was found to be 15.42 and 26.65, respectively.

Following the study of Organisation for Economic Co-operation and Development (OECD, 2013) and (Ozkul, 2009) on the effects of climate change on Gediz and Büyük Menderes watersheds, it is expected that approximately 20% of the surface runoff will decrease by 2030 and the reduction will increase to approximately 35% and over 50% by 2050 and 2100, respectively. It was also noted that the reduced surface runoff potential of the watersheds is expected to cause serious water stress problems among users.

Two hydrological studies (Yücel et al., 2015; Sen et al., 2011) are warning that warming in snow-fed watersheds will contribute to changes in the river flows seasonality. According to both studies, there is an earlier shift in spring streamflow timing in the year. The runoff peak of the main snowmelt in the spring reaches days earlier across the region, resulting in a reduction in the fractions of the river discharge in the spring and early summer. Yücel et al.'s study (2015) was carried out that 15 streamflow stations are selected in the Eastern Anatolia region of Turkey which are in the Tigris, Euphrates, Çoruh and Aras basin. Also, according to a regional climate change simulation based on a high emission scenario, by the end of the century, it is expected that the surface runoff of the Aras, Euphrates and Tigris basins will decrease by 11.6%, 23.5% and 28.5%, respectively. In the Çoruh basin, there is an increase of approximately 4% in surface runoff.

The study of Bağçaci et al. (2021) show that the summer temperature increase in Turkey is expected to be between 2.0 °C and 3.5 °C in the long term using CMIP6 SSP2–4.5 based simulations. Same study also finds maximum temperature rise looks more homogeneous across the country in the long term, reaching a record high of

around 6.5 °C using SSP5–8.5 simulations. Also, they stated that much of the Turkey's territory will be exposed to the adverse effects of the climate change, and extreme heat will likely become more frequent.

In a study of Fujihara et al. (2008) conducted in the Seyhan basin, a decrease of 118 mm (52%) in the output of the MRI-CGCM2 (climate model under the SRES A2 scenario) and 139 mm (61%) in the output of the CCSR/NIES/FRCGC-MIROC (climate model under the SRES A2 scenario) is expected in the annual river flow of the basin. Therefore, the existing water resources in the Seyhan Basin will reduce significantly in the future (Fujihara et al., 2008).

2.4 Modelling Studies

2.4.1 Hydrological Models

Water cycle or hydrological cycle is the circulation of water that takes place between the earth's atmosphere, ocean, and land. Water frequently changes its state between solid, liquid, and gas phases through the cycle. Surface runoff consists of the precipitation that does not seep into the soil and passes from the land surface to rivers, streams, lakes, etc. which are surface waters. Surface runoff varies over time with the characteristics of the basin and location. Runoff is significant part of the water cycle, and it helps balance it. Below equation shows the water balance equation. Also, Figure 2-11 shows simple diagram of the water cycle.

$$Q_s = P - ET - \Delta SM - \Delta GW$$

where, Q_s: Surface runoff, P: Precipitation, ET: Evapotranspiration, ΔSM: Soil moisture changes, ΔGW: Groundwater storage changes

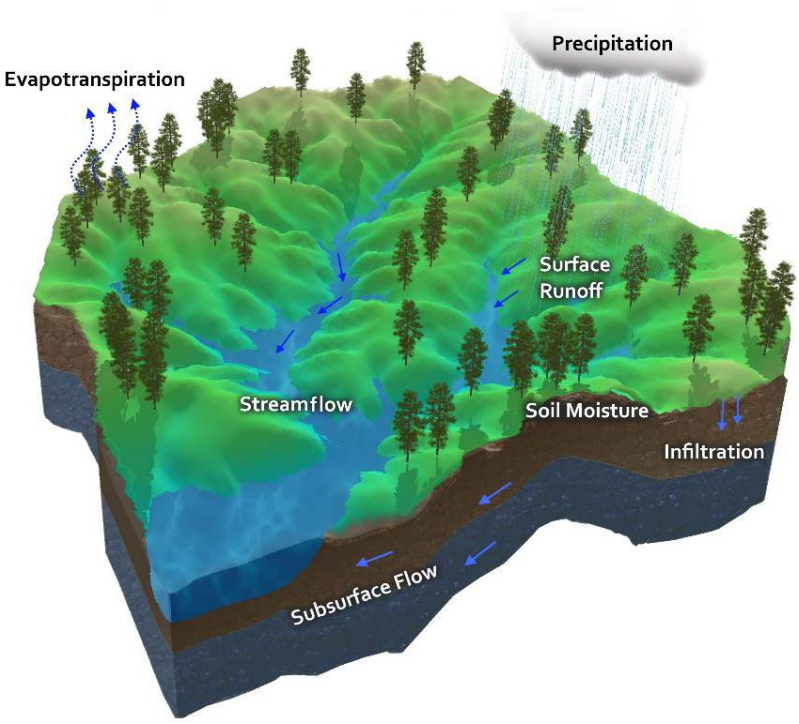

Figure 2-11 Simple Diagram of Water Cycle (Sitterson et al., 2017)

The main elements of hydrological models are surface runoff, precipitation, infiltration, evapotranspiration, groundwater runoff, etc. There is an interaction between these elements and a basin or watershed can be thought of as an area where hydrological elements are integrated. Hydrological modelling represents the hydrological elements or processes and enables the formulation of mathematical models of the interaction between these processes (Islam, 2011).

Models are simplified examples or representations of a real-world system. The best model can be defined as having the least model parameter and model complexity and giving the most realistic result at the same time. Models are substantially used to evaluate system respond or behavior and to comprehend existing hydrological processes. A rainfall-runoff model can be identified as a set of equations that allow the runoff estimation from various model parameters used to understand watershed properties. Hydrological models are accepted as a significant tool for the management of water and environmental resource (Devi et al., 2015).

Types of hydrological models

Types of hydrological models depend on model's structure. Structure of a model can change from simple to complex. Empirical, conceptual, and physically based models are the model structures that use for the hydrological purposes. Table 2-1 shows the basic structure of hydrological models. While empirical models can be considered as the simplest model, physical models can be considered as complex one (Sitterson et al., 2017).

Table 2-1 Basic structure of hydrological models (Sitterson et al., 2017)

	Empirical	**Conceptual**	**Physical**
Method	Non-linear relationship between inputs and outputs, black box concept	Simplified equations that represent water storage in catchment	Physical laws and equations based on real hydrologic responses
Strengths	Small number of parameters needed, can be more accurate, fast run time	Easy to calibrate, simple model structure	Incorporates spatial and temporal variability, very fine scale
Weaknesses	No connection between physical catchment, input data distortion	Does not consider spatial variability within catchment	Large number of parameters and calibration needed, site specific
Best Use	In ungauged watersheds, runoff is the only output needed	When computational time or data are limited.	Have great data availability on a small scale
Examples	Curve Number, Artificial Neural Networks	HSPF , TOPMODEL , HBV , Stanford	MIKE-SHE , KINEROS , VIC , PRMS

Empirical models are primarily observation-based models and attempt to characterize the response of the system in the consideration of the available data. These models are also known as metric models. They are relatively easily applied to ungauged basins by regional analysis, associating the model features (time to unit hydrograph peak, percentage of runoff, etc.) with climatic and physical descriptors of the basin. However, this should be considered that although empirical models based on available data and have been used to ungauged basins, the results often lack formal specification of confidence limits. Artificial Neural Networks and Data Based Mechanistic modelling are among the most interesting approaches for empirical

models in the recent times. Artificial Neural Networks use available data to comprehend the processes of rainfall-runoff and Data Based Mechanistic is developed as an empirical transfer function model based on the available data (Pechlivanidis et al., 2011).

Conceptual models are the models that comprehend flow processes by interconnecting components of hydrological processes. These models are comprised of a series of interconnected reservoirs that symbolize the physical elements in a basin. They are defined as the models between physical and empirical models. Conceptual models use equations which are semi empirical, and both the field data and the calibration are used to analyze the model parameters. Conceptual models differ in their complexity, and these complexities depend on the balance equations used to reflect the hydrological components. Long-term hydrological and meteorological recording is required to perform the calibration. They are best used in situations where there is a limited time and properties of the basin are not comprehensively analyzed. HBV model, HSPF and TOPMODEL are the examples of such models (Sitterson et al., 2017).

Physical models are a type of model built on understanding of the physics in relation to hydrological processes. Both large amount of data and computational time are needed for these models. It is accepted that it is possible to collect all the data which is required for the model either from the laboratory or from the field. Physically based models provide an insight into a process that gives a better understanding of the hydrological system. However, it is not easy to operate and develop such models in terms of economy and time. Generally, these models can be applied at fine scales. MIKE SHE, VIC are the examples of such models (Jajarmizadeh et al., 2012).

Hydrological models can also be categorized in spatial structure which are lumped models, semi-distributed models and fully-distributed models. Figure 2-12 shows the spatial structure visualization of hydrological models. A is the lumped model. B is the semi-distributed model divided by sub-basins. C is the fully-distributed model divided by grid cells.

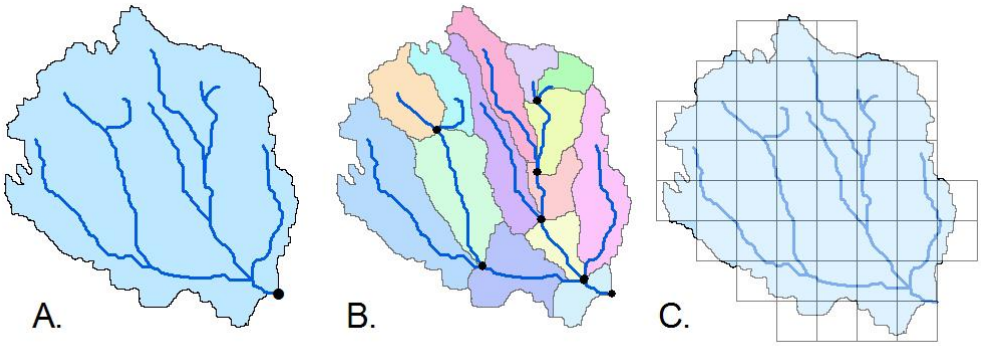

Figure 2-12 Spatial structure visualization of hydrological models (Sitterson et al., 2017)

In lumped models, it is considered as a single homogeneous area. Averaged input values are used in these models. For example, precipitation and temperature values are accepted equally distributed. For this reason, there is no spatial variability for the variables of input and output (Daniel et al., 2011)

According to Daniel et al. (2011) and Sitterson et al. (2017), semi-distributed models can be thought as a combination of many lumped models. In other words, basin consists of the small sub-basins each of which is a lumped model. Basin can be divided by many sub-basins in semi-distributed model for different usage purposes. Vegetation zone, slope, precipitation regime, runoff characteristics or elevation can be one of the purposes of dividing basin to sub-basins. There is spatial variability in semi-distributed models compared to lumped models. Semi-distributed models need less computational time, data, and parameter compared to fully-distributed models. Physically based models or conceptual models can be operated with semi-distributed models based on input data. HBV model, TOPMODEL are some examples of semi-distributed conceptual models. Şorman et al. (2009) applied the HBV model for the first time in Turkey and the aim of their study was to show that it is possible to model and forecast the snowmelt flow in the eastern part of Turkey.

Fully-distributed models known as distributed model are the most complex one. There is a spatial heterogeneous for the input values. These models divided by grid

cells and each grid cell has its input, output, and parameter. Since such models are grid based, they provide wider range of basin information. These models also are prone to being physically based. There is a data-intensive because all inputs of these models are temporary and spatially distributed. Computational and setting up time is longer than the lumped and semi-distributed models and also fully-distributed models need powerful computer sources. MIKESHE and WRF-Hydro models are some examples of fully-distributed physical models (Jajarmizadeh et al., 2012; Sitterson et al., 2017). Kilicarslan et al. (2021) used the WRF-Hydro model in a study and investigated the effect of sea surface temperature products of different resolutions on the simulations of excessive precipitation that caused important flooding on the basins of the Eastern Black Sea and Mediterranean in Turkey. Table 2-2 shows comparison of the hydrological models on the spatial basis.

Table 2-2 Comparison of the hydrological models on a spatial basis (Sitterson et al., 2017)

	Lumped	**Semi-Distributed**	**Distributed**
Method	Spatial variability is disregarded; entire catchment is modeled as one unit	Series of lumped and distributed parameters	Spatial variability is accounted for
Inputs	All averaged data by catchment	Both averaged and specific data by sub-catchment	All specific data by cell
Strengths	Fast computational time, good at simulating average conditions	Represents important features in catchment	Physically related to hydrological processes
Weaknesses	A lot of assumptions, loss of spatial resolution, not ideal for large areas	Averages data into sub-catchment areas, loss of spatial resolution	Data intense, long computational time
Examples	Empirical and conceptual models, machine learning	Conceptual and some physical models, TOPMODEL , SWAT	Physically distributed models, MIKESHE VELMA

2.4.2 HBV

HBV (Hydrologiska Byråns Vattenbalansavdelning) is a hydrological rainfall-runoff model which simulates the runoff. It was first developed by Sten Bergstöm at Swedish Meteorological and Hydrological Institute. HBV is most common rainfall-runoff model for the Scandinavian countries (Bergström, 1992).

There are various hydrological rainfall-runoff models that run at varying degree of difficulty. The HBV model is a mathematical water balance model that describes hydrological processes as simple as possible but with a sufficiently robust model structure.

HBV model is a semi-distributed conceptual model which provides to divide basin to different sub-basins, vegetation, and elevation regions (Bergström, 1992). HBV is a conceptual model which is well-known worldwide, and it has been performed more than 90 countries and it is also used for research about 50 PhD thesis all over the world (Bergström & Lindström, 2015).

Figure 2-13 shows the general overview of the structure of the routines in the HBV model and Figure 2-14 shows general structure of the HBV model.

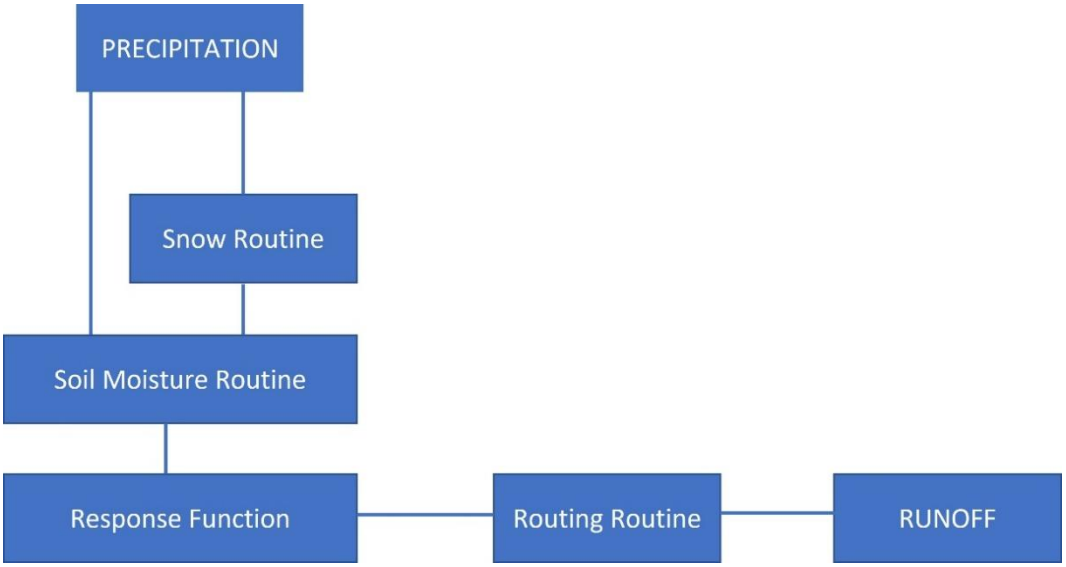

Figure 2-13 Schematic HBV Model Structure (Seibert, 2005)

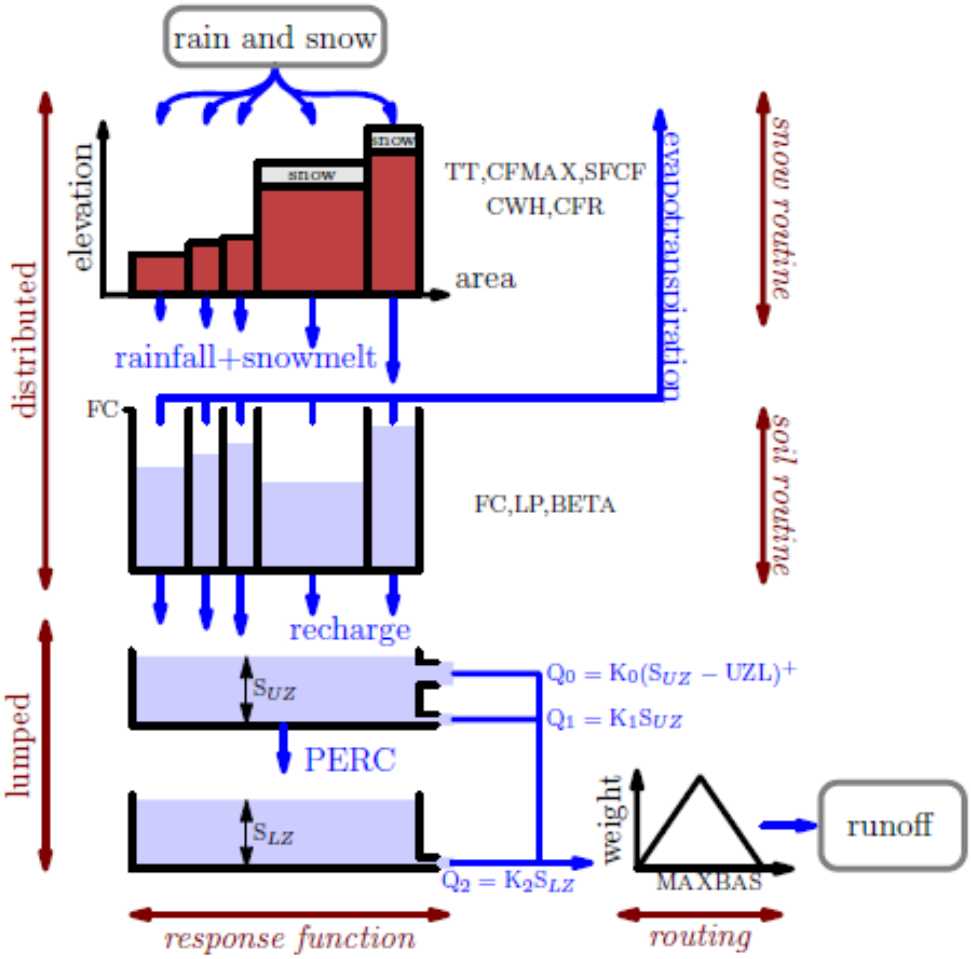

Figure 2-14 General Structure of HBV Model (Driessen et al., 2010)

The overall water balance equation of HBV model can be described as:

$$P - E - Q = \frac{d}{dt}(SP + SM + UZ + LZ + Lakes)$$

where P is precipitation, E is evaporation, Q is runoff, SP is snowpack, SM is soil moisture, UZ is upper groundwater zone, LZ is lower groundwater zone and $Lakes$ is the term which means change in the lake storage (Driessen et al., 2010).

The input and output data required by the routines of the HBV model are summarized in Table 2-3. The data that appear as inputs in all routines except the snow routine are model outputs, that is, the values calculated by the HBV model.

Table 2-3 Input and Output Data of the HBV model routines

Routines	Input Data	Output Data
Snow Routine	Precipitation, Temperature	Snowpack, Snow melt
Soil Routine	Potential Evaporation, Precipitation, Snow melt	Actual Evaporation, Soil Moisture, Groundwater Recharge
Response Function	Groundwater Recharge, Potential Evaporation	Runoff, Groundwater Levels
Routing Routine	Runoff	Simulated Runoff

Snow Routine

This routine computes accumulation of snow and snowmelt and also works separately for each zone of both elevation and vegetation. Threshold temperature (TT) is a temperature value that determine the precipitation whether snow or rain. If air temperature is below the TT, precipitation becomes snow or air temperature is above TT, it becomes rain. Accumulation of snow is adjusted by snowfall correction factor parameter (SFCF) in order to calculate missing winter evaporation and systematic errors in snowfall. CFMAX is a degree day factor which helps to calculate the snowmelt. CFR is a refreezing coefficient that helps to calculate liquid water in the snow. CWH is a parameter which is water holding capacity and before any runoff can occur, this value must be exceeded. If there are two vegetation zones in the catchment, the number of these parameters is doubled (Bergström, 1992).

Some equations of snow routine of HBV model are shown below. Also, Table 2-4 shows the snow routine parameters of HBV model

$$Melt = CFMAX * (T - TT)$$

$$Refreezing = CFR * CFMAX * (TT - T)$$

Table 2-4 Snow routine parameters

Parameter	Description	Unit
TT	Threshold temperature	°C
CFMAX	Degree day factor	mm/Δt*°C
SP	Seasonal variability	-
SFCF	Snowfall correction factor	-
CFR	Refreezing coefficient	-
CWH	Water holding capacity	-

Soil Routine

Changes in the soil moisture (SM) of the basin due to infiltration from the snow routine are controlled by this routine. FC, LP, and BETA are the three parameters that controls soil routine of HBV model. FC is the maximum soil moisture storage, LP is the soil moisture threshold value at which actual evapotranspiration (AET) reaches potential evapotranspiration (PET), and BETA is a soil shape calibration parameter which defines the relative contribution to runoff from a precipitation or snowmelt. The relationship between the FC, LP, BETA, and precipitation is shown below figures and equations (Seibert, 2005). Also, Table 2-5 shows the soil routine parameters of HBV model.

$$\frac{recharge}{P(t)} = \left(\frac{SM(t)}{FC}\right)^{BETA}$$

$$E_{actual} = E_{potential} * \min\left(\frac{SM(t)}{FC * LP}, 1\right)$$

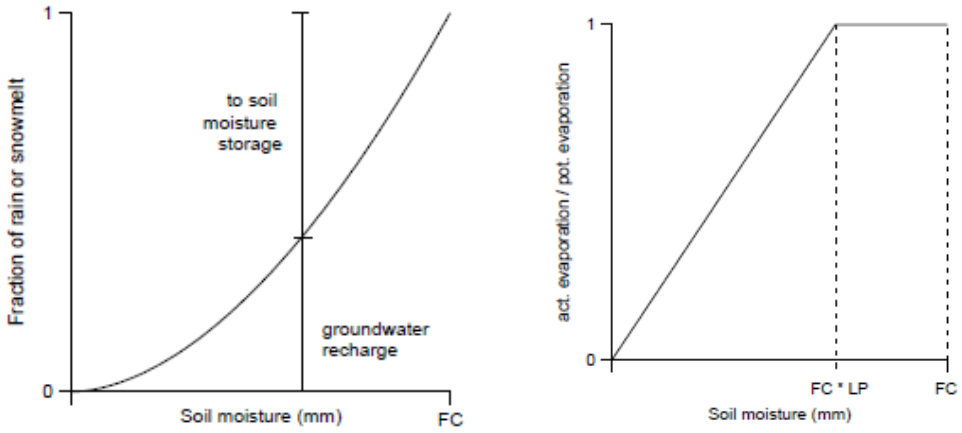

Figure 2-15 Summary of soil routine of HBV Model (Seibert, 2005)

According to the given equations, 3 different evaluations can be made regarding the soil:

- When the soil is dry (low SM/FC), groundwater recharge is low because only a small part of the precipitation increases the soil moisture (most of the precipitation is lost due to high evapotranspiration).
- When the soil moisture is at the field capacity (SM/FC equal to 1), no more precipitation can be stored as soil moisture and precipitation directly turns into the runoff. This can result in high flows even if average precipitation events occur.
- When the soil is moist (high SM/FC), most of the precipitation is available to increase soil moisture storage in the upper layer.

Table 2-5 Soil routine parameters

Parameter	Description	Unit
FC	Maximum soil moisture storage	mm
LP	Soil moisture threshold value	-
BETA	Soil shape calibration parameter	-

Response Function

This routine that obtains recharge from the soil routine consist of two reservoirs called SUZ (Storage in upper zone) and SLZ (Storage in lower zone). All excess water from the soil layer is redirected to fill the upper reservoir. Second, it is discharged towards the lower reservoir according to a percolation rate which is controlled by the percolation coefficient. The sum of the surface flow (Q0), subsurface flow (Q1) and baseflow (Q2) is the global outflow and is controlled by the recession coefficients K0, K1 and K2, respectively. However, K1 is consistently controlling the outflow from the upper reservoir, and only K0 is activated when the water level exceeds an UZL threshold (Ouatiki et al., 2020).

Response function of the HBV model is shown in Figure 2-16. Equation of this routine is also shown below. Table 2-6 shows the response function routine parameters of HBV model.

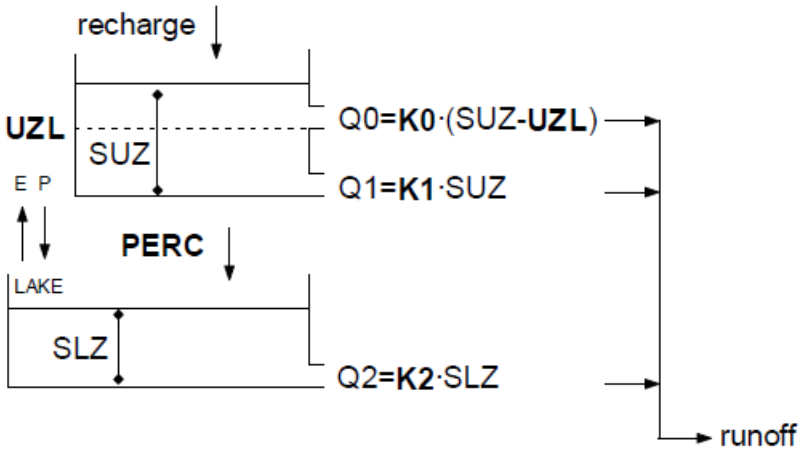

Figure 2-16 Response function of the HBV model (Seibert, 2005)

recharge = input from soil routine
SUZ = storage in upper zone
SLZ = storage in lower zone
UZL = threshold parameter
PERC = maximum percolation to lower zone
K_i = Recession coefficient
Q_i = runoff component

$$Q_{GW}(t) = (K_2 * SLZ) + (K_1 * SUZ) + K_0 * \max(SUZ - UZL, 0)$$

Outflow from the upper zone of the storage (SUZ) exits the reservoirs three ways. Q_0, Q_1, and Perc are these three possible ways. Outflow from the lower zone of the storage (SLZ) can be calculated from SUZ reservoirs (only percolation) and Q_2 (Mendez & Calvo-Valverde, 2016).

Table 2-6 Response function parameters

Parameter	Description	Unit
UZL	Threshold parameter	mm
PERC	Maximum percolation ratio	mm/Δt
Alpha	Non-linearity coefficient	-
K_0	Recession coefficient	1/Δt
K_1	Recession coefficient	1/Δt
K_2	Recession coefficient	1/Δt

Routing Routine

A filter (MAXBAS) is used to smooth the generated flow. MAXBAS is a free parameter of the HBV model. Also, it is only one parameter of routing routine of the HBV model. The total flow from the upper and lower zone reservoirs can be smoothed using the Muskingum method or a simple triangular weight function by the parameter of MAXBAS. Flow hydrograph comparison before and after MAXBAS is shown in Figure 2-17. The figure on the left shows generated flow and before MAXBAS parameter has been applied. The figure on the right shows obtained flow and after MAXBAS parameter has been applied. The middle figure is the MAXBAS which is a triangular weight function. Equation of this routine is also shown below (Bergström, 1992).

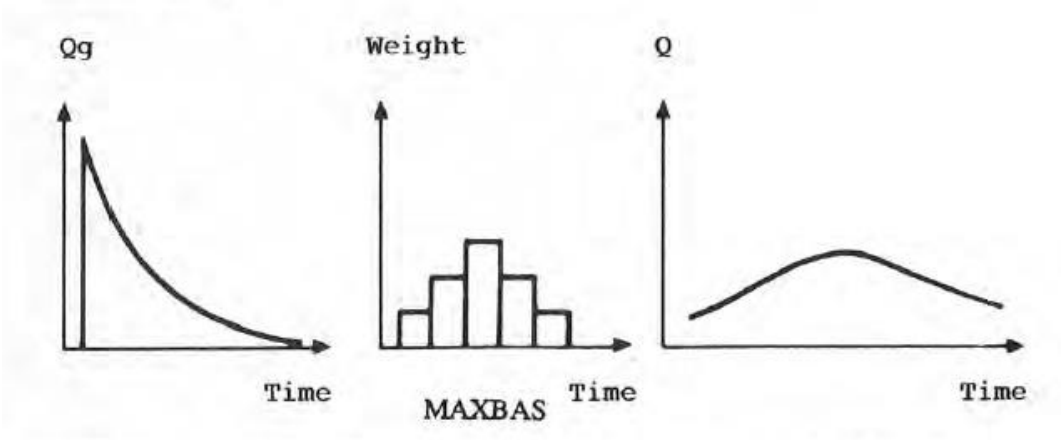

Figure 2-17 Flow hydrograph comparison before and after MAXBAS (Bergström, 1992)

$$Q_{sim}(t) = \sum_{i=1}^{MAXBAS} c(i) * Q_{GW}(t - i + 1)$$

$$c(i) = \int_{i-1}^{i} \left(\frac{2}{MAXBAS}\right) - \left| u - \frac{MAXBAS}{2} \right| * \frac{4}{MAXBAS^2} du$$

CHAPTER 3

STUDY AREA AND METHODOLOGY

3.1 Kızılırmak Basin

3.1.1 Kızılırmak Basin Area

Kızılırmak basin is located between 37º 56' and 41º 44' north latitudes and 32º 48' and 38º 24' east longitudes and located in the eastern part of the Central Anatolia Region in our country. Kızılırmak basin has the longest river which is fully located and the second largest drainage area in Turkey. Total drainage area is about 82.221 km^2 and the area of the Kızılırmak basin corresponds to approximately 10 percent of Turkey. Kızılırmak rises from Sivas-İmranlı surroundings and passes through the provincial lands of Kayseri, Nevşehir, Aksaray, Kırşehir, Ankara, Kırıkkale, Çankırı, Çorum, Sinop and Samsun, respectively, and flows into the Black Sea from the Bafra Plain in Samsun. The location of the Kızılırmak basin on the map of Turkey and physical map is given Figure 3-1.

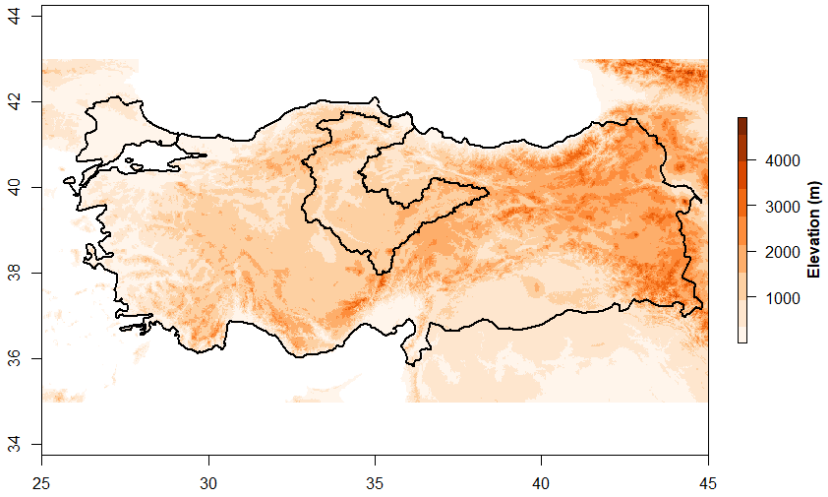

Figure 3-1 Location and Physical Map of the Kızılırmak Basin

Kızılırmak basin is adjacent to the Fırat-Dicle basin in the east, Yeşilırmak basin in the north, Batı Karadeniz basin in the northwest, Sakarya basin in the west, Konya Kapalı basin in the southwest and Seyhan basin in the south. Political map of Kızılırmak basin is shown Figure 3-2.

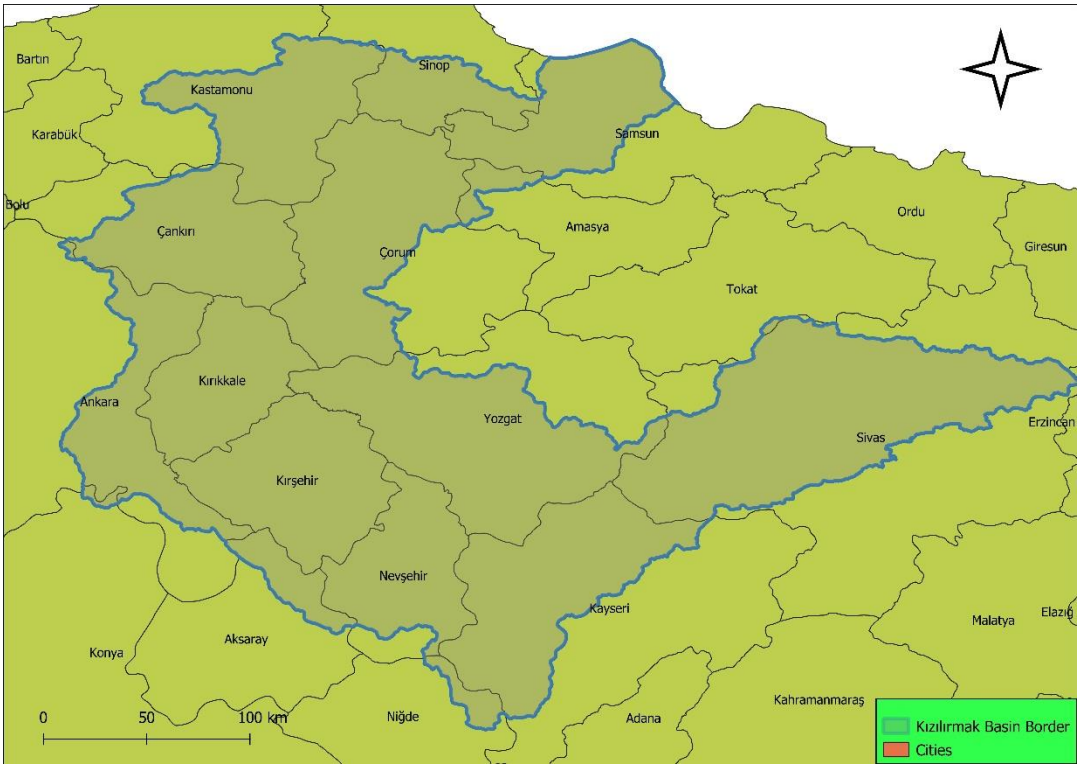

Figure 3-2 Political Map of the Kızılırmak Basin

The highest elevation of the basin is Mount Erciyes near Kayseri province and the lowest elevation is Bafra, where reaches the downstream of the Black Sea. It changes from 3895 m to 0 m and average elevation of the basin is 1260 m (SYGM, 2019). Hypsometric curve of the Kızılırmak basin is shown Figure 3-3.

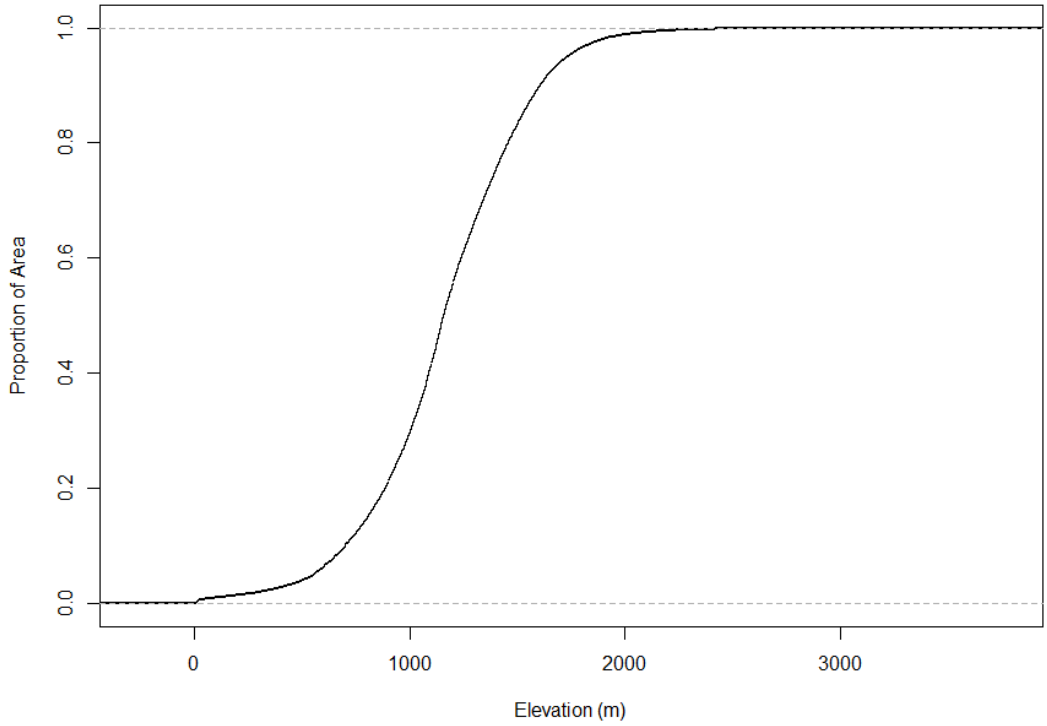

Figure 3-3 Hypsometric Curve of the Kızılırmak Basin

There are 11 dams on the mainstream of Kızılırmak river. These dams are called İmranlı Dam, Çermikler Dam, Yamula Dam, Bayramhacılı Dam, Hirfanlı Dam, Kesikköprü Dam, Kapulukaya Dam, Obruk Dam, Boyabat-Kepez Dam, Altınkaya Dam and Derbent Dam respectively. Locations of these dams are shown in Figure 3-4.

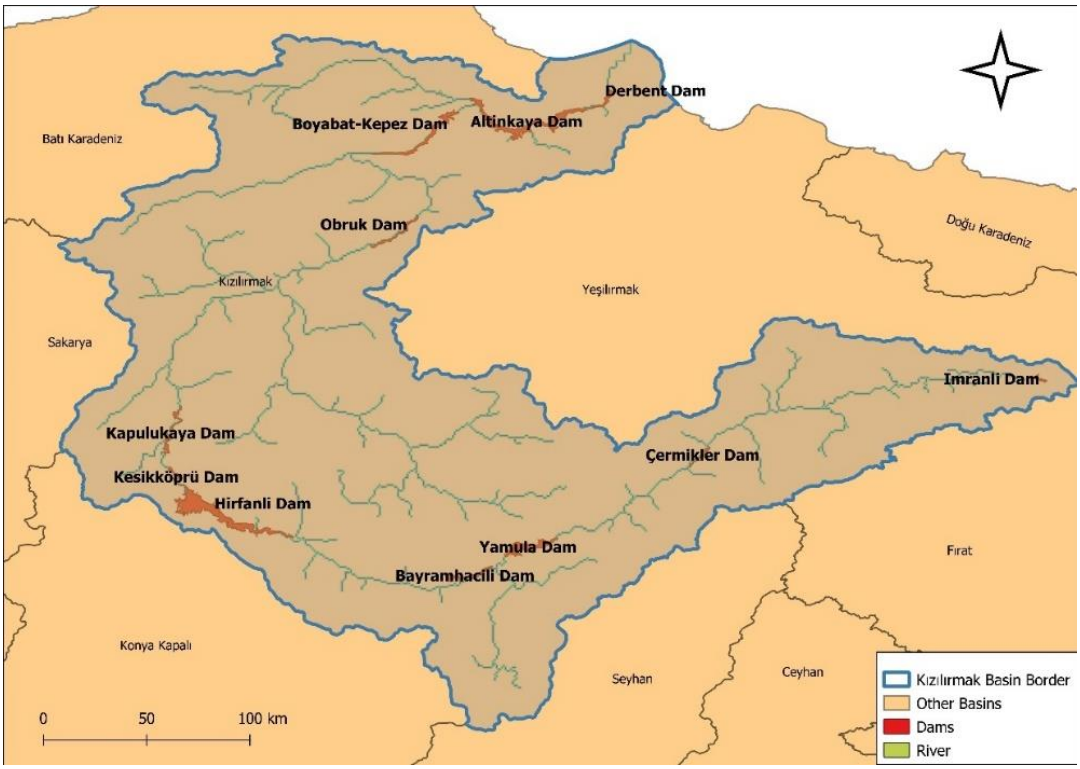

Figure 3-4 Location of Dams on Kızılırmak Mainstream

Since the Kızılırmak river is a long river, Kızılırmak basin covers a large area. The Kızılırmak basin has the climatic characteristics of the Black Sea region in the northern parts and Central Anatolia region in the southern parts. For this reason, it is possible to see the meteorological features specific to the geographical regions of the Black Sea and Central Anatolia regions in the Kızılırmak basin. The Black Sea region has a Black Sea climate, with warm winters, cool summers, and it is rainy in all seasons. The daily and annual temperature differences in the Black Sea climate are less when compared to other climate types in Turkey. Although the most precipitation falls in the winter season and the least in the summer season, there is not much difference in the amount of precipitation between the seasons. In the Central Anatolia region, there is a continental climate. In this region, winters are cold and often snowy, and summers are hot and dry. In the continental climate, annual and daily temperature differences are high. In winter, the temperature often drops below zero.

When the precipitation and temperature data of the Kızılırmak basin are analyzed; it is seen that average annual precipitation increases towards the northern part of the basin (in the direction of the Black Sea region). According to the data obtained from the meteorological observation stations in the Kızılırmak basin, the average total precipitation value was found to be 444.3 mm/year using the Thiessen Polygons method and it is 461 mm/year using the arithmetic mean. Also, the annual mean temperature for the Kızılırmak basin was found to be 10.5°C (SYGM, 2019).

3.1.2 Sub-basins in the Kızılırmak Basin

Given Kızılırmak basin has many dams regulating the runoff water, the volume of the water is more dominated by the water management decisions rather than the nature of the hydrological cycle. Accordingly, an accurate model simulation results are not expected at the downstream locations of major dams. Some preliminary hydrological modelling simulations are performed over different locations of the main stream of Kızılırmak basin, and indeed very poor or insignificant runoff NSE results are found (results are not shown). Accordingly, branches of Kızılırmak basin that are not regulated and have natural flow are considered for hydrological modelling simulations in this study. Among the available stations that have near natural flow conditions at the up-stream, the ones that have as high catchment area as possible are preferred. As a result, only three sub-catchments of Kızılırmak basin could be determined for this study (Figure 3-5), where the stream gauge stations have DSI id of E15A035 (Kızılırmak - Söğütlühan), E15A041 (Delice Çayı - Çadırhöyük) and E15A045 (Gökırmak - Purtulu). Three sub-basin areas were created with the help of these stream gauge stations. E15A035 stream gauge station represents SB 1535. E15A041 stream gauge station represents SB 1541. E15A045 stream gauge station represents SB 1545.

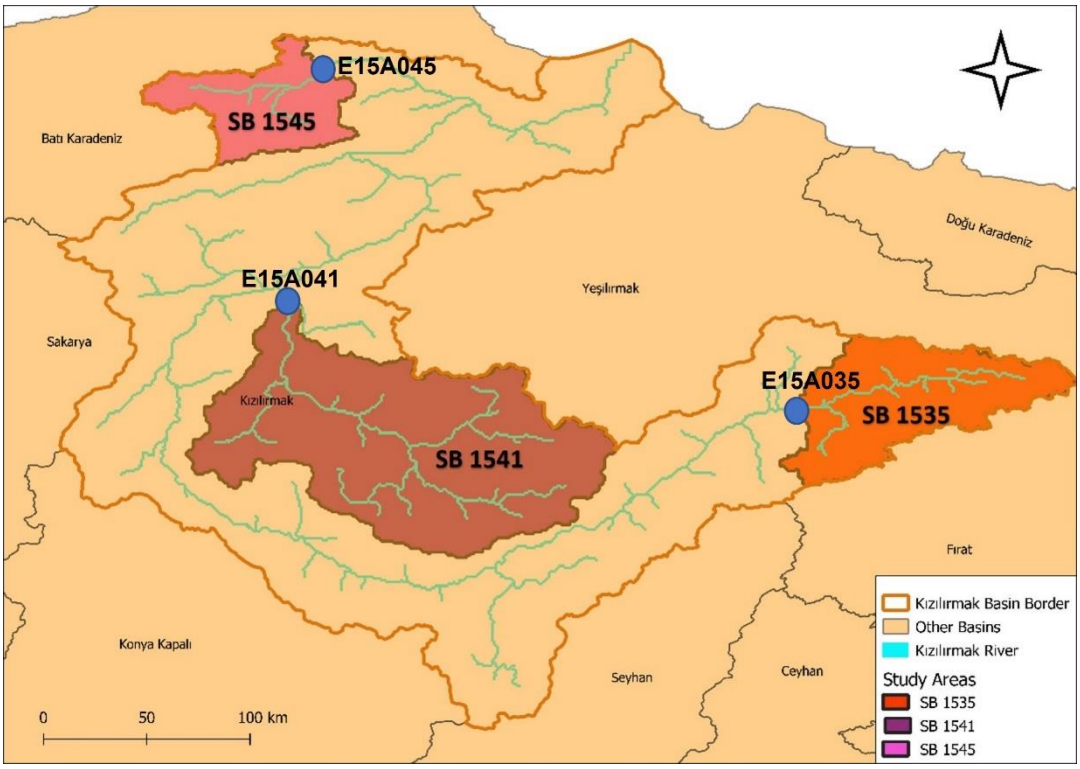

Figure 3-5 Location of Sub-basin Areas

Also, in order to increase the representativeness of the basin, areas from the upper, middle and lower region of the basin were selected when carrying out the modelling studies. Another reason for choosing these 3 sub-basins: Sub-basin 1535 (SB 1535) includes an area that rises of Kızılırmak and is upper region of the basin, Sub-basin 1541 (SB 1541) is in the middle of the basin and is on one of the largest branches of the Kızılırmak, Sub-basin 1545 (SB 1545) is on the lower region of the basin and close to the point where Kızılırmak flows into the Black Sea. In addition, there are significant differences between these 3 sub-basins in terms of the annual average temperature and annual total precipitation (Table 3-1). Hypsometric curve and average temperature and precipitation graphs of 3 sub-basins are shown in Figure 3-6 and Figure 3-7.

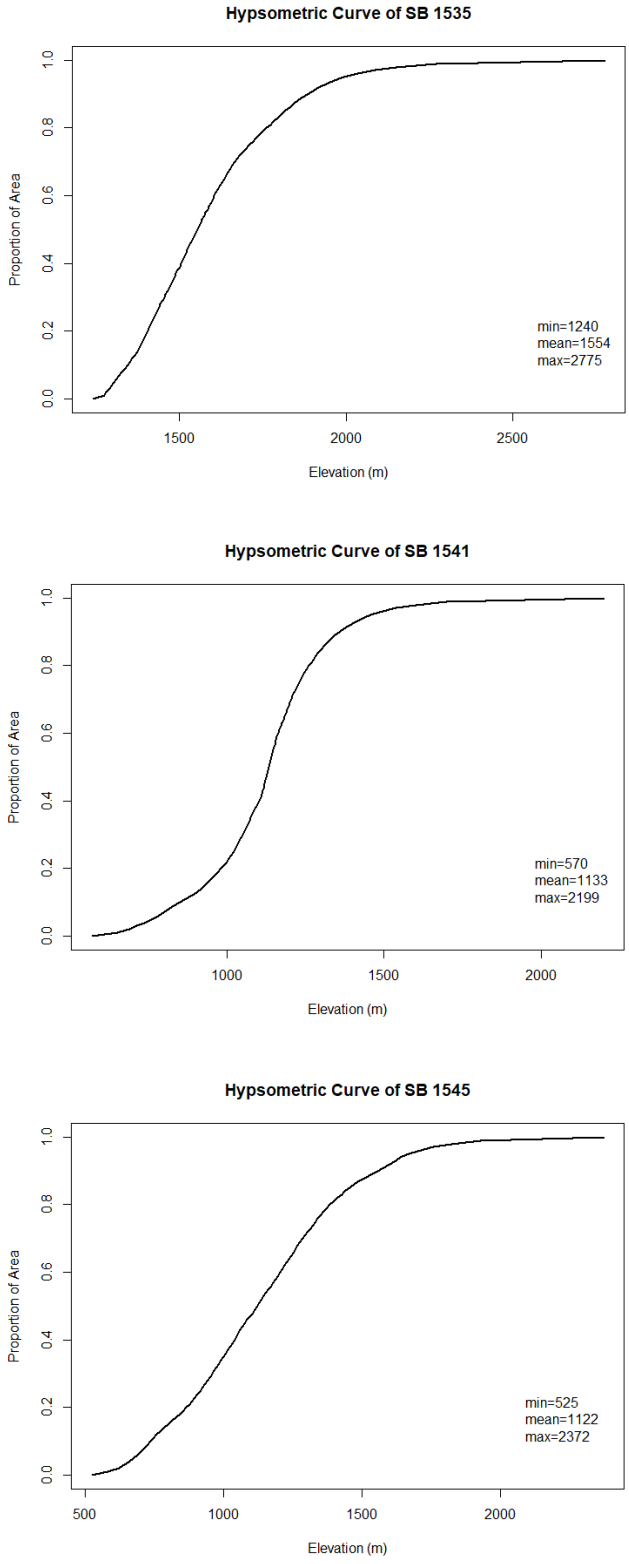

Figure 3-6 Hypsometric Curve of the Sub-basins

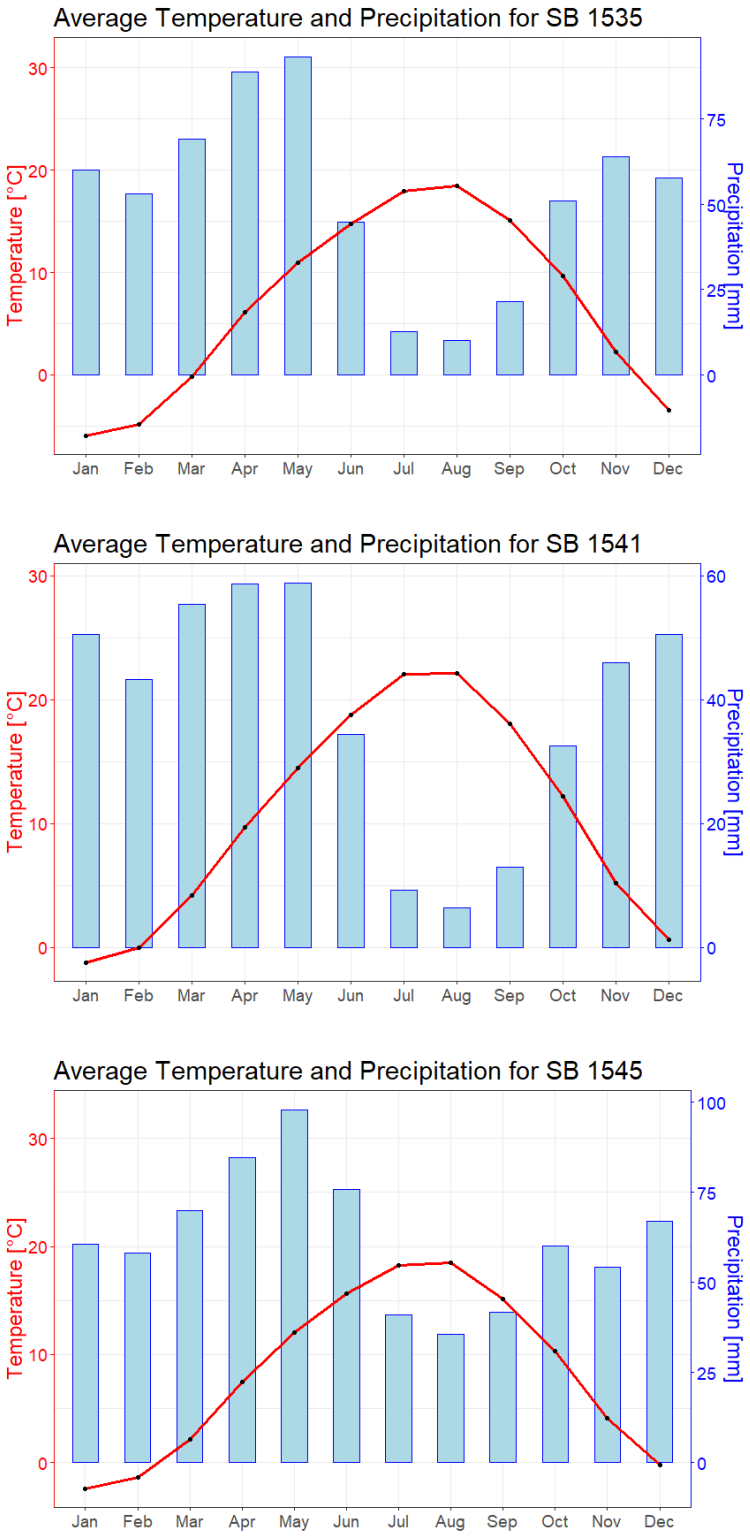

Figure 3-7 Average Temperature and Precipitation of the Sub-basins

For 3 sub-basins, May is the rainiest month, while August is the driest month. Also, while January is the coldest month, August is the hottest month.

Also, average temperature, precipitation, and areas of the 3 sub-basins are shown in Table 3-1. The fact that the average temperature and precipitation values are different from each other is significant for the representativeness of the Kızılırmak basin during the modelling studies.

Table 3-1 Average temperature, precipitation, and areas of the 3 sub-basins

Sub-basin	Area (km^2)	Average Temperature (°C) (from ERA5-LAND)	Average Precipitation (mm/year) (from ERA5-LAND)
SB 1535	6607.5	6.8	626
SB 1541	16762.8	10.6	429
SB 1545	3931.5	8.3	747

Table 3-2 shows Köppen-Geiger climate classification of 3 sub-basins between the years of 1992-2021. Percentage values indicated in Table 3-2 show what percentage of those sub-basins are included in which Köppen-Geiger climate classification (Dsb: Warm, dry-summer continental climate, Csa: Hot-summer Mediterranean climate, Dsa: Hot, dry-summer continental climate, Cfb: Temperate oceanic climate, Dfb: Warm-summer humid continental climate) (Peel et al., 2007).

Table 3-2 Köppen-Geiger climate classification of 3 sub-basins

Sub-basin/ Climate Classification	Dsb	Csa	Dsa	Cfb	Dfb
SB 1535	100%	-	-	-	-
SB 1541	33%	16%	51%	-	-
SB 1545	7%	-	-	7%	86%

3.2 HBV Model

Calibration and Validation Processes of the Model

Models have some unknown coefficients that are parameters. In process of hydrological modelling, hydrological parameters are necessary to calibrate taking into consideration the different conditions of the study area. Calibration of a model generally comprises of adjusting the model parameters to redefine the response of a basin within a certain accuracy range. In other words, calibration of a model is to estimate these parameters which cannot be obtained from the study area using the past data or records. Therefore, calibration can be done when long term records are available (Yılmaz et al., 2010). Figure 3-8 shows the schematic representation of the model calibration.

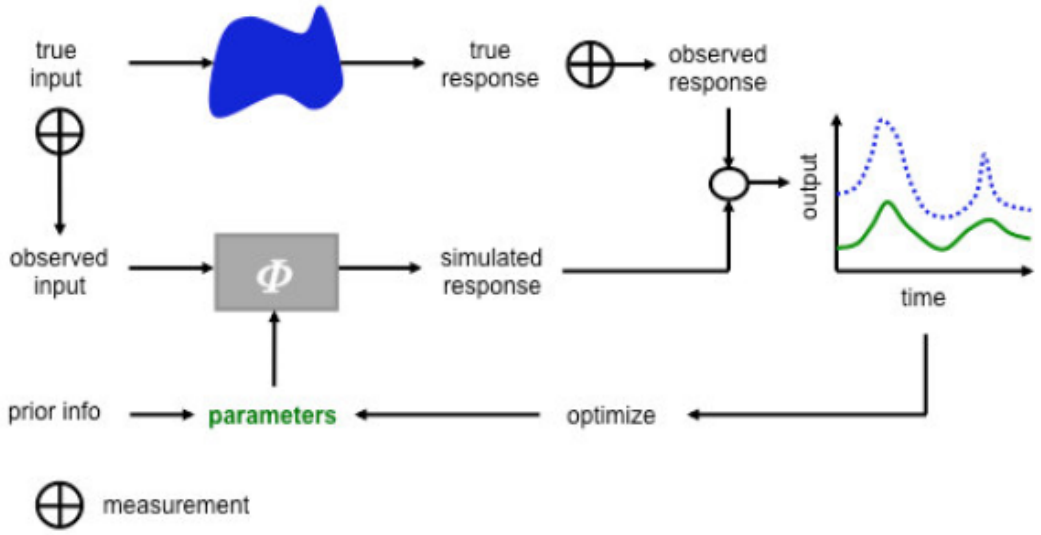

Figure 3-8 A schematic representation of the model calibration
(Yılmaz et al., 2010)

Calibration of a model can be divided into two parts which are manually or automatically (Yılmaz et al., 2010). Manual calibration is a trial-and-error procedure. In order to perform calibration manually, good knowledge of physical characteristics of the basin is required and also it requires a good analysis of working principle and structure of the model. In addition, manual calibration needs expert hydrologists to

perform successful calibration. However, this method requires time and labor intensive and when there are many parameters, there will be an increase in the difficulties of manual calibration method in order to estimate the parameters correctly (Yılmaz et al., 2010). When the parameters are performed automatically by a computer, this method is automatic calibration. This method is objective and fast when compared to the manual calibration. Automatic calibration can be thought as an optimization problem. Automatic calibration method uses single mathematical criteria which can be objective function in order to get best parameter set. However, this method is often insufficient to properly quantify the simulation of all the significant features of the system stated in the observations (Madsen, 2000).

The basis for the determining the model parameters is to minimize the error between simulated and observed discharge. Calibration stops when acceptable ratio (statistical criterion) is achieved with the observations (Bergström, 1992). There are many statistical criteria to evaluation the model performance. Nash-Sutcliffe Efficiency (NSE) and Root Mean Squared Error (RMSE) are two of the important performance criteria (Ouatiki et al., 2020).

$$NSE = 1 - \frac{\sum_{i=1}^{n}(Q_i^{obs} - Q_i^{sim})^2}{\sum_{i=1}^{n}(Q_i^{obs} - \overline{Q}^{obs})^2}$$

$$RMSE = \sqrt{\frac{\sum_{i=1}^{n}(Q_i^{obs} - Q_i^{sim})^2}{n}}$$

where, Q^{obs} : Observed surface runoff, Q^{sim} Simulated surface runoff, $\overline{Q}^{obs}$: Observed mean surface runoff

NSE was proposed by Nash and Sutcliffe (1970) to evaluate the predictive accuracy of the hydrological models. NSE shows the goodness of fit the observed and simulated data to the 1:1 line of the graph. NSE is sensitive to extreme values and calculated NSE value range from -∞ to 1.

When NSE value is above 0.50, we can say that evaluation of daily runoff simulations is satisfactory (Moriasi et al., 2015). In addition, when NSE value is above 0.55, we can say that evaluation of monthly runoff simulations is satisfactory (Moriasi et al., 2015).

The square root of mean square error (MSE) is called the root mean square error (RMSE). MSE is also referred to as the standard error of estimation in regression analysis. RMSE calculates the difference between simulated and measured values. The unit is the same as the simulated and measured results. A value of 0 indicates perfect fit to the data. It is widely accepted that the lower RMSE, the better the model performance (Moriasi et al., 2015).

It is extremely important to use separate data sets for model calibration and validation in hydrological modelling studies. The content and length of the data set to be used during the calibration of the model is highly significant in the optimization of the parameters. Also, the data set to be used during calibration should include various hydrological events such as drought, flood, high flow, low flow, etc. It is important to determine the parameters of the model because of the variety in these hydrological events and to perform a good performance during the validation to be used later using these parameters. 5-10 years is sufficient for the calibration of the HBV model (Seibert, 2005). It is also important to note that calibration and validation data sets have similar statistical properties (Seibert, 2005).

Monte Carlo simulation, Batch simulation, and Genetic Algorithm and Powell optimization (GAP) are three methods for calibration of the HBV model. Monte Carlo simulation is performed based on randomly selected sets of parameters. Many simulations can be run in the Monte Carlo simulation and some objective functions (NSE, RMSE, etc.) can be used for the model efficiency. Selected objective function is calculated for each model run (default value is 1000) and it is used to sort different sets of parameters based on their performance. Batch simulation is used when there are predefined parameter sets. This simulation can also assess the model performance. What distinguish this simulation from others is that the parameter sets

to be used for the evaluation of model performance are known in advance (Seibert & Vis, 2012).

GAP optimization is another method for the calibration of the HBV model. Principles of evolution is used by GAP method to develop a set of optimal parameters gradually. The algorithm starts with a randomly selected parameter set with a default value of 50 (Hedberg, 2015). The performances of the parameter sets are evaluated and two of the parameter sets are used to create the next set of parameters, known as the next generations. The two contributing sets of parameters are selected on the basis of their probabilities which are defined by various goodness of fit criteria. New parameters are then evolved out of parameter values from the old values (default value of p is 0.82) or out of random values between the old values (default value of p is 0.16) or are evolved as a mutation (default value of p is 0.02). The process continues until no new set of parameters is better than the previous generation, or the process ends when it reaches the maximum number of generations entered (default value is 5000) (Hedberg, 2015). GAP optimization has two steps. This is the first step of GAP optimization. Fine-tuning of the results is the second step. The second step involves performing a local optimization that use a method called Powell's quadratic method for better model fit. Powell's quadratic method is the iterative process, with the default value of 1000 iterations. An optimized set of parameters is obtained with each calibration. Calibration should be repeated more than once to minimize the risk of detecting a change due to parameter uncertainties. If the model is calibrated n times in total, n different optimal parameter sets are obtained (Hedberg, 2015).

In this study, GAP optimization is used for the calibration of the HBV model. Each parameter has lower and upper limit. If any parameter has reached one of the limits at the end of the calibration, it is necessary to expand the range of the upper and lower limit and calibration should be repeated. Number of model runs was chosen 5000 (default value) and number of runs for local optimization was chosen 1000 (default value) in this study. Model calibrated 100 times in total and objective function of this study are Reff (model efficiency) and LogReff (efficiency for

log(Q)). Also, the elevation of the sub-basins was entered as a percentage weighted. Minimum and maximum elevation of the sub-basins were entered as lower and upper limits for the elevation of precipitation and elevation of temperature parameters. Figure 3-9 shows the values GAP optimization window.

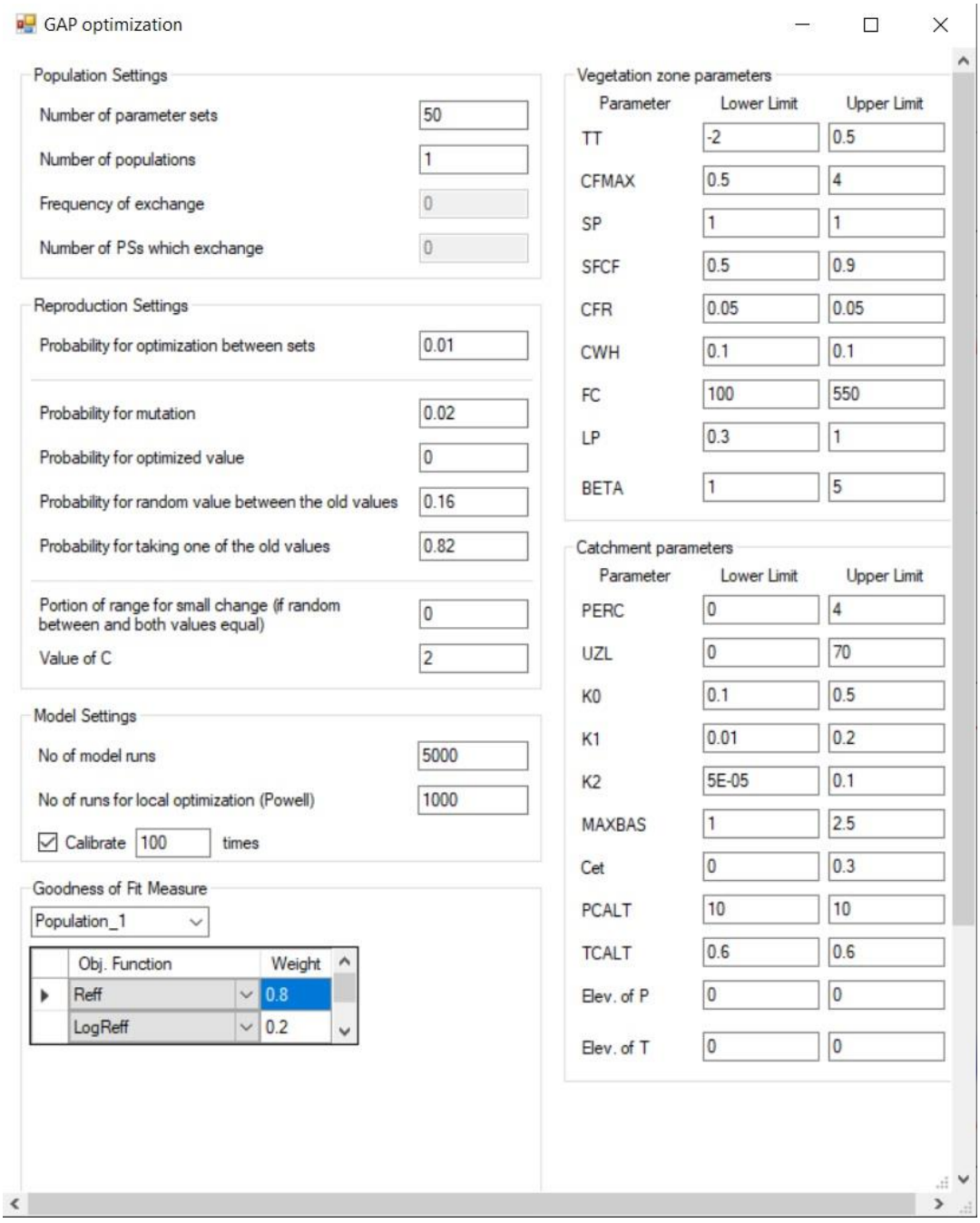

Figure 3-9 GAP optimization window

HBV-Light Model

In this study, HBV-light model is used. According to Seibert and Vis (2012), HBV-light model has been developed by Uppsala University at Sweden using Microsoft Visual Basic. It is a computer-based model and easy to use for educational and research purposes. HBV-light model can easily run with the little time and model knowledge. It is easy to see and interpret observed and simulated time series and parameter values at the same time in a window. Main window of the HBV-light model is shown in Figure 3-10.

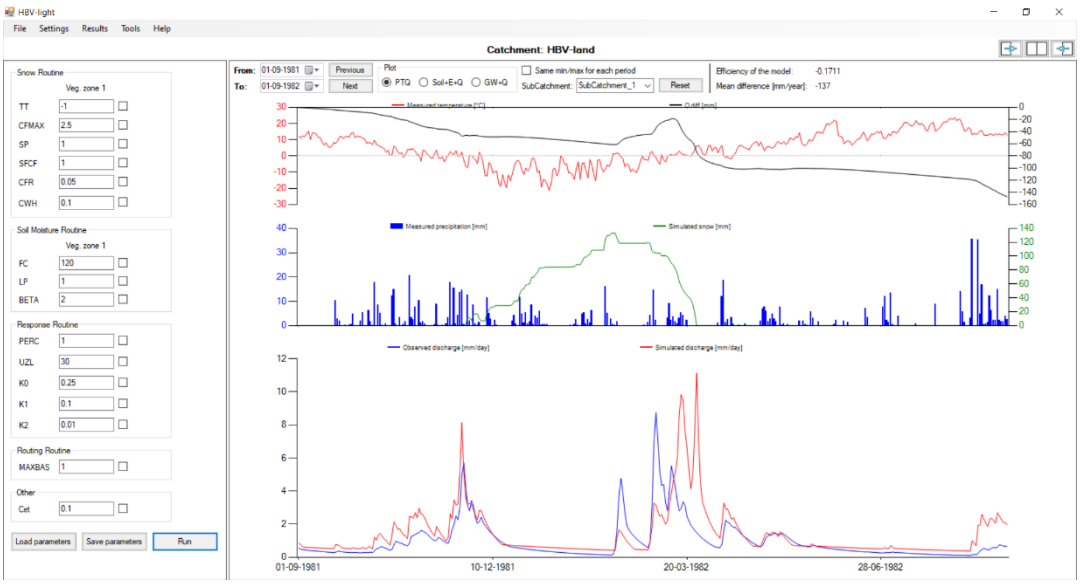

Figure 3-10 Main window of HBV-light model

Warming up period is used in the HBV-light model. It refers to the time the simulation will run before obtaining final results and helps the meteorological conditions and parameter values to adapt to normal operating conditions (Vis et al., 2015; Birundu & Mutua, 2017). One year warming up period is usually sufficient (Seibert & Vis, 2012).

3.3 Datasets

In this study, future surface runoff projections over three sub-basins of Kızılırmak basin are obtained by running HBV model. Firstly, the validation of ERA5-Land datasets was performed with the ground station-based meteorological station dataset (precipitation and temperature) and ERA5-Land datasets were used for historical temperature and precipitation values (chapter 4.1). Then, 56 different GCM/RCM couple datasets (temperature and precipitation) were downloaded for both the historical and the future periods. Later, obtained historical GCM/RCM couple datasets were validated using ERA5-Land datasets. Following the results of the validation, 10 worst performing (with lowest accuracy) among 56 datasets were eliminated (chapter 4.2). Remaining 46 datasets were used in this study to investigate the impact of climate change in this study. These 46 RCM-based temperature and precipitation datasets for the historical period were corrected using ERA5-Land datasets. Then, correction factors (chapter 3.4) from the historical simulations (between ERA5-Land and RCM -based temperature and precipitation datasets) were later applied to future temperature and precipitation projections to correct the future datasets (chapter 4.3). Later, HBV-Light model was run for the historical period using ERA5-Land precipitation and temperature datasets to obtain historical runoff simulations and the calibration parameters of the HBV-Light model (chapter 4.5). Later, these calibration parameters were utilized in HBV-Light future projection simulations to obtain future runoff simulations using 46 projection datasets (chapter 4.6). After obtaining an ensemble of 46 runoff projections for the future, their ensemble mean was taken so that future runoff dataset-based analyses to be done. Multi-model ensemble is widely used for the climate models (Crawford et al., 2019; Feng et al., 2011; Hagedorn et al., 2005). For this reason, in this study, ensemble mean of 46 models was used. Below details are given for above summarized methodology.

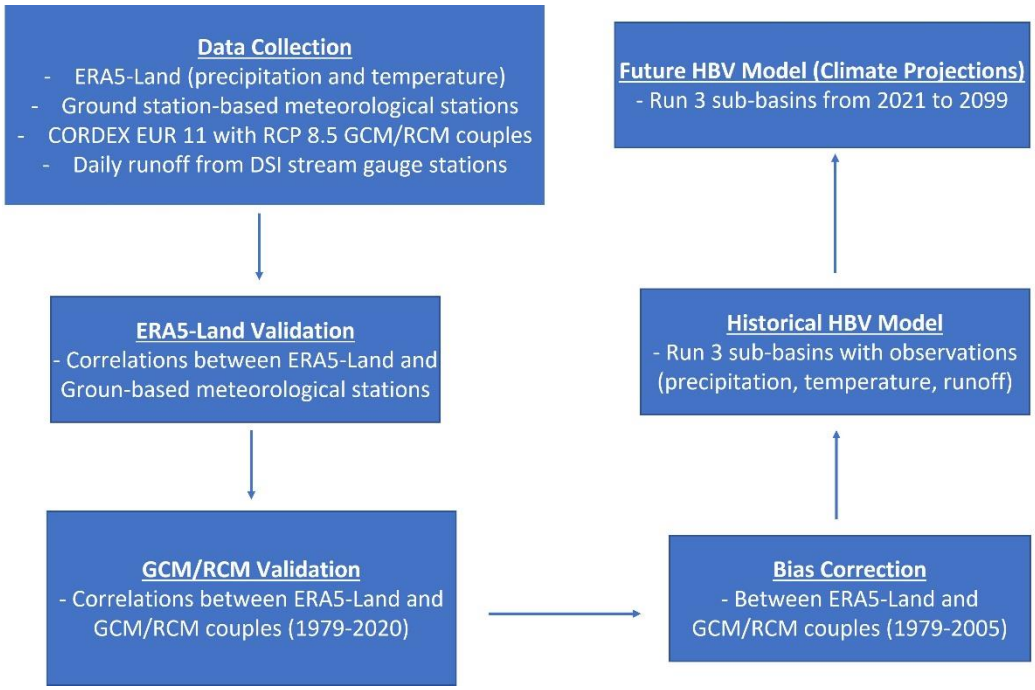

Figure 3-11 Flowchart of Analysis

3.3.1 Ground Station-Based Meteorological Stations

In this study, ground station-based meteorological station dataset (precipitation and temperature) was used for the validation of ERA5-Land. In Bağçaci et al.'s study (2021), ERA5 precipitation and near-surface temperature data were validated with ground station-based meteorological stations.

Meteorological stations which were used for the validation of ERA5-Land is shown in Figure 3-13. There are 2 meteorological stations for SB 1535 (17716: Zara Station, 17090: Sivas Station). There are 5 meteorological stations for SB 1541 (17760: Boğazlıyan Station, 17140: Yozgat Station, 17732: Çiçekdağı Station, 17756: Kaman Station, 17730: Keskin Station). There are 1 meteorological station for SB 1545 (17074: Kastamonu Station).

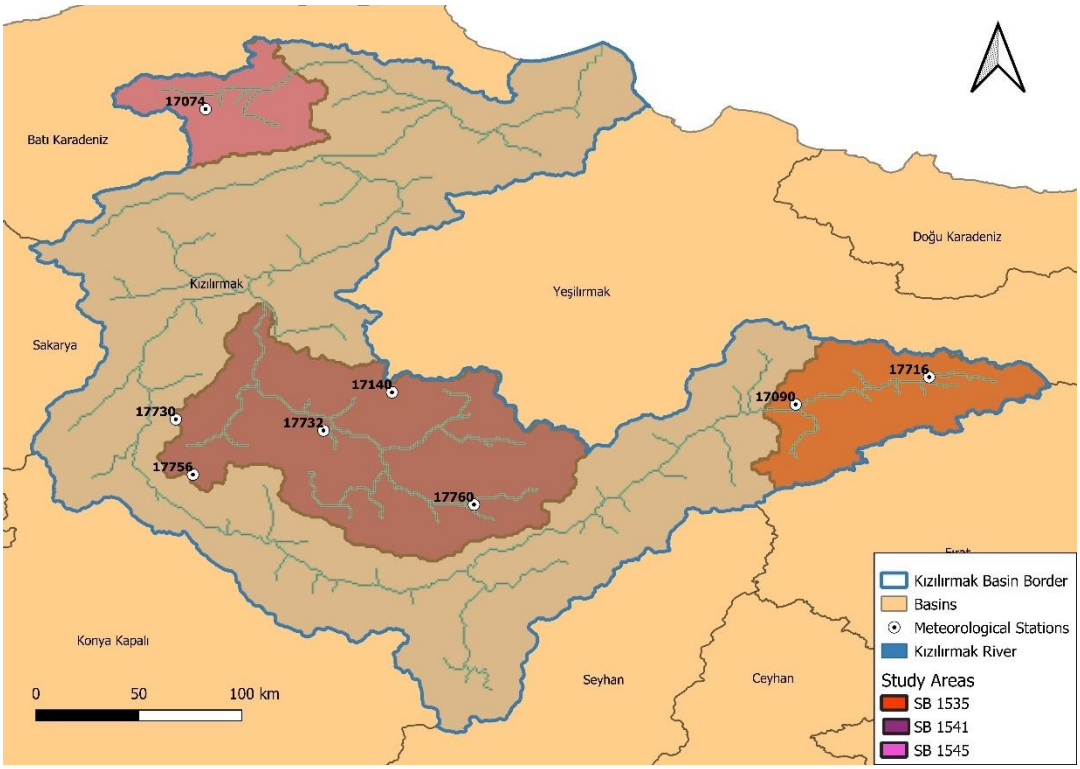

Figure 3-12 Location of meteorological stations within the 3 sub-basins

3.3.2 Climate Change Datasets (GCM/RCM)

Global Circulation Models (GCMs) are widely preferred in studies to understand the effects of large-scale climate change and may have an important role in understanding and explaining future changes in the global climate. GCMs provide limited information at the regional scale compared to the global scale and GCMs are not favored at sub-regional scales on the impacts of climate change on hydrology and water resources. Since GCMs have coarse spatial resolutions, they do not efficiently resolve the earth's surface structure at these scales. Regional climate models are used, which is a common procedure to obtain high scale regional information. This method is the process of dynamically downscaling GCM outputs and is performed using RCM. In recent years, RCMs have been used more and more in understanding the effects of climate change on water resources and hydrology with different scenarios (Bozkurt & Şen, 2012).

Taking measurements give information about climatic events that have happened in the past and that are likely to happen in the near future. Climate models can be used in order to predict likely to happen changes in climate parameters. These models can be divided into two main approaches: dynamic and statistical climate models. GCM which is Global Circulation or Global Climate Model, RCM which is Regional Climate Model, AOGCM which is Coupled Atmosphere Ocean Global Climate Model, ESM which is Earth System Model, are the examples of dynamical climate models. Although GCMs and AOGCMs are extremely simple models, these models give information about the most important physical processes that define our climate system. However, these models are limited by coarse spatial resolution on the effects of global climate. Resolution of these models can vary from 3° to 1.2° for the world. For the specific regions, RCMs are used using the GCMs outputs and they allow to reassess the climate at smaller scales. Resolution of the RCMs is very high compared to GCMs and can vary from 0.5° to 0.025° which is about 50 km to 3 km. With the help of the RCMs, impacts of the climate change can be reevaluated for the regional or local level. Statistical models are the second climate model types. They enable statistical relationships to be established between characteristics of local climate and historical large-scale processes. Markov chains, principle component analysis, weather generator, or linear methods are the examples of statistical models (Anders et al., 2014).

Table 3-3 Advantages and Disadvantages of Dynamical and Statistical Method (Trzaska & Schnarr, 2014)

	Dynamical downscaling	Statistical downscaling
Advantages	• Based on consistent, physical mechanism • Resolves atmospheric and surface processes occurring at sub-GCM grid scale • Not constrained by historical record so that novel scenarios can be simulated • Experiments involving an ensemble of RCMs are becoming available for uncertainty analysis	• Computationally inexpensive and efficient, which allows for many different emissions scenarios and GCM pairings • Methods range from simple to elaborate and are flexible enough to tailor for specific purposes • The same method can be applied across regions or the entire globe, which facilitates comparisons across different case studies • Relies on the observed climate as a basis for driving future projections • Can provide point-scale climatic variables for GCM-scale output • Tools are freely available and easy to implement and interpret; some methods can capture extreme events
Disadvantages	• Computationally intensive • Due to computational demands, RCMs are typically driven by only one or two GMC/emission scenario simulations • Limited number of RCMs available and no model results for many parts of the globe • May require further downscaling and bias correction of RCM outputs • Results depend on RCM assumptions; different RCMs will give different results • Affected by bias of driving GCM	• High quality observed data may be unavailable for many areas or variables • Assumes that relationships between large and local-scale processes will remain the same in the future (stationarity assumptions) • The simplest methods may only provide projections at a monthly resolution

Table 3-3 show advantages and disadvantages of dynamical and statistical method. Both models have advantages as well as disadvantages. Selection of the appropriate method based on both the requested spatial and temporal resolution of climate information and time and resource limitation. Generally, if there is a time and financial limitation, the most appropriate method is the statistical method. Dynamical methods are firstly used to survey the climate on larger areas by large climate institutions and regional assessment projects (Trzaska & Schnarr, 2014).

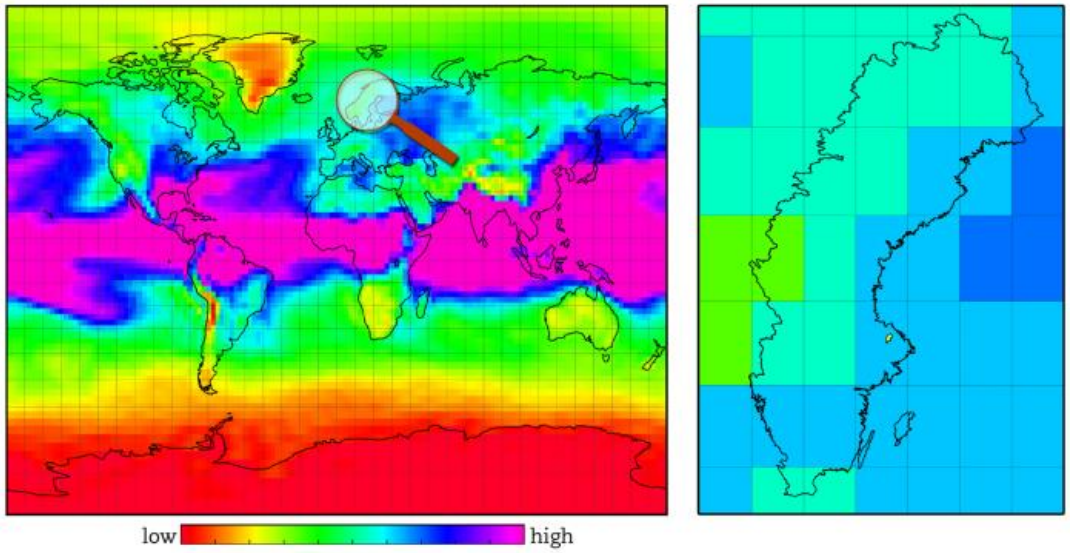

Figure 3-13 GCM with a resolution of 2.5° × 2.5° over all continents (Teutschbein, 2013)

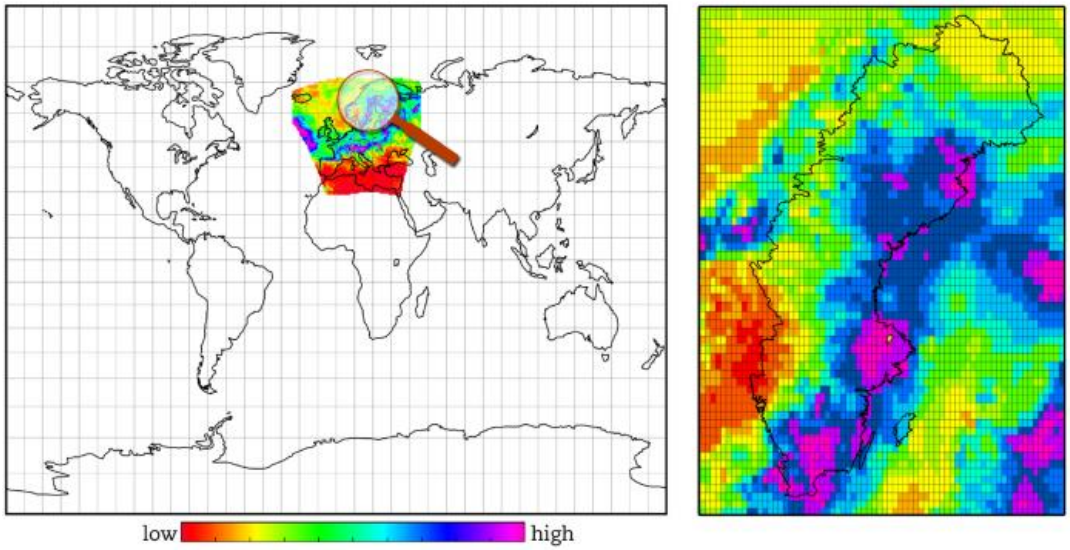

Figure 3-14 RCM with a resolution of 0.22° × 0.22° over Europe (Teutschbein, 2013)

CMIP5 (The Coupled Model Intercomparison Project Phase 5) (Taylor et al., 2012) is a project of the WCRP (World Climate Research Programme) to provide Fifth Assessment of IPCC Report with time dependent environmental variables. Database of the CMIP5 provides access to variable outputs from each model and these outputs are usually available as time series until 2100. Time steps of the outputs may vary

on a daily, monthly, or annual basis. Variable time projections of the models are evaluated in four different Representative Concentration Pathways (RCPs). Although each RCP contains the same categories of data, outputs can vary widely and reflect different emission scenarios over time depends on the socioeconomic assumptions (specific to each RCP). There are four types of RCPs. These are listed in Table 3-4 (Moss et al., 2010).

Table 3-4 Types of representative concentration pathways (Moss et al., 2010)

Name	Radiative Forcing	Concentration	Pathway shape
RCP 8.5	>8.5 W/m^2 in 2100	> ~1370 CO_2-eq in 2100	Rising
RCP 6	~6 W/m^2 at stabilization after 2100	~850 CO_2-eq (at stabilization after 2100)	Stabilization without overshoot
RCP 4.5	~4.5 W/m^2 at stabilization after 2100	~650 CO_2-eq (at stabilization after 2100)	Stabilization without overshoot
RCP 2.6	peak at ~3W/m^2 before 2100 and then decline	peak at ~490 CO_2-eq before 2100 and then decline	Peak and decline

According to Christensen et al. (2018), considering the long-term economic growth projections, there is at least a 35% probability of CO_2 concentrations exceeding defaults in RCP 8.5 by 2100. Also, Schwalm et al. (2020) stated that RCP 8.5 scenario is the best match for mid-century according to current and stated policies, with still very reasonable CO_2 emission levels in 2100. Furthermore, Barredo et al. (2017) and Riahi et al. (2011) are the examples of some studies that use RCP 8.5. Therefore, RCP 8.5 emission scenario was used for this study.

In Europe, a major effort has been developed in the CORDEX framework to downscale the projections of GCMs from the 5th Coupled Model Intercomparison

Project (CMIP5) for nearly a decade. EURO-CORDEX covers Europe at two different spatial resolutions, 0.11° (EUR-11, 12.5km) and 0.44° (EUR-44, 50 km) (Vautard et al., 2021). In this study, due to the higher spatial resolution, dataset of EUR-11 was used. Figure 3-15 shows the EURO-CORDEX model domain at 0.11° spatial resolution.

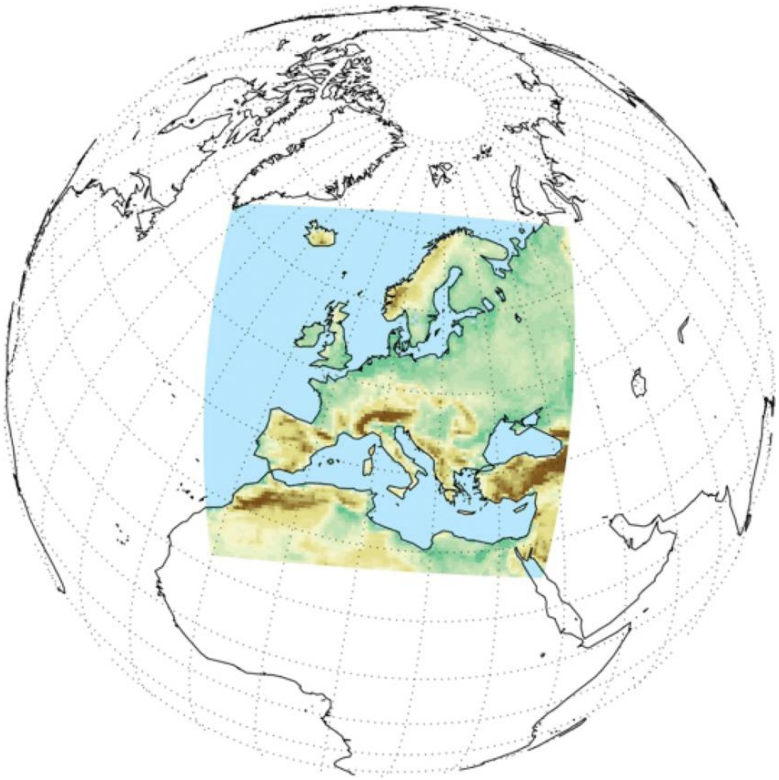

Figure 3-15 EURO-CORDEX model domain at 0.11° spatial resolution (EURO-CORDEX community, 2021)

In this study, daily precipitation and temperature datasets were downloaded and used from 56 GCM/RCM model couples with RCP 8.5 emission scenario using CMIP5 experiments between 2021 and 2099 future scenarios. Downloaded precipitation and temperature datasets are non-corrected values. Then, these downloaded datasets are corrected using a correction factor (chapter 3.4) for each month and ERA5-Land datasets were used to calculate these correction factor. 56 GCM/RCM model couples are listed in Table **3-5**.

Table 3-5 GCM/RCM model couples

ID	GCM	RCM
1	CCCma-CanESM2	CLMcom-CCLM4-8-17
2	CCCma-CanESM2	GERICS-REMO2015
3	CNRM-CERFACS-CNRM-CM5	CLMcom-CCLM4-8-17
4	CNRM-CERFACS-CNRM-CM5	CLMcom-ETH-COSMO-crCLIM-v1-1
5	CNRM-CERFACS-CNRM-CM5	CNRM-ALADIN53
6	CNRM-CERFACS-CNRM-CM5	CNRM-ALADIN63
7	CNRM-CERFACS-CNRM-CM5	DMI-HIRHAM5
8	CNRM-CERFACS-CNRM-CM5	GERICS-REMO2015
9	CNRM-CERFACS-CNRM-CM5	ICTP-RegCM4-6
10	CNRM-CERFACS-CNRM-CM5	IPSL-WRF381P
11	CNRM-CERFACS-CNRM-CM5	KNMI-RACMO22E
12	CNRM-CERFACS-CNRM-CM5	MOHC-HadREM3-GA7-05
13	CNRM-CERFACS-CNRM-CM5	RMIB-UGent-ALARO-0
14	CNRM-CERFACS-CNRM-CM5	SMHI-RCA4
15	ICHEC-EC-EARTH	CLMcom-ETH-COSMO-crCLIM-v1-1
16	ICHEC-EC-EARTH	DMI-HIRHAM5
17	ICHEC-EC-EARTH	KNMI-RACMO22E
18	ICHEC-EC-EARTH	SMHI-RCA4
19	IPSL-IPSL-CM5A-MR	DMI-HIRHAM5
20	IPSL-IPSL-CM5A-MR	GERICS-REMO2015
21	IPSL-IPSL-CM5A-MR	IPSL-WRF381P
22	IPSL-IPSL-CM5A-MR	KNMI-RACMO22E
23	IPSL-IPSL-CM5A-MR	SMHI-RCA4
24	MIROC-MIROC5	CLMcom-CCLM4-8-17
25	MIROC-MIROC5	GERICS-REMO2015
26	MOHC-HadGEM2-ES	CLMcom-CCLM4-8-17
27	MOHC-HadGEM2-ES	CLMcom-ETH-COSMO-crCLIM-v1-1
28	MOHC-HadGEM2-ES	CNRM-ALADIN63

Table 3-5 GCM/RCM model couples

ID	GCM	RCM
29	MOHC-HadGEM2-ES	DMI-HIRHAM5
30	MOHC-HadGEM2-ES	GERICS-REMO2015
31	MOHC-HadGEM2-ES	ICTP-RegCM4-6
32	MOHC-HadGEM2-ES	IPSL-WRF381P
33	MOHC-HadGEM2-ES	KNMI-RACMO22E
34	MOHC-HadGEM2-ES	MOHC-HadREM3-GA7-05
35	MOHC-HadGEM2-ES	SMHI-RCA4
36	MOHC-HadGEM2-ES	UHOH-WRF361H
37	MPI-M-MPI-ESM-LR	CLMcom-CCLM4-8-17
38	MPI-M-MPI-ESM-LR	CLMcom-ETH-COSMO-crCLIM-v1-1
39	MPI-M-MPI-ESM-LR	CNRM-ALADIN63
40	MPI-M-MPI-ESM-LR	DMI-HIRHAM5
41	MPI-M-MPI-ESM-LR	ICTP-RegCM4-6
42	MPI-M-MPI-ESM-LR	IPSL-WRF381P
43	MPI-M-MPI-ESM-LR	KNMI-RACMO22E
44	MPI-M-MPI-ESM-LR	MOHC-HadREM3-GA7-05
45	MPI-M-MPI-ESM-LR	MPI-CSC-REMO2009
46	MPI-M-MPI-ESM-LR	SMHI-RCA4
47	MPI-M-MPI-ESM-LR	UHOH-WRF361H
48	NCC-NorESM1-M	CLMcom-ETH-COSMO-crCLIM-v1-1
49	NCC-NorESM1-M	CNRM-ALADIN63
50	NCC-NorESM1-M	DMI-HIRHAM5
51	NCC-NorESM1-M	GERICS-REMO2015
52	NCC-NorESM1-M	ICTP-RegCM4-6
53	NCC-NorESM1-M	IPSL-WRF381P
54	NCC-NorESM1-M	KNMI-RACMO22E
55	NCC-NorESM1-M	MOHC-HadREM3-GA7-05
56	NCC-NorESM1-M	SMHI-RCA4

3.3.3 ERA5-Land

ERA5-Land data set was used for precipitation and temperature data used as input in the HBV-light model. ERA5-Land is a publicly available dataset for the period from 1950 to the present. The information of surface variables (humidity, air temperature, soil temperature total precipitation) is provided hourly and in high resolution by ERA5-Land. ERA5-Land is a replica of the land component of the ERA5 climate reanalysis with better spatial resolution. ERA5-Land contains information about uncertainties for all variables at reduced spatial and temporal resolutions. It combines model data with observations from around the world, using the laws of physics to create a globally complete and consistent dataset. ERA5-Land generates data from 1950 to the present that gives an accurate description of the past climate. It is a grid-based dataset and grid spaces is about 9 km (0.1^0 * 0.1^0) (Climate Data Store, 2022).

Table 3-6 Data Description of ERA5-LAND (Climate Data Store, 2022)

Data type	Gridded
Projection	Regular latitude-longitude grid
Horizontal coverage	Global
Horizontal resolution	0.1° x 0.1°; Native resolution is 9 km
Vertical coverage	From 2 m above the surface level, to a soil depth of 289 cm
Vertical resolution	4 levels of the ECMWF surface model: Layer 1: 0 -7cm, Layer 2: 7 -28cm, Layer 3: 28-100cm, Layer 4: 100-289cm Some parameters are defined at 2 m over the surface
Temporal coverage	January 1950 to present

Table 3-6 Data Description of ERA5-LAND (Climate Data Store, 2022)

Temporal resolution	Hourly
File format	GRIB
Update frequency	Monthly with a delay of about three months relatively to actual date

Precipitation in ERA5-Land

ERA5-Land data set provides hourly precipitation data. Precipitation data is the accumulation of liquid and frozen water from rain and snow that falls on the earth. It represents the total amount of water accumulated over a given period of time. The units are water equivalent depth in meters. This is the depth the water will have when evenly distributed over the grid box. Last hour of a day gives the total precipitation of that day.

Temperature in ERA5-Land

Temperature parameter of ERA5-Land data set express the air temperature at a height of 2 m above the surface of land, sea, or in-land waters. Since ERA5-Land provides hourly data, the arithmetic average of the temperatures in a day was taken as input to the HBV-light model and this process was repeated for each day.

In this study, ERA5-Land dataset (precipitation and temperature) cropped over study area were used in hydrological modelling studies for the historical period because ground station-based meteorological stations located in the sub-basins do not have continuous data (some missing data) (HBV model requires daily precipitation and temperature data) and there are also few meteorological stations representing the sub-basins (i.e., SB 1545 has only 1 meteorological station, while SB 1535 has 2.)

3.3.4 Runoff Observations

Runoff observation data was obtained from the General Directorate of State Hydraulic Works (DSİ) stream gauge annual report. This report is prepared separately for each year and has been published publicly until 2015. This report provides daily runoff data at stream gauge stations (if not closed) basin-based in Turkey. The runoff observations in the report may not be natural runoff data. Therefore, while selecting the sub-basins, the areas with as little interference as possible have been taken into consideration. Available observations for 3 sub-basins are listed in Table 3-7.

Table 3-7 Available Runoff Observation Dates

SUB-BASINS	DATES
SB 1535	01.10.1979-30.09.2011
SB 1541	01.10.1996-30.09.2010
SB 1545	01.10.1998-30.09.2011

Since there are limited data at the runoff observation station, the dates the model was run were also different from each other. For this reason, the HBV model was run between the dates when the data of the runoff observation station was available.

3.3.5 Datasets in the HBV-LIGHT Model

Model inputs

In the HBV-light model, daily precipitation, daily average temperature, daily observed runoff, and potential evapotranspiration data are used as the inputs to generate daily simulation runoff. These four types of data must be available to run the model. Optionally, long term daily mean temperature values can be used in order to add extra flexibility to the model. The long term mean of potential evapotranspiration for a given day of the year can be corrected using deviations from

the long term mean of temperature. A correction factor, C_{ET}, is used in this process (Seibert, 2005). In this study, these five types of data (daily precipitation, daily temperature, daily runoff, monthly potential evapotranspiration, and long term daily mean temperature) were used.

Precipitation and Temperature in the HBV-Light model

Daily precipitation and temperature values obtained from ERA5-Land data set are used as inputs in the HBV-Light model.

Long term daily mean temperature in the HBV-Light model

Long term daily mean temperature data was obtained from temperature values obtained from ERA5-Land data set.

Potential evapotranspiration in the HBV-Light model

Potential evapotranspiration (PET) is the amount of water process of transferring from the soil to the atmosphere. This can take place directly or through plants when water is available for this process to occur. There are some available methods to calculate it. Potential evapotranspiration can be calculated using formulas frequently used in the literature, such as Thornthwaite, Penman-Monteith (Portela, 2019). Thornthwaite (1948) method based on temperature. Thornthwaite is calculated monthly. Its formula is given below.

$$\mathrm{PET} = 16 * d * \left(\frac{10 * T}{I}\right)^{a}$$

T: monthly mean temperature (in °C)

I: annual thermal index (summation of monthly indices)

d: correlation factor that depends on latitude and month

a: an exponent that depends on I

According to Seibert (2005), PET can be calculated 3 ways for the HBV-light model input.

- 12 values which is long term monthly mean values
- 365 values which is long term daily mean values
- Daily values

In this study, Thornthwaite method was used for the calculation of monthly evapotranspiration. When we compare the Thornthwaite method with the Penman-Monteith method, Penman-Monteith method depends on the average maximum and average minimum air temperatures and requires the average air relative humidity and global solar radiation. This causes the Penman-Monteith method to be complex. However, in Thornthwaite method, average temperature and latitude is enough for the calculation. As a result, the Penman-Monteith method's need for extra data and the complexity of the formulas have caused common usage of the simpler Thornthwaite method, with the argument that the accuracy obtained with the Penman-Monteith method is not important (Kumar et al., 1987).

Long term monthly mean PET values are sufficient for the HBV-light model (Bergström, 1992; Seibert, 2005). Also, according to Idrizovic et al.'s study (2018), they conducted a study about different PET inputs in the Toplica River watershed in Serbia and they found that the HBV-light model was not sensitive to the use of the daily or monthly average PET value. They observed that the HBV-light model is almost at the same efficiency level with the average daily and monthly values, with the daily PET values. They concluded that HBV-light model was insignificantly sensitive to different PET input data types. In addition, according to Oudin et al. (2005), it is not necessary to seek daily observed PET data as input to a rainfall-runoff model. A long-term mean PET data would also work.

Runoff in the HBV-Light model

In this study, daily runoff observation data was obtained from the stream gauge annual report of the General Directorate of State Hydraulic Works (DSI). Then, these obtained data were used as input in the HBV-Light model.

3.4 Bias Correction

If a near-accurate result is to be obtained, it is important to know that the outputs of the general circulation model cannot be used in hydrological or other impact models without some sort of preliminary bias correction (Piani et al., 2010). For the climate modelers, it is common to show projections of future precipitation and regional and global temperature in relation to statistical changes. Therefore, modelers use bias correction techniques that correct the density histogram ranges. This usually includes some methods that using the observed and simulated cumulative distribution functions. Histogram equalization, quantile mapping or statistical downscaling are some examples of these methods in the literature (Piani et al., 2010).

Bias Correction in Precipitation Series

Correction factor was performed for precipitation series for each GCM/RCM model couple separately using ERA5-Land precipitation dataset and as a result, the correction factor was calculated for each model (46 models) and for each month (12 months) and for each sub-basin (3 sub-basins).

The historical ERA5-Land precipitation values (1979-2005) were divided by the historical GCM/RCM model precipitation values (1979-2005) and the correction factor was calculated for each model and for each month and for each sub-basin. Then, this correction factor was multiplied by not corrected future RCM model precipitation values (2021-2099). As a result, corrected future precipitation values (2021-2099) were calculated. Formulation of this processes was given below.

$$\text{Correction factor}_{(m,r)} = \text{ERA5-Land}_{(m,y1)} / \text{RCM historical}_{(m,y1,r)}$$

$$\text{corrected RCM}_{(m,y2,r)} = \text{Correction factor}_{(m,r)} * \text{not corrected RCM}_{(m,y2,r)}$$

m: is the months

y1: years of bias correction (1979-2005)

r: GCM/RCM model couples (There are 46 models)

y2: years of climate projections (2021-2099)

Bias Correction in Temperature Series

Correction factor was performed for temperature series for each GCM/RCM model couple separately using ERA5-Land temperature dataset and as a result, the correction factor was calculated for each model (46 models) and for each month (12 months) and for each sub-basin (3 sub-basins).

The historical GCM/RCM model temperature values were subtracted from the historical ERA5-Land temperature values (1979-2005) and the correction factor was calculated for each model and for each month and for each sub-basin. Then, when this correction factor and the not corrected future RCM model temperature values (2021-2099) are added, the corrected future temperature values (2021-2099) were calculated. Formulation of this processes was given below.

$$\text{Correction factor}_{(m,r)} = \text{ERA5-Land}_{(m,y1)} - \text{RCM historical}_{(m,y1,r)}$$

$$\text{corrected RCM}_{(m,y2,r)} = \text{Correction factor}_{(m,r)} + \text{not corrected RCM}_{(m,y2,r)}$$

m: is the months

y1: years of bias correction (1979-2005)

r: GCM/RCM model couples

y2: years of climate projections (2021-2099)

CHAPTER 4

RESULTS AND DISCUSSION

4.1 ERA5-Land Validation

In this study, ground station-based meteorological stations within the sub-basins were used to validate the ERA5-Land datasets. For this reason, daily and yearly correlation values between ERA5-Land and MGM station was performed. Table 4-1 shows the daily and yearly correlation values for precipitation and temperature.

Table 4-1 Correlation Values for 3 sub-basins

	Daily Correlation for Temperature	Daily Correlation for Precipitation	Yearly Correlation for Temperature	Yearly Correlation for Precipitation
SB 1535	0.98	0.44	0.94	0.78
SB 1541	0.92	0.52	0.97	0.92
SB 1545	0.98	0.36	0.93	0.79

In our study, there is no continuous data at the meteorological stations (the HBV model requires daily precipitation and temperature values) and there are few meteorological stations representing the sub-basins (i.e., SB 1545 is represented by only 1 ground station-based meteorological station, while there are 65 grids in the ERA5-Land dataset). For these reasons, in this study, ERA5-Land precipitation and temperature dataset were used in hydrological modelling studies for the historical period.

4.2 GCM/RCM Validation

Sorting of the performances of the precipitation and temperature outputs obtained from the RCM/GCM model couples and eliminating the 10 lowest performing models among 56 models is a step which is applied in this study. Daily correlations between the ERA5-Land datasets and the temperature and precipitation data obtained from the GCM/RCM model couples are first calculated. This process is repeated for each model (56 GCM/RCM) and each sub-basin (3 sub-basins). Then, there are six correlation values for a model (three temperature and precipitation). Then, by taking the average of these correlation values, 10 GCM/RCM model couples with the lowest correlation are determined, and these 10 models are eliminated. There is no specific way to specify the number of models with the lowest performance to be eliminated. In this study, the value of 10 was chosen arbitrary. Eliminated 10 GCM/RCM model couples are listed in Table 4-2. Also, daily correlation values for each model and for each sub-basin between the ERA5-Land datasets and GCM/RCM model couples are shown in appendices A.

Table 4-2 Eliminated 10 GCM/RCM model couples

ID	GCM	RCM
26	MOHC-HadGEM2-ES	CLMcom-CCLM4-8-17
27	MOHC-HadGEM2-ES	CLMcom-ETH-COSMO-crCLIM-v1-1
29	MOHC-HadGEM2-ES	DMI-HIRHAM5
30	MOHC-HadGEM2-ES	GERICS-REMO2015
31	MOHC-HadGEM2-ES	ICTP-RegCM4-6
33	MOHC-HadGEM2-ES	KNMI-RACMO22E
34	MOHC-HadGEM2-ES	MOHC-HadREM3-GA7-05
35	MOHC-HadGEM2-ES	SMHI-RCA4
36	MOHC-HadGEM2-ES	UHOH-WRF361H
42	MPI-M-MPI-ESM-LR	IPSL-WRF381P

Overall, 46 GCM/RCM model couples were analyzed for this study.

4.3 Bias Correction

Correction factor was performed for precipitation and temperature series for each GCM/RCM model couple separately using ERA5-Land precipitation and temperature dataset and as a result, the correction factor was calculated for each model (46 models) and for each month (12 months) and for each sub-basin (3 sub-basins). This process was performed between 1979 and 2005. Corrected precipitation and temperature values were calculated for each of the 3 sub-basins.

For Precipitation

The gridded data sets were used in this study. However, before the hydrological modelling studies, the average precipitation values for each sub-basin were obtained by taking the average of the grid values within the sub-basin boundaries of the gridded precipitation data. After obtaining the daily time series for each sub-basin for both the RCM and ERA5-Land data sets, bias correction was performed, and corrected precipitation values were obtained. Then, these obtained values were used in daily time series for future periods in hydrological modelling studies.

Table 4-3 shows the correction factor for precipitation that is ensemble mean of 46 GCM/RCM model couples. If the correction factor is close to 1, RCM and ERA5-Land data sets are close to each other.

Table 4-3 Correction Factor for Precipitation (Ensemble Mean of 46 Models)

	Average Correction Factor												
	Jan	**Feb**	**Mar**	**Apr**	**May**	**June**	**July**	**Aug**	**Sep**	**Oct**	**Nov**	**Dec**	**Ave.**
SB 1535	0.89	0.95	1.05	1.21	1.20	1.25	2.76	0.94	0.95	1.18	1.11	0.86	1.20
SB 1541	0.92	0.89	0.97	0.97	0.93	1.03	1.84	0.82	0.76	1.02	0.97	0.90	1.01
SB 1545	1.05	1.11	1.10	1.15	1.04	1.14	2.43	1.63	1.14	1.29	1.03	1.13	1.27

	Average Correction Factor												
	Jan	**Feb**	**Mar**	**Apr**	**May**	**June**	**July**	**Aug**	**Sep**	**Oct**	**Nov**	**Dec**	**Ave.**
Ave.	0.95	0.98	1.04	1.11	1.06	1.14	2.34	1.13	0.95	1.16	1.04	0.96	

According to Table 4-3, January and September have the lowest correction factor (0.95) and July has the highest correction factor (2.34) when taking averages of 3 sub-basins correction factor.

Also, ensemble mean of corrected precipitation and non-corrected precipitation (original 46 model outputs) for 3 sub-basins are shown in appendices D.

For Temperature

The gridded data sets were used in this study. However, before the hydrological modelling studies, the average temperature values for each sub-basin were obtained by taking the average of the grid values within the sub-basin boundaries of the gridded temperature data. After obtaining the daily time series for each sub-basin for both the RCM and ERA5-Land datasets, bias correction was performed, and corrected temperature values were obtained. Then, these obtained values were used in daily time series for future periods in hydrological modelling studies.

Table 4-4 shows the correction factor for temperature that is ensemble mean of 46 GCM/RCM model couples. If the correction factor is close to 0, RCM and ERA5-Land data sets are close to each other.

Table 4-4 Correction Factor for Temperature (Ensemble Mean of 46 Models)

	Average Correction Factors												
	Jan	**Feb**	**Mar**	**Apr**	**May**	**June**	**July**	**Aug**	**Sep**	**Oct**	**Nov**	**Dec**	**Ave.**
SB 1535	0.04	-0.20	0.01	0.87	0.86	0.21	0.13	0.90	1.75	2.09	0.97	0.21	0.65

	Average Correction Factors												
	Jan	**Feb**	**Mar**	**Apr**	**May**	**June**	**July**	**Aug**	**Sep**	**Oct**	**Nov**	**Dec**	**Ave.**
SB 1541	0.14	-0.29	-0.14	0.67	1.01	0.85	0.92	1.40	1.82	1.84	0.90	0.34	0.79
SB 1545	-0.74	-0.89	-0.71	0.31	0.56	0.23	0.17	0.92	1.50	1.64	0.64	-0.17	0.29
Ave.	-0.19	-0.46	-0.28	0.62	0.81	0.43	0.41	1.07	1.69	1.86	0.84	0.13	

According to Table 4-4, December has the lowest correction factor (0.13) and October has the highest correction factor (1.86) when taking averages of 3 sub-basins correction factor.

Also, ensemble mean of corrected temperature and non-corrected temperature (original 46 model outputs) for 3 sub-basins are shown in appendices D.

Also, performance of bias correction of RCM simulations was investigated utilizing ERA5-Land and RCM simulations for precipitation and temperature values during the periods [2006-2020] and [1979-2005].

$$\Delta P = [RCM\_P_{(2006\text{-}2020)} / RCM\_P_{(1979\text{-}2005)}] - [EL\_P_{(2006\text{-}2020)} / EL\_P_{(1979\text{-}2005)}]$$

$$\Delta T = [RCM\_T_{(2006\text{-}2020)} - RCM\_T_{(1979\text{-}2005)}] - [EL\_T_{(2006\text{-}2020)} - EL\_T_{(1979\text{-}2005)}]$$

where EL refer to ERA5-Land product, RCM refer to climate model historical values, and _P and _T refer to precipitation and temperature. Average results for ΔP and ΔT are given below in Table 4-5.

Table 4-5 Performance of bias correction

Sub-basin	ΔP (%)	ΔT [°]
SB 1535	0.07	-0.2
SB 1541	0.06	-0.2
SB 1545	0.06	-0.6

Considering RCM model simulations are corrected using correction factors obtained utilizing datasets between 1979 and 2005, the difference between the two periods ([2006-2020] and [1979-2005]) show the consistency of the correction implemented to RCM datasets. Overall, the results shown in Table 4-5 imply the corrected RCM and ERA5-Land datasets are consistent.

4.4 Trend Analysis of Precipitation and Temperature

Yearly averages of historical precipitation and temperature values (1979-2020) from ERA5-Land and yearly averages of future precipitation and temperature values from ensemble mean of 46 GCM/RCM model couples for the Kızılırmak Basin and 3 sub-basins are given in Table 4-6.

Table 4-6 Yearly Average Historical and Future Precipitation and Temperature Values

	1979-2020 (ERA5-Land)		2021-2060 (GCM/RCM)		2061-2099 (GCM/RCM)	
	P	T	P	T	P	T
SB 1535	626	6.8	607	8.5	571	11.3
SB 1541	459	10.6	441	12.2	408	14.7
SB 1545	747	8.3	726	9.8	697	12.2
Kızılırmak	544	9.8	525	11.4	490	13.9

P: Precipitation (mm/year), T: Temperature (°C)

It is seen that temperature values tend to increase, and precipitation values tend to decrease throughout the Kızılırmak Basin. The average temperature between 2061 and 2099 is expected to be around 4 °C higher than the 1979-2020 average, while precipitation values are expected to be around 10% lower. Figure 4-1 and Figure 4-2 show the historical and future temperature and precipitation graph for the Kızılırmak Basin and 3 sub-basins, respectively.

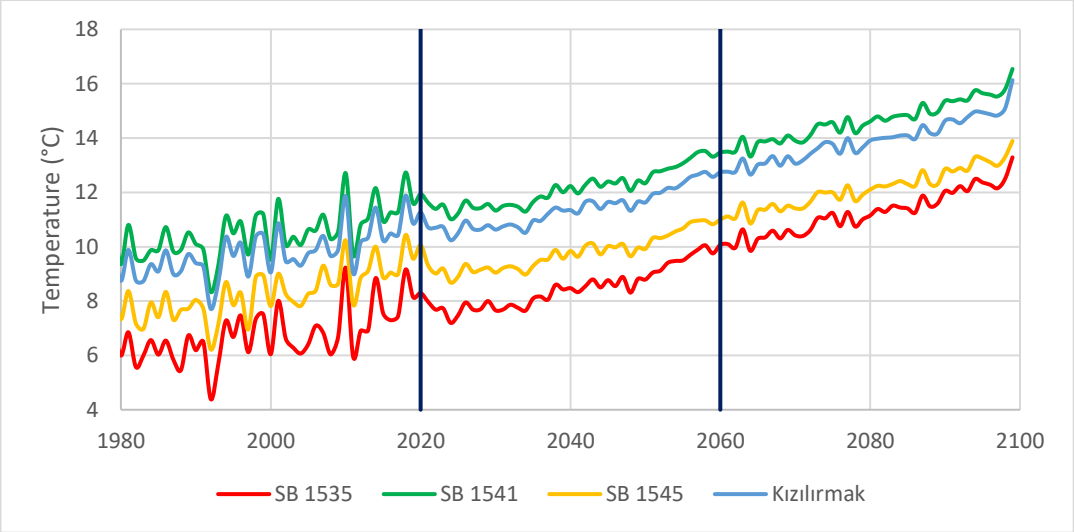

Figure 4-1 Historical (ERA5-Land) and Future (GCM/RCM) Temperature Graph for the Kızılırmak Basin and 3 sub-basins

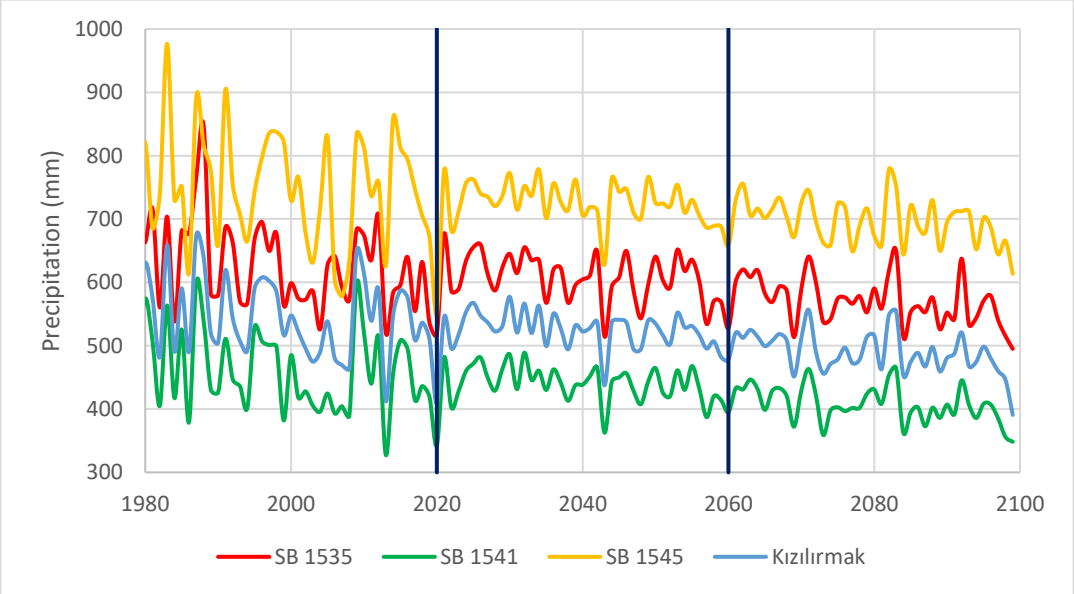

Figure 4-2 Historical (ERA5-Land) and Future (GCM/RCM) Precipitation Graph for the Kızılırmak Basin and 3 sub-basins

When the effect of climate change on water resources project is analyzed specifically for the Kızılırmak basin (SYGM, 2016), it is seen that an increase in temperatures and a decrease in precipitation are expected for the future periods. We can say that there is a consistency between this study and SYGM's study in terms of changes in the precipitation and temperature due to the climate change (Table 4-7).

Table 4-7 Comparison of Earlier and Current Study

	Precipitation				Temperature			
Source	Reference Period	mm/ year	Future Period	Change	Reference Period	°C	Future Period	Change
SYGM 2016*	1971-2000	~450*	2061-2100	~-5% **	1971-2000	~10*	2061-2100	~+4°C **
Barkış 2022	1979-2020	544	2061-2099	-10% (Entire Kızılırmak)	1979-2020	9.8	2061-2099	+4.1°C (Entire Kızılırmak)

* İKLİM DEĞİŞİKLİĞİNİN SU KAYNAKLARINA ETKİSİ PROJESİ Proje Nihai Raporu EK 17 – Kızılırmak Havzası

** values extracted from figure or tables in SYGM 2016 report

4.5 HBV-LIGHT Model Runoff Simulations - Historical Period

HBV-Light model was run in the following time periods considering the daily runoff observations. Precipitation and temperature ERA5-Land data are available from 1950 to the present, but limited runoff observations are available. Appropriate time intervals were determined, and the models were run. For this reason, the calibration and validation time periods for 3 sub-basins were different. These periods were shown in Table 4-8.

Table 4-8 Calibration and validation periods for the sub-basins

AREAS	DATES		
	Warming-Up	Calibration	Validation
SB 1535	01.10.1979-30.09.1980	01.10.1980-30.09.2000	01.10.2000-30.09.2011
SB 1541	01.10.1996-30.09.1997	01.10.1997-30.09.2005	01.10.2005-30.09.2010
SB 1545	01.10.1998-30.09.1999	01.10.1999-30.09.2006	01.10.2006-30.09.2011

Calibrated HBV model parameter values for 3 sub-basins are shown in Table 4-9.

Table 4-9 Calibrated HBV Model Parameter Values

HBV Model Parameters	SB 1535	SB 1541	SB 1545
TT	-0.18	-0.29	-1.37
CFMAX	4.98	4.81	3.3
SP	0.5	0.69	0.75
SFCF	1.65	2.19	1.95
CFR	0.05	0.25	0.02
CWH	0.1	0.03	0.05
FC	463	555	540
LP	0.33	0.1	0.47
BETA	1.14	2.59	2.08
PERC	0.2	0.07	0.46
UZL	48.8	59.3	3.33
K0	0.29	0.42	0.28
K1	0.12	0.09	0.12
K2	0.002	0.001	0.01
MAXBAS	2.07	2.23	2.48
Cet	0.16	0.01	0.21

Simulated and observed surface runoff potentials, NSE, RMSE, R^2 and bias in percentage is given in Table 4-10 and Table 4-11.

Table 4-10 Some statistical values for 3 sub-basins in calibration period

Calibration Period						
	Simulated Runoff (m^3/s)	Observed Runoff (m^3/s)	NSE (daily and monthly)	RMSE (m^3/s) (daily and monthly)	R^2 (daily and monthly)	Bias (%)
SB 1535	40.4	41.3	0.87 / 0.93	22.21 / 13.95	0.87 / 0.94	-2.2
SB 1541	12.0	13.3	0.66 / 0.75	9.41 / 6.86	0.67 / 0.76	-10.0
SB 1545	11.5	11.6	0.81 / 0.90	7.29 / 4.29	0.81 / 0.90	-0.6

Table 4-11 Some statistical values for 3 sub-basins in validation period

Validation Period						
	Simulated Runoff (m^3/s)	Observed Runoff (m^3/s)	NSE (daily and monthly)	RMSE (m^3/s) (daily and monthly)	R^2 (daily and monthly)	Bias (%)
SB 1535	34.7	29.9	0.78 / 0.87	18.71 / 12.9	0.81 / 0.90	16.1
SB 1541	11.1	11.3	0.25 / 0.35	11.08 / 9.56	0.41 / 0.47	-1.7
SB 1545	10.6	10.6	0.61 / 0.73	8.99 / 6.25	0.61 / 0.73	0.1

Evaluation of the daily model simulations are performed using both daily and monthly time series, where daily values (in m^3/s) are averaged to obtained monthly time series (in m^3/s). When NSE value is above 0.50, we can say that evaluation of daily runoff simulations is satisfactory (Moriasi et al., 2015). In addition, when NSE value is above 0.55, we can say that evaluation of monthly runoff simulations is satisfactory (Moriasi et al., 2015).

4.5.1 SB 1535

Considering daily and monthly NSE values in the evaluation of the runoff simulations (Moriasi et al., 2015), overall HBV-Light model simulations yield highly accurate simulations (0.87 and 0.93 for the daily and the monthly time series, respectively), over SB 1535 sub-basin during the calibration period (Figure 4-3).

When independent validation period is simulated, HBV-Light model results are still considered accurate, because NSE values are in the satisfactory range (0.78 and 0.87 for the daily and the monthly time series, respectively) (Figure 4-4).

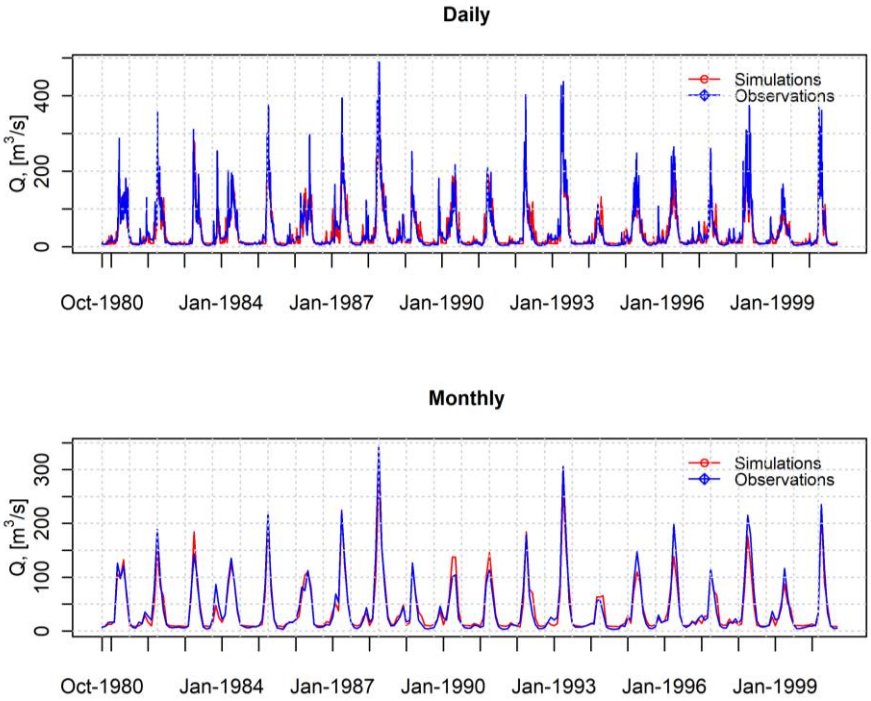

Figure 4-3 Comparison of the observed and the simulated runoff for SB 1535 during the calibration period using daily and monthly time series

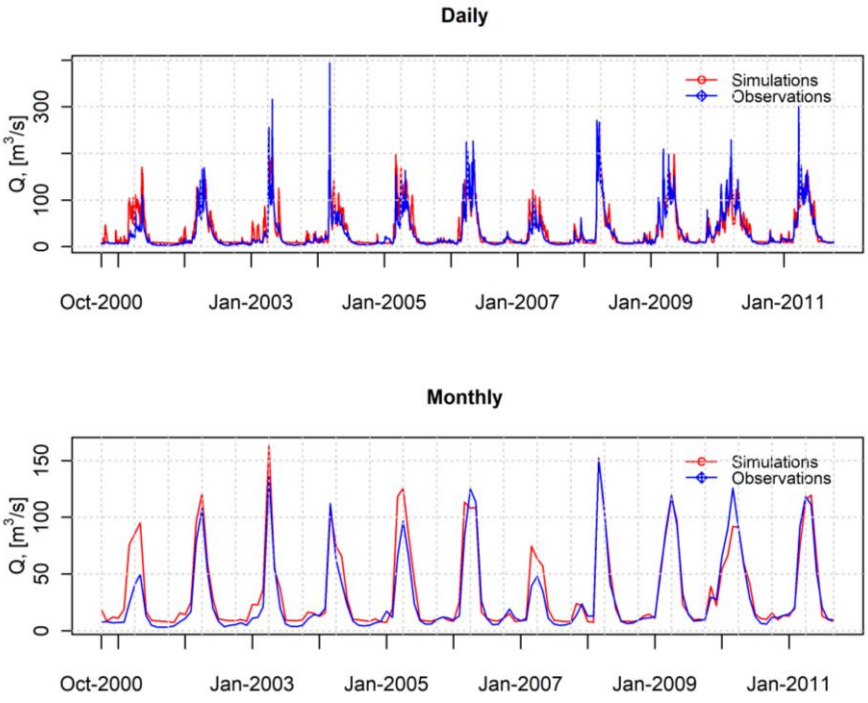

Figure 4-4 Comparison of the observed and the simulated runoff for SB 1535 during the validation period using daily and monthly time series

In addition, GCM/RCM based historical HBV model simulations were also performed. Surface runoff potential based on historical GCM/RCM (1979-2005) and simulation (based on ERA5-Land dataset) and observation (from DSI stream gauge station) is shown in Figure 4-5.

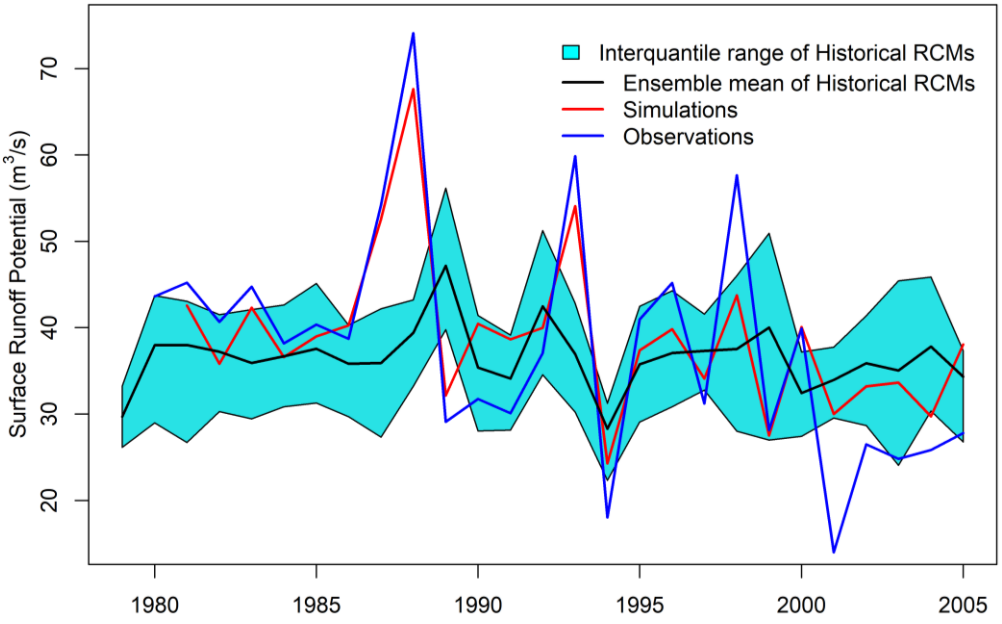

Figure 4-5 Surface runoff potential based on historical GCM/RCM, simulation and observation for SB 1535

4.5.2 SB 1541

Considering daily and monthly NSE values in the evaluation of the runoff simulations (Moriasi et al., 2015), overall HBV-Light model simulations yield accurate simulations (0.66 and 0.75 for the daily and the monthly time series, respectively), over SB 1541 sub-basin during the calibration period (Figure 4-6).

When independent validation period is simulated, it cannot be said that performance of the model is successful because daily and monthly NSE values are less than 0.5 (0.25 and 0.35 for the daily and the monthly time series, respectively) (Figure 4-7).

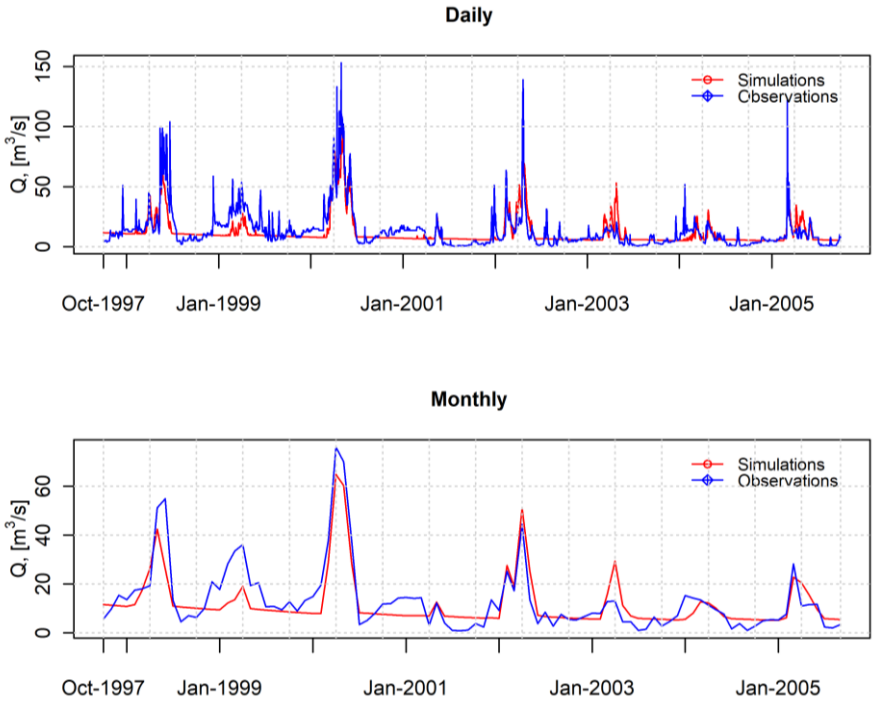

Figure 4-6 Comparison of the observed and the simulated runoff for SB 1541 during the calibration period using daily and monthly time series

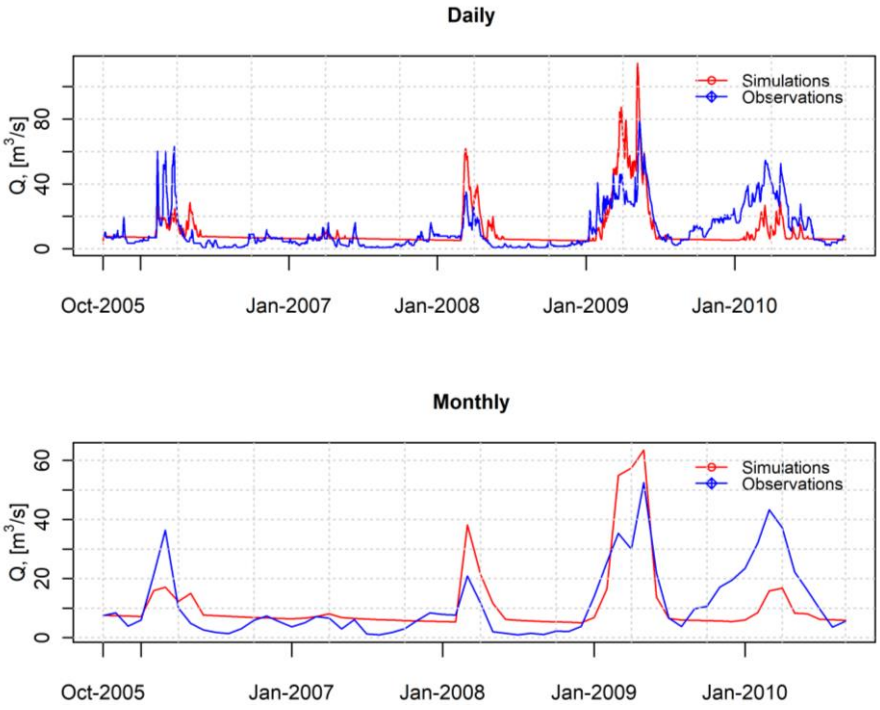

Figure 4-7 Comparison of the observed and the simulated runoff for SB 1541 during the validation period using daily and monthly time series

In addition, GCM/RCM based historical HBV model simulations were also performed. Surface runoff potential based on historical GCM/RCM (1979-2005) and simulation (based on ERA5-Land dataset) and observation (from DSI stream gauge station) is shown in Figure 4-8.

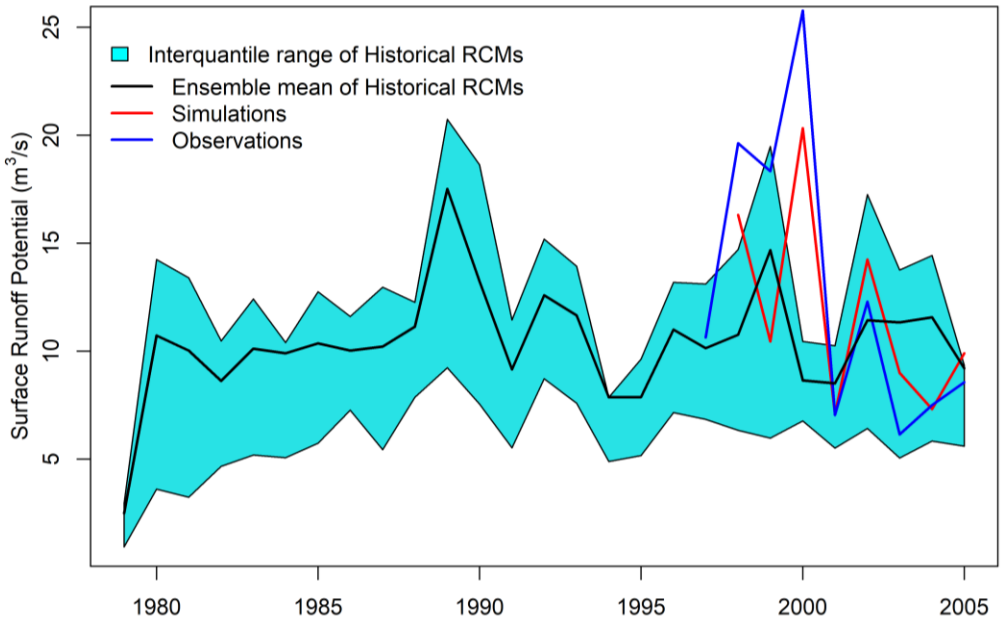

Figure 4-8 Surface runoff potential based on historical GCM/RCM, simulation and observation for SB 1541

4.5.3 SB 1545

Considering daily and monthly NSE values in the evaluation of the runoff simulations (Moriasi et al., 2015), overall HBV-Light model simulations yield highly accurate simulations (0.81 and 0.90 for the daily and the monthly time series, respectively), over SB 1545 sub-basin during the calibration period (Figure 4-9).

When independent validation period is simulated, HBV-Light model results are still considered accurate, because NSE values are in the satisfactory range (0.61 and 0.73 for the daily and the monthly time series, respectively) (Figure 4-10).

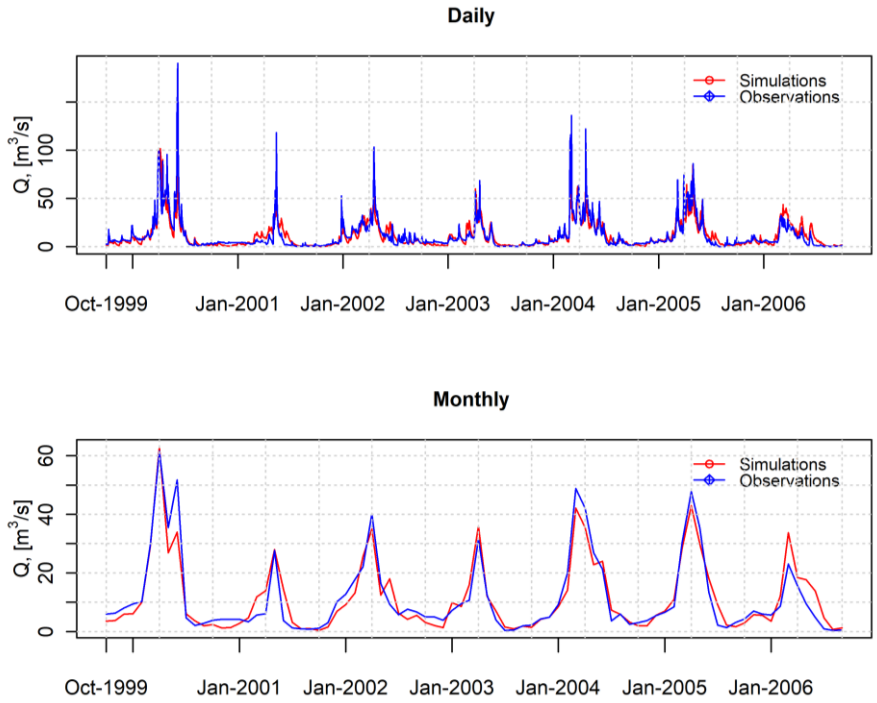

Figure 4-9 Comparison of the observed and the simulated runoff for SB 1545 during the calibration period using daily and monthly time series

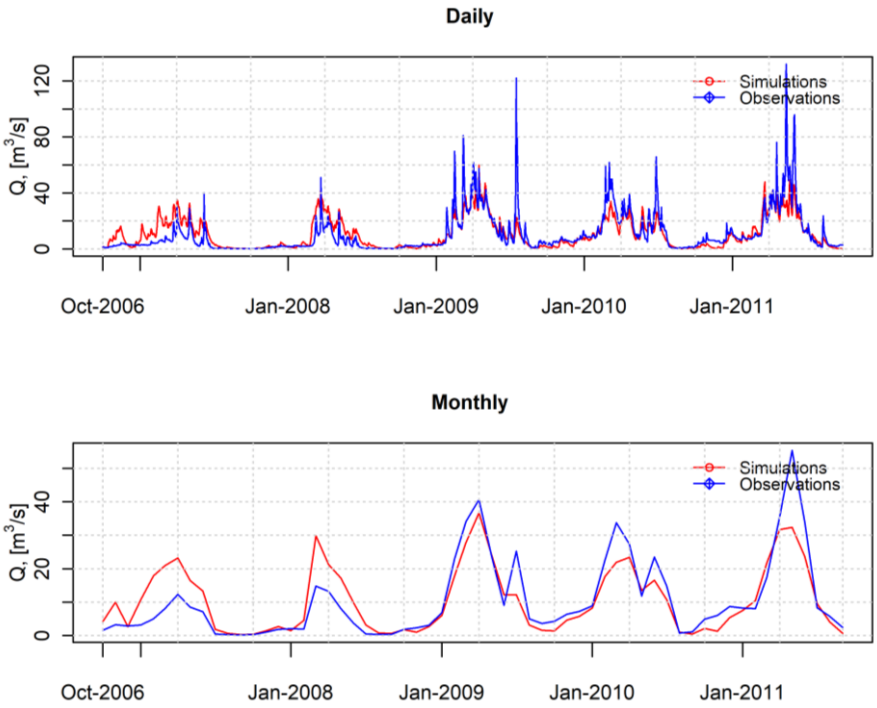

Figure 4-10 Comparison of the observed and the simulated runoff for SB 1545 during the validation period using daily and monthly time series

In addition, GCM/RCM based historical HBV model simulations were also performed. Surface runoff potential based on historical GCM/RCM (1979-2005) and simulation (based on ERA5-Land dataset) and observation (from DSI stream gauge station) is shown in Figure 4-11.

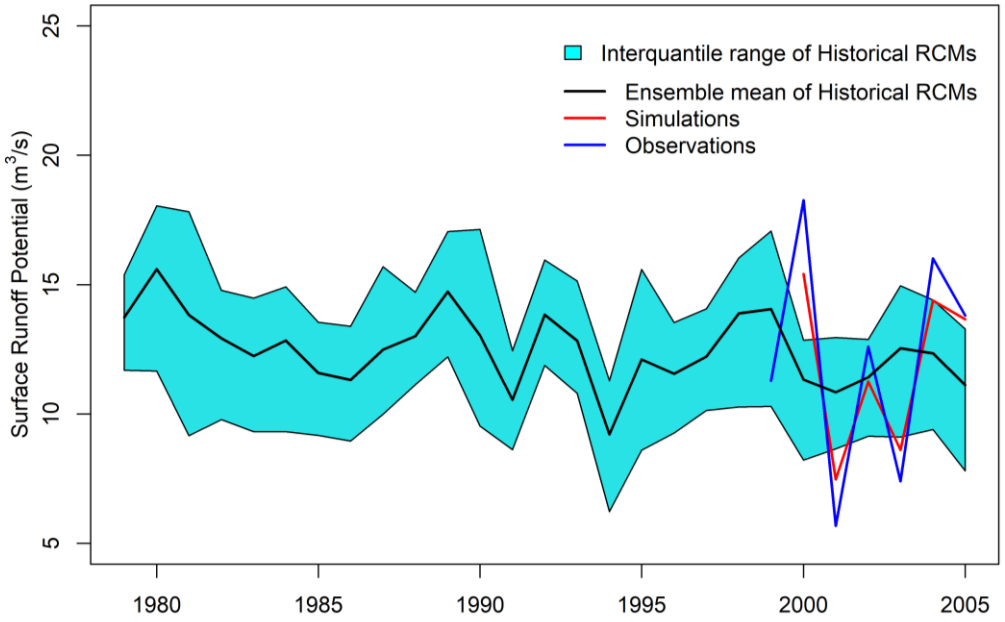

Figure 4-11 Surface runoff potential based on historical GCM/RCM, simulation and observation for SB 1545

4.5.4 Discussions of Historical Simulations

The model runs for the subbasins SB 1535 and SB 1545 show HBV model successfully simulates the baseflow and the peak flows, for the validation and especially the calibration periods (i.e., yields daily NSE values 0.87 & 0.81 for calibration and 0.78 & 0.61 for validation periods). However, for SB 1541, the model yields satisfactory result during the calibration period (i.e., daily NSE values 0.66) but very poor performance during independent validation period (daily NSE of 0.25). The poor performance of HBV model for the SB 1541 is further investigated through the simulated and observed runoff and precipitation values given below (Figure 4-12). Overall, during the calibration period (01.10.1997-30.09.2005) the model

accurately captures the observed runoff values while during the validation period the model misses one of the three spring runoff values greatly, hence the daily NSE values decrease considerably to 0.25. To investigate the reason for the model to miss the spring 2010 runoff values, the precipitation estimates obtained from ERA5-Land and MGM station-based observations are compared (Figure 4-13). Even though the precipitation during early months of 2010 from ERA5-Land is high and consistent with MGM-based observations, the runoff response of HBV does not follow the observations. Similar inconsistency also exists for spring 1999 that HBV simulations does not capture high observed flows despite relatively high precipitation input. Yet the relation is not always so clear that precipitation values similar to spring 2010 also exist during spring 2004 yet the observed flows are almost at as low levels as spring 2010. Accordingly, the inconsistency between simulated and observed runoff estimates in this study could not be resolved with a high confidence.

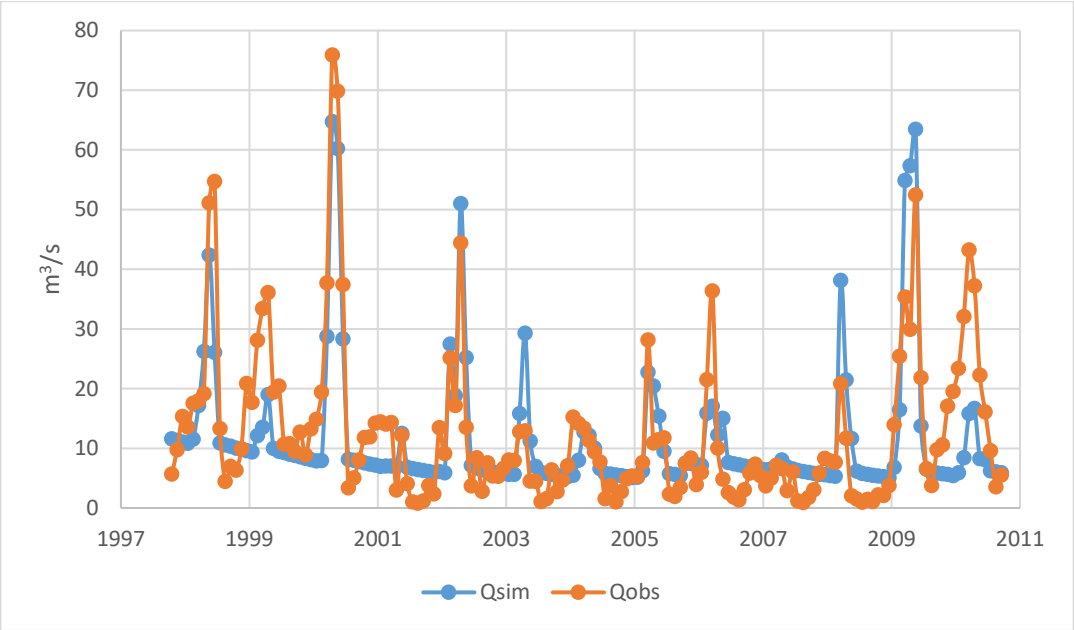

Figure 4-12 Surface runoff simulations and DSI observations for SB 1541

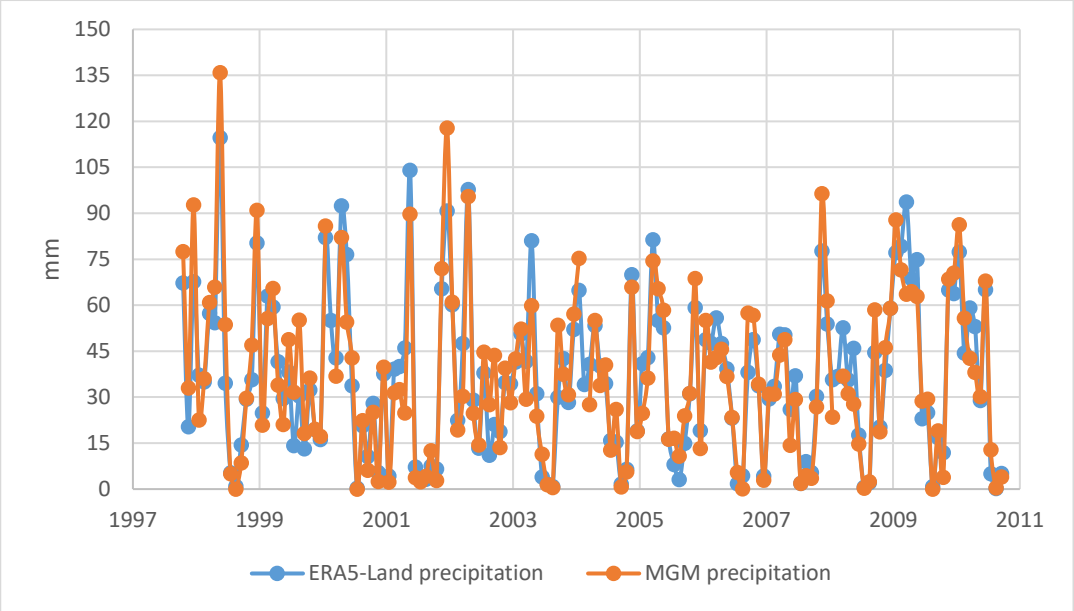

Figure 4-13 Precipitation of ERA5-Land and MGM observations for SB 1541

4.6 HBV-LIGHT Model Runoff Simulations - Comparisons of Historical and Future Projection

Changes in the surface runoff potential because of the climate change between the years of 2021-2099 were investigated using the HBV hydrological model. The surface runoff potential of each sub-basin was calculated by running 46 models separately, then the average of the results of the 46 models was taken and the surface runoff potential of that sub-basin was calculated.

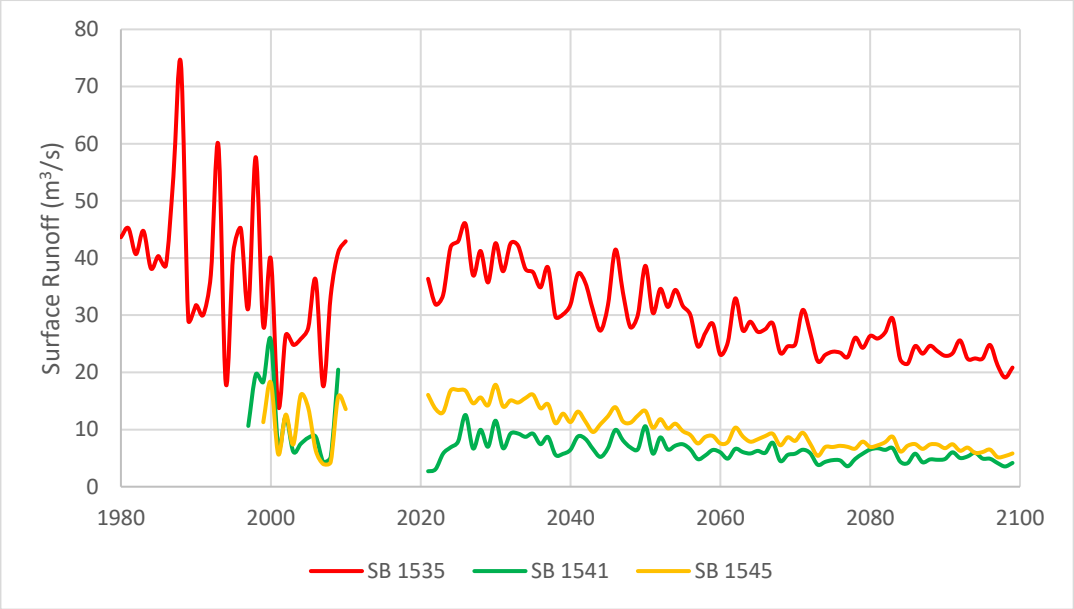

Figure 4-14 Historical and Future Surface Runoff Potential Graph for 3 sub-basins

Figure 4-14 shows the yearly average historical and future surface runoff potential graph for 3 sub-basins and Table 4-12 shows the yearly average historical and future surface runoff potential values. It can be seen that surface runoff potential tends to decrease for the 3 sub-basins.

Table 4-12 Historical and Future Surface Runoff Potential Values

	Current Situation		2021-2060	2061-2099
	Observed Surface Runoff (m^3/s)	Simulated Surface Runoff (m^3/s)	Surface Runoff (m^3/s)	Surface Runoff (m^3/s)
SB 1535	37.4 (1980-2011)	38.4 (1980-2011)	34.6	24.8 (↓34%)
SB 1541	12.4 (1997-2010)	11.6 (1997-2010)	7.3	5.3 (↓57%)
SB 1545	11.2 (1999-2011)	11.1 (1999-2011)	12.7	7.3 (↓35%)

Surface runoff potential was calculated for each model couple separately using the HBV hydrological model. For 3 sub-basins, the surface runoff potential of the future period was re-run with the parameters calculated in the calibration period specified in Table 4-9 using the HBV model. Then, surface runoff potential for 3 sub-basins

was calculated by taking the ensemble mean of the outputs of the 46 GCM/RCM model couples calculated. Detailed analysis of the change in the surface runoff potential for 3 sub-basins is given below.

4.6.1 SB 1535

The surface runoff potential for the SB 1535 between the years 2021-2099 is shown in Figure 4-15.

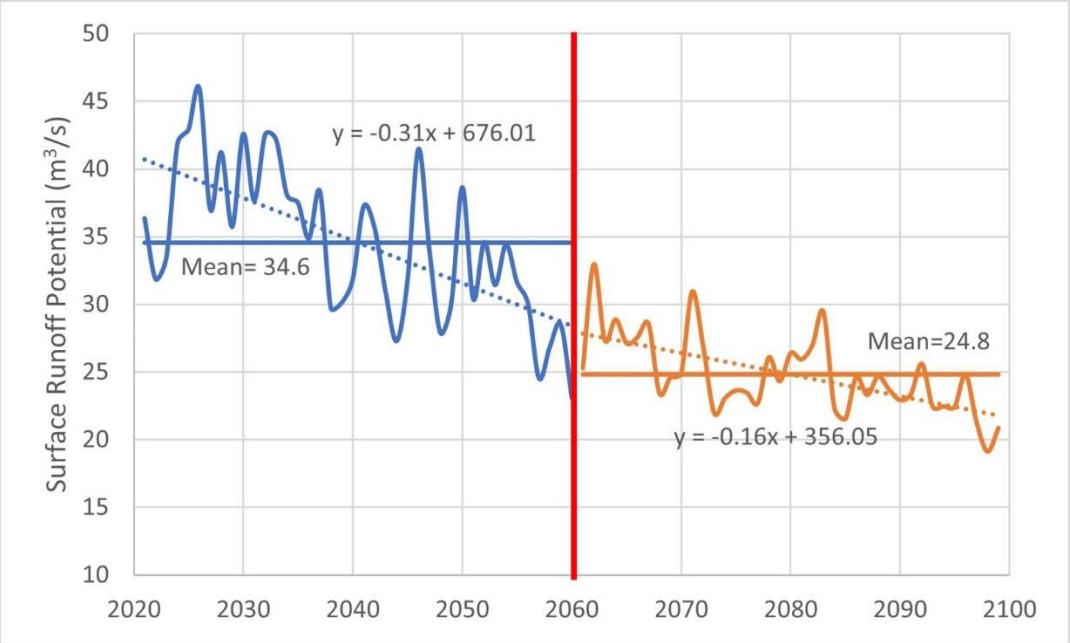

Figure 4-15 Change of surface runoff potential over the years for SB 1535 (Ensemble mean of 46 model outputs)

According to Figure 4-15, it can be said that there is a decrease in the surface runoff potential until 2100. While the decrease between 2021-2060 is 7% compared to current situation, this rate of decrease dramatically increases to 34% in the period of 2061-2099.

Ensemble mean of 46 RCM models and their interquartile ranges of surface runoff potential for SB 1535 is shown in Figure 4-16.

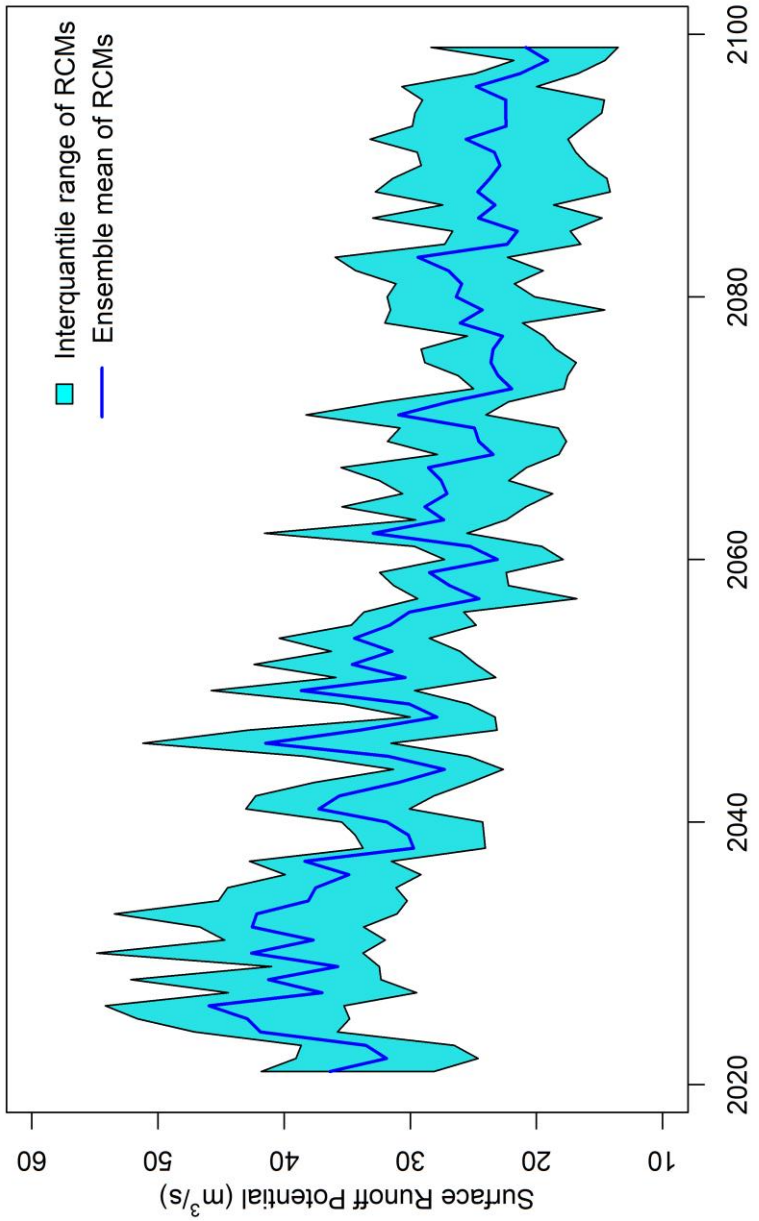

Figure 4-16 Yearly Surface Runoff Trends for SB 1535 (Ensemble mean and Interquartile ranges of 46 models)

4.6.2 SB 1541

The surface runoff potential for the SB 1541 between the years 2021-2099 is shown in Figure 4-17.

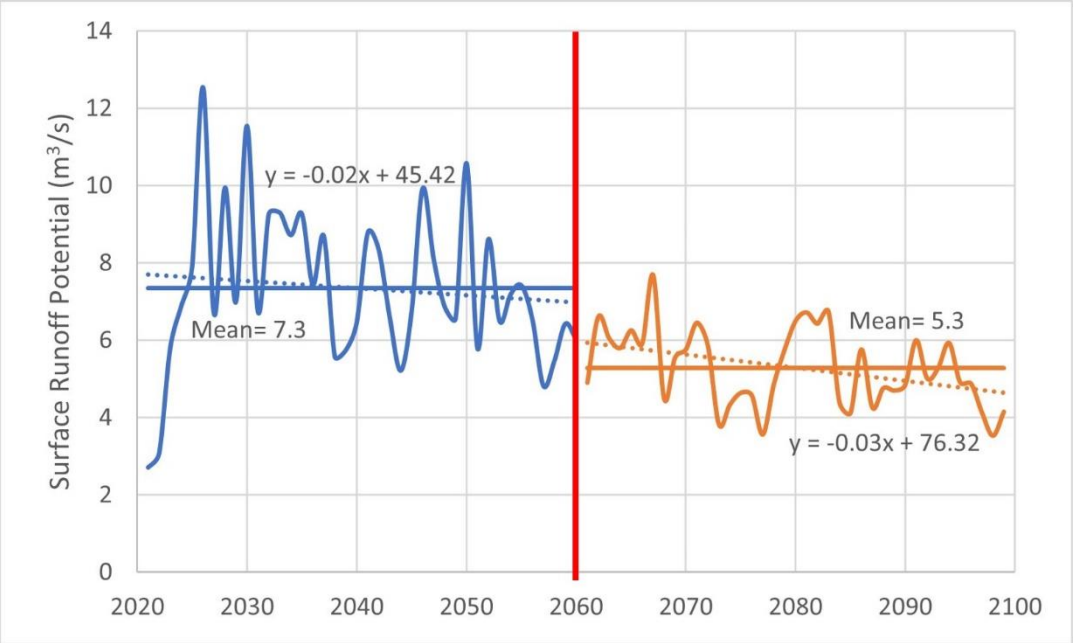

Figure 4-17 Change of surface runoff potential over the years for SB 1541 (Ensemble mean of 46 model outputs)

According to Figure 4-17, it can be said that there is a decrease in the surface runoff potential until 2100. The decreases in the surface runoff potential for SB 1541 are striking. While the decrease between 2021-2060 is 41% compared to current situation, this rate of decrease dramatically increases to 57% in the period of 2061-2099.

Ensemble mean of 46 RCM models and their interquartile ranges of surface runoff potential for SB 1541 is shown in Figure 4-18.

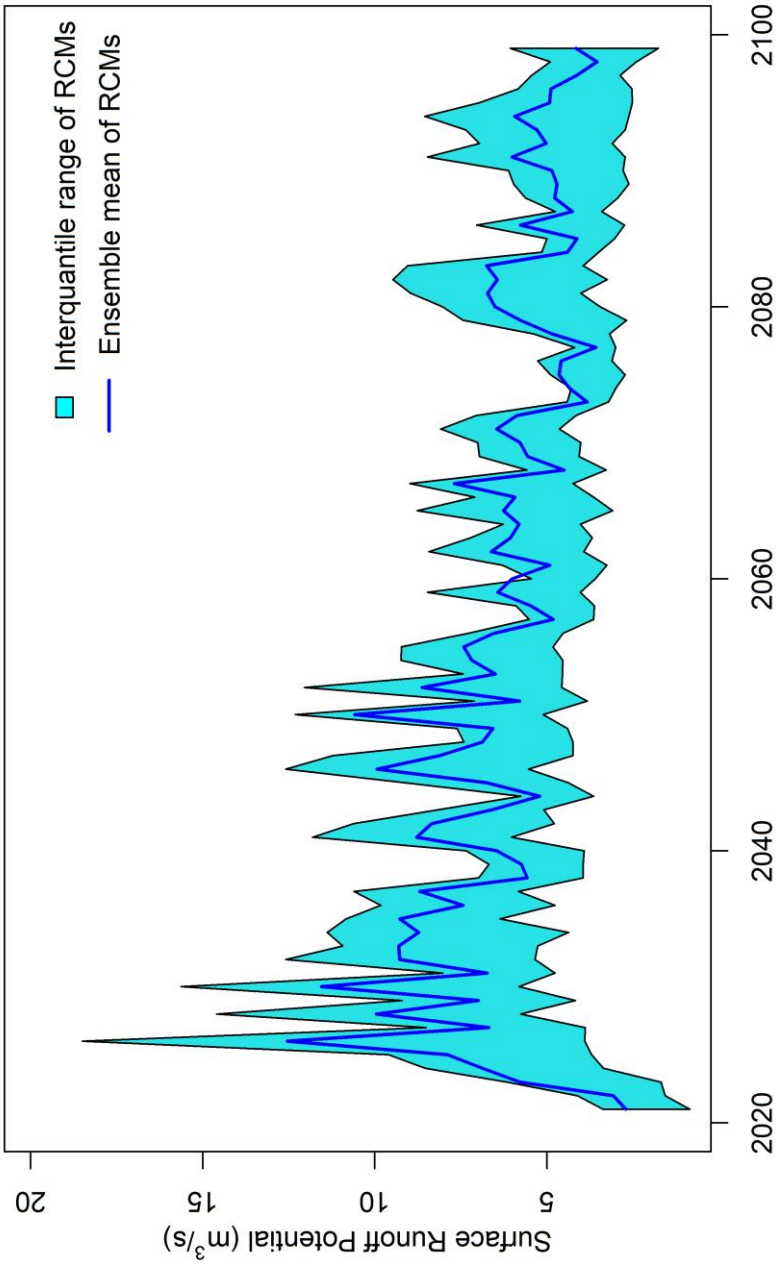

Figure 4-18 Yearly Surface Runoff Trends for SB 1541 (Ensemble mean and Interquartile ranges of 46 models)

4.6.3 SB 1545

The surface runoff potential for the SB 1545 between the years 2021-2099 is shown in Figure 4-19.

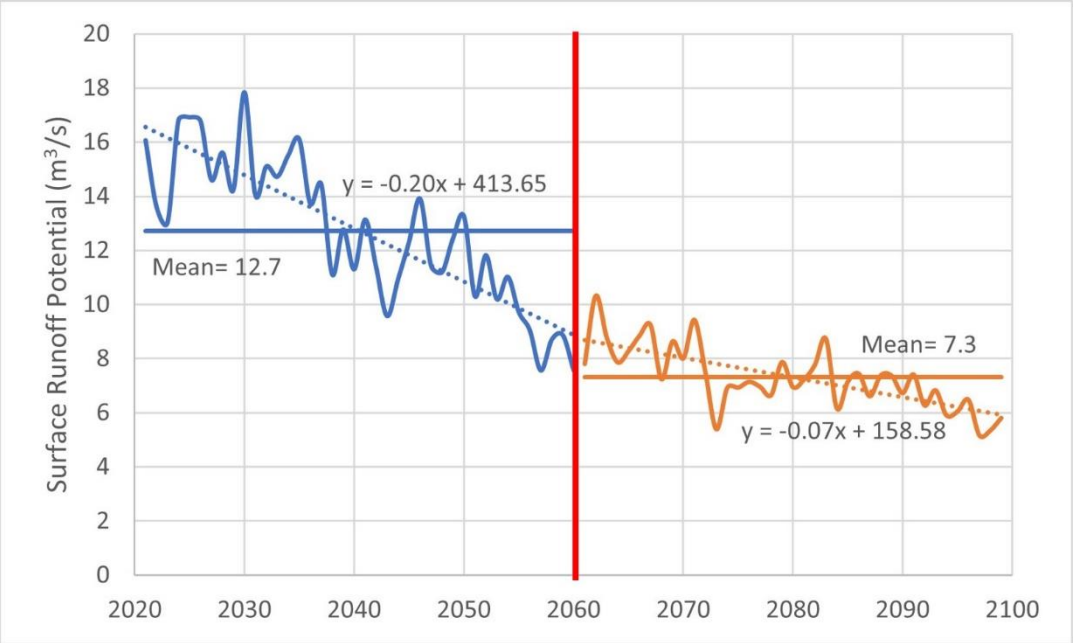

Figure 4-19 Change of surface runoff potential over the years for SB 1545 (Ensemble mean of 46 model outputs)

According to Figure 4-19, it can be said that there is a decrease in the surface runoff potential until 2100. There is a 35% decrease compared to current situation in the period of 2061-2099.

Ensemble mean of 46 RCM models and their interquartile ranges of surface runoff potential for SB 1545 is shown in Figure 4-20.

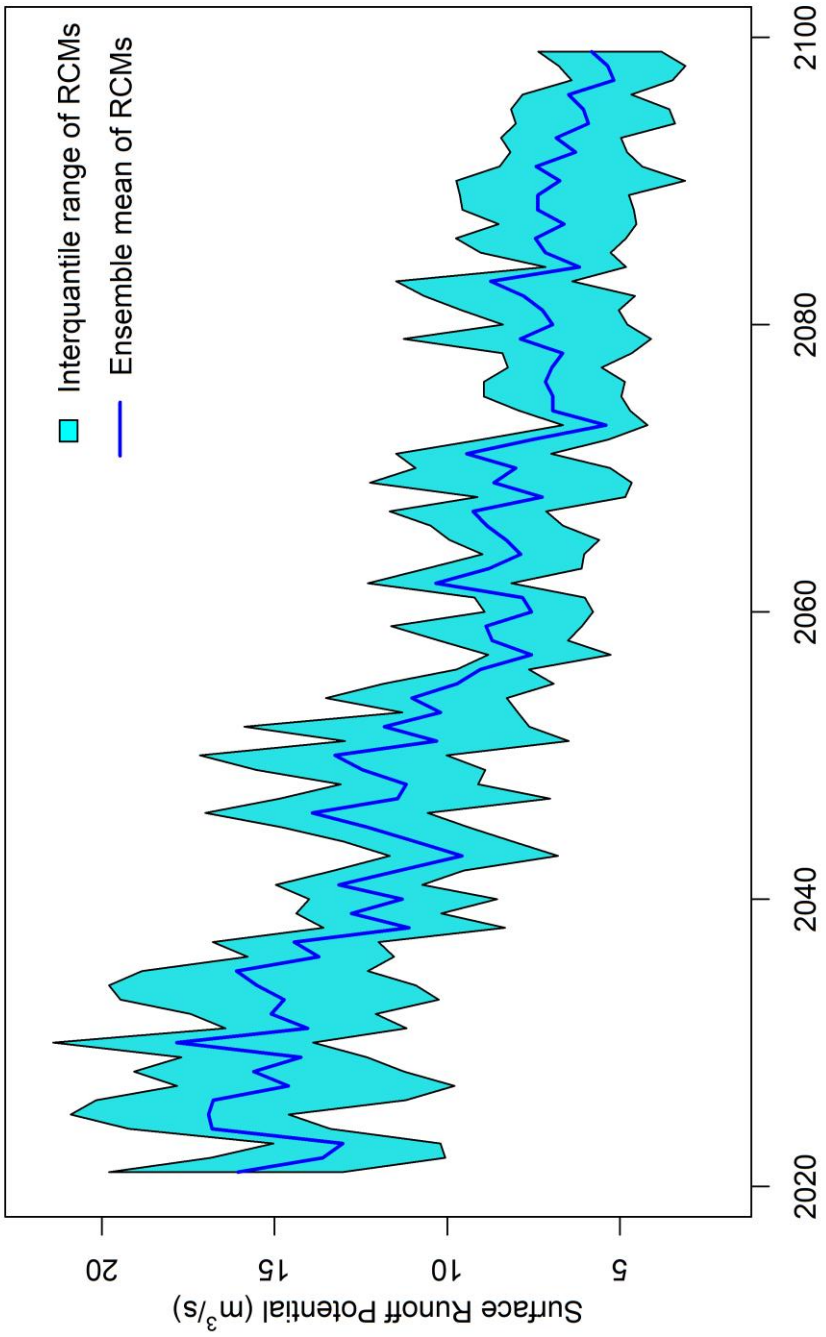

Figure 4-20 Yearly Surface Runoff Trends for SB 1545 (Ensemble mean and Interquartile ranges of 46 models)

4.6.4 Discussions of Future Simulations

The surface runoff potential of SB 1545 shows an increase in the 2021-2060 period compared to the current situation between 1999-2011 period (Table 4-12). However, when the precipitation values in Table 4-6 are examined, there is a decrease when average for the period 1979-2020 (747 mm/year) is compared against the average for the period 2021-2060 (726 mm). Annual average precipitation is 715 mm/year for the period when the model was run (01.10.1999 - 30.09.2011) for the SB 1545. Since the annual average precipitation is 726 mm/year in the 2021-2060 period, there is an increase in the surface runoff potential following the increase in the precipitation relative to the HBV model calibration and validation period between 1999 and 2011.

Comparison of historical and future precipitation, temperature and surface runoff potential is shown in Table 4-13. The precipitation and the temperature values until 2020 are from ERA5-Land and between 2021 and 2099 are from ensemble mean of RCMs. Observed surface runoff potential (Q_{OBS}) are from DSI stream gauge stations (some values are missing because the data are available between the dates the model was run). Simulated surface runoff potential (Q_{RCM}) are from the historical and future HBV model results. Historical simulation results are between 1979 and 2005 and future simulation results are between 2021-2099. When we examine the precipitation data in 10-year periods, precipitation values towards the end of the century is much lower when compared against current conditions. This is also valid for the surface runoff potential for 3 sub-basins. When we examine the temperature data in Table 4-13, overall the temperature increases during almost all periods compared against the previous period.

Overall, there is a decrease in the surface runoff potential in all 3 sub-basins (the rate of the decrease will be between 34% and 57% (Table 4-12) of the current multi-decadal averages). The decreasing runoff potential result under the influence of climate change over Kızılırmak basin is consistent with the previous studies found over other basins in the literature. According to Aktaş (2014), 15-20% decrease will

be expected in the surface flow after 2040 in Turkey. Also, for Büyük Menderes and Gediz basins, Ozkul (2009) and OECD (2013) stated that there will be a decrease in the surface runoff potential approximately 35% and 50% by 2050 and 2100, respectively. In addition, Yücel et al. (2015) stated that there will be a decrease in the surface runoff in Aras, Euphrates, and Tigris watersheds due to the climate change (11.6%, 23.5%, 28.5% respectively).

Table 4-13 Comparison of Precipitation (from ERA5-Land until 2020 and RCM beyond 2020), Temperature (similar to precipitation), and Surface Runoff (Q_{OBS} and Q_{RCM}). P: Precipitation (mm/year), T: Temperature (°C), Q_{OBS}: Observed Surface Runoff Potential from DSI (m^3/s), Q_{RCM}: Simulated Historical (1979-2005) and Simulated Future (2021-2099) Surface Runoff Potential (m^3/s)

Decadal Period	SB 1535				SB 1541				SB 1545			
	P	T	Q_{OBS}	Q_{RCM}	P	T	Q_{OBS}	Q_{RCM}	P	T	Q_{OBS}	Q_{RCM}
1980-1989	673	6.2	44.9	38.2	494	10.0	-	10.9	780	7.6	-	13.1
1990-1999	632	6.5	38.0	36.5	464	10.2	-	10.9	773	7.9	-	12.3
2000-2005	581	6.6	26.5	34.9	426	11.2	10.4	10.1	726	8.2	12.3	11.6
2006-2009	622	6.7	32.0	-	447	9.7	10.7	-	663	8.7	8.8	-
2010-2019	608	7.7	-	-	453	11.4	-	-	752	9.3	-	-
2020-2029	614	7.8	-	38.5	441	11.5	-	6.9	717	9.2	-	15.3
2030-2039	616	8.0	-	37.4	450	11.7	-	8.2	741	9.3	-	14.5
2040-2049	596	8.6	-	32.8	435	12.3	-	7.4	720	9.9	-	11.8
2050-2059	602	9.5	-	31.1	432	13.0	-	6.9	713	10.6	-	10.0
2060-2069	582	10.3	-	26.9	419	13.7	-	5.9	709	11.3	-	8.5
2070-2079	576	10.9	-	24.8	410	14.3	-	5.0	699	11.8	-	7.3
2080-2089	570	11.4	-	24.9	408	14.8	-	5.4	697	12.3	-	7.3
2090-2099	551	12.3	-	22.5	394	15.6	-	4.9	680	13.1	-	6.2

When the effect of climate change on water resources project (SYGM, 2016) is analyzed specifically for the Kızılırmak basin, it is seen that a decrease in the surface runoff similar to the one found in this study is expected for the future periods. We

can say that there is a consistency between this study and SYGM's study in terms of changes in the surface runoff due to the climate change (Table 4-14).

Table 4-14 Comparison of Earlier and Current Study for Surface Runoff Potential

	Surface Runoff Potential		
Source	Reference Period	Future Period	Change
SYGM 2016*	1973-2012	2061-2100	~-48% **
Barkış 2022	Observation dates	2061-2099	-[34% - 57%] (3 sub-basins)

* İKLİM DEĞİŞİKLİĞİNİN SU KAYNAKLARINA ETKİSİ PROJESİ Proje Nihai Raporu EK 17 – Kızılırmak Havzası

** values extracted from figure or tables in SYGM 2016 report

Total three climate models were used in the study of SYGM and their results (given in Table 4-14) is ensemble mean of these 3 models based on the RCP 8.5 scenario. In our study, modeling studies were carried out over 3 sub-basins of Kızılırmak basin, however in SYGM's study, the entire Kızılırmak was modeled. According to SYGM's study, the ensemble mean of the outputs of the 3 models says that there will be a decrease of approximately 48% in the surface runoff potential of the Kızılırmak basin. In our study, the surface runoff potential of the 3 sub-basins decreases by 34%, 57% and 35%, respectively, where it is not directly possible to simulate the runoff potential over entire Kızılırmak basin via HBV model in the absence of reliable runoff data (i.e., NSE values between simulations and the observations greater than 0.50) during the historical period. The reason an estimate over entire Kızılırmak basin is not performed because the dams (in particular Yamula, Hirfanlı, Kesikköprü, and Altınkaya) regulate the flow significantly, hence calibration via ordinary HBV model yields not successful results. If detailed and accurately acquired observational data about the managed water would be available, then flow estimates near natural flow conditions could be obtained. However, in reality there are too many unknowns and such accurate estimates could not be

obtained. This condition prevents accurate hydrological model simulations to be obtained over entire Kızılırmak basin, where one of the best available option to study the basins water potential becomes investigation of the sub-basins of entire catchment.

CHAPTER 5

CONCLUSIONS AND RECOMMENDATIONS

The aim of this study is to evaluate the expected change in the surface runoff potential that will occur due to climate change in the Kızılırmak Basin until 2100. HBV-light hydrological model was used in this study. ERA5-Land datasets were used for historical precipitation and temperature datasets used as input of the model. By using the CMIP5 experiments, historical and future daily precipitation and temperature values from 56 GCM/RCM model couples were downloaded from CORDEX EUR-11 with 0.11^0 spatial resolution, with the RCP 8.5 emission scenario. Correlation evaluation was performed between ERA5-Land dataset and 56 GCM/RCM model couples and 10 models with the poorest daily correlation were eliminated. Also, values from CORDEX EUR-11 are not bias corrected so bias correction was performed. After performing the bias correction, the parameters calibrated with the HBV hydrological model were used for the future periods and expected changes in the surface runoff potential of 3 sub-basins between the years of 2021 and 2099 were investigated.

Temperature values tend to increase the Kızılırmak Basin. This increase has been at a dramatic level in the last period (2061-2099). The average temperature between the years of 2061 and 2099 is approximately 4 °C higher than the average of 1979-2020. Average precipitation between 2061 and 2099 is around 10% lower than the average between 1979 and 2020 over entire Kızılırmak basin. Runoff simulations performed using HBV model during calibration period were on average 4.3 % lower than the observations (i.e., dry bias) and during validation period 4.8% higher than the observations (i.e., wet bias). Daily NSE value ranges from 0.66 to 0.87 during the calibration period and 0.25 to 0.78 during the validation period and monthly NSE value ranges from 0.75 to 0.93 during the calibration period and 0.35 to 0.87 during the validation period. These results show that the HBV hydrological model can

accurately (Moriasi et al., 2007) reflect the watershed conditions in the sub-basins modeled in the Kızılırmak basin and the model calibration stages have been successfully carried out.

The total area of the 3 sub-basins investigated in detail corresponds to approximately one-third of the Kızılırmak Basin. Overall, the current surface runoff potential is expected to decrease in all 3 sub-basins between 2061 and 2099, where the rate of the decrease will be between 34% and 57% of the current multi-decadal averages. Considering the consistency between the temperature and the precipitation patterns between the three sub-basins and entire Kızılırmak basin, the surface runoff potential of entire Kızılırmak basin is also expected to decrease at a similar rate. Therefore, it is concluded that the surface runoff potential of Kızılırmak basin is expected to be impacted from the climate change considerably.

Currently, in this study, only the future surface runoff potential of three sub-basins of Kızılırmak basin is investigated. On the other hand, the impact of the expected change on available water structures (i.e., change in dam reservoir levels) or the future planned structures (e.g., future dam projects) or the water related future projects (e.g., new irrigation areas) are not considered. In a future study, the impact of this expected change (i.e., a decrease in surface runoff potential between 34% and 57%) over existing and future water related projects and infrastructures should be investigated. In particular, drinking water quality change under this expected future surface runoff potential change should be also investigated as it directly impacts the health of the society living in the capital and the surrounding cities. Overall, water allocation plans should be revised under these expected changes and scenarios.

In this study, only the impact of the expected change in the climate over the surface runoff potential is investigated. On the other hand, an investigation of the agricultural water need, where on average 70% of the water potential is used for irrigation purposes over Turkey, is not performed. Accordingly, in a future study, an investigation of the current water uses and the future water requirements of the crops as well as the total irrigation requirement of the crops that are grown inside

Kızılırmak basin should be performed to understand whether or not the future water potential will be sufficient for the irrigation needs over the Kızılırmak basin. If insufficient, then perhaps, alternative crops should be identified under the future expected water potential availability conditions.

This study is currently implemented using CMIP5-based climate projection datasets, as dynamically downscaled high resolution CMIP6 projections over Turkey are not yet available. In the future, once these simulations are available, then this study should be repeated to investigate the expected change under the latest climate change scenarios using CMIP6-based projections. Similarly, on the most pessimistic carbon emission scenario (i.e., RCP8.5) is considered in this study. In a future study, other scenarios (e.g., RCP4.5) could be also investigated to see the possible range of the expected change in surface potential of Kızılırmak basin.

REFERENCES

Aktaş, Ö. (2014). Impacts of climate change on water resources in Turkey. *Environmental Engineering and Management Journal, 13*, 881-889. doi:10.30638/eemj.2014.092

Anders, I., Stagl, J., Auer, I., & Pavlik, D. (2014). Climate Change in Central and Eastern Europe. In S. Rannow, & M. Neubert (Eds.), *Managing Protected Areas in Central and Eastern Europe Under Climate Change. Advances in Global Change Research* (Vol. 58, pp. 17-30). Dordrecht: Springer. doi:10.1007/978-94-007-7960-0_2

ASKİ. (2022, September 17). *Kızılırmak-Kesikköprü Barajı*. Retrieved from ANKARA SU VE KANALİZASYON İDARESİ GENEL MÜDÜRLÜĞÜ: https://www.aski.gov.tr/TR/ICERIKDETAY/Kizilirmak-Kesikkopru-Baraji/32/9

Bağçaci, S. Ç., Yucel, I., Düzenli, E., & Yilmaz, M. T. (2021). Intercomparison of the expected change in the temperature and the precipitation retrieved from CMIP6 and CMIP5 climate projections: A Mediterranean hot spot case, Turkey. *Atmospheric Research, 256*. doi:10.1016/j.atmosres.2021.105576

Balov, M., & Altunkaynak, A. (2020). The impacts of climate change on the runoff volume of Melen and Munzur Rivers in Turkey based on calibration of WASMOD model with multiobjective genetic algorithm. *Meteorology and Atmospheric Physics, 132*, 85-98. doi:10.1007/s00703-019-00676-7

Barredo, J., Caudullo, G., & Mauri, A. (2017). *Mediterranean habitat loss under RCP4.5 and RCP8.5 climate change projections.* In European Commision. JRC Technical Reports. doi:10.2760/622174

Bergström, S. (1992). *THE HBV MODEL - its structure and applications.* Norrköping: SMHI RH No 4.

Bergström, S., & Lindström, G. (2015). Interpretation of runoff processes in hydrological modelling—experience from the HBV approach. *Hydrological Processes*, 3535-3545.

Birundu, A., & Mutua, B. (2017). Analyzing the Mara River Basin Behaviour through Rainfall-Runoff Modeling. *International Journal of Geosciences, 8*, 1118-1132. doi:10.4236/ijg.2017.89064

Bozkurt, D., & Şen, Ö. (2012). Climate change impacts in the Euphrates–Tigris Basin based on different model and scenario simulations. *Journal of Hydrology, 480*, 149-161. doi:10.1016/j.jhydrol.2012.12.021

Christensen, P., Gillingham, K., & Nordhaus, W. (2018). Uncertainty in forecasts of long-run economic growth. *Proceedings of the National Academy of Sciences of the United States of America, 115*(21), 5409-5414. doi:10.1073/pnas.1713628115

Climate Data Store. (2022, April 22). *ERA5-Land hourly data from 1950 to present*. doi:10.24381/cds.e2161bac

Crawford, J., Venkataraman, K., & Booth, J. (2019). Developing climate model ensembles: A comparative case study. *Journal of Hydrology, 568*, 160-173. doi:10.1016/j.jhydrol.2018.10.054

Dadaser-Celik, F., Çelik, M., & Dokuz, A. (2012). Associations between stream flow and climatic variables at Kızılırmak River Basin in Turkey. *Global NEST Journal, 14*(3), 354-361.

Daniel, E., Camp, J., LeBoeuf, E., Penrod, J., Dobbins, J., & Abkowitz, M. (2011). Watershed Modeling and its Applications: A State-of-the-Art Review. *The Open Hydrology Journal, 5*, 26-50. doi:10.2174/1874378101105010026

Devi, G., Ganasri, B., & Dwarakish, G. (2015). A Review on Hydrological Models. *Aquatic Procedia, 4*, 1001-1007. doi:10.1016/j.aqpro.2015.02.126

Driessen, T. L., Hurkmans, R. T., Terink, W., Hazenberg, P., Torfs, P. J., & Uijlenhoet, R. (2010). The hydrological response of the Ourthe catchment to climate change as modelled by the HBV model. *Hydrology and Earth System Sciences*, 651-665.

Efe, R. (1996). Kızılırmağın Akım ve Rejim Özellikleri. *Öneri Dergisi, 1*(4), 39-60. doi:10.14783/maruoneri.710445

Ercan, B., Yağcı, A., Yilmaz, A., Yuce, M., & Unsal, M. (2019). Annual Runoff Modelling of Kızılırmak Basin by Artificial Intelligent Techiques. *Fresenius Environmental Bulletin, 28*(9), 6651-6660.

Ersoy, N. (2022). *Impact of Climate Change over the Variability of Drought Characteristics over 25 Basins of Turkey (Master's Thesis).* Ankara: Middle East Technical University.

EURO-CORDEX community. (2021). *Guidance for EURO-CORDEX climate projections data use.*

Feng, J., Lee, D.-K., Fu, C., Tang, J., Sato, Y., Kato, H., . . . Mabuchi, K. (2011). Comparison of four ensemble methods combining regional climate simulations over Asia. *Meteorology and Atmospheric Physics, 111*, 41-53. doi: 10.1007/s00703-010-0115-7

Fujihara, Y., Tanaka, K., Watanabe, T., Nagano, T., & Kojiri, T. (2008). Assessing the Impacts of Climate Change on the Water Resources of the Seyhan River Basin in Turkey: Use of Dynamically Downscaled Data for Hydrologic Simulations. *Journal of Hydrology, 353*, 33-48.

Güner Bacanlı, Ü., Dikbaş, F., & Baran, T. (2012). Kuraklık Analizinde Entropi Yöntemi. *VII. Ulusal Hidroloji Kongresi*, (pp. 101-112). Isparta. doi:10.13140/RG.2.1.3118.0329

Hagedorn, R., Doblas-Reyes, F., & Palmer, T. (2005). The rationale behind the success of multi-model ensembles in seasonal forecasting – I. Basic

concept. *Tellus A: Dynamic Meteorology and Oceanography, 57*(3), 219-233. doi:10.3402/tellusa.v57i3.14657

Hao, Z., Singh, V., & Hao, F. (2018). Compound Extremes in Hydroclimatology: A Review. *Water*.

Hedberg, S. (2015). *Regional Quantification of Climatic and Anthropogenic Impacts on Streamflows in Sweden (Master's thesis).* Uppsala: Department of Earth Sciences, Uppsala University.

Höök, M., Li, J., Johansson, K., & Snowden, S. (2012). Growth rates of global energy systems and future outlooks. *Natural Resources Research*, 23-41.

Idrizovic, D., Pocuca, V., Gregoric, E., Matovic, G., & Djurovic, N. (2018). Evaluation of HBV-light Model Efficiency with Different Potential Evapotranspiration Inputs. *10th Eastern European Young Water Professionals Conference*, (pp. 63-69). Zagreb.

IPCC. (2014). *Climate Change 2014: Mitigation of Climate Change. Working Group III Contribution to the Fifth Assessment Report of the Intergovernmental Panel on Climate Change.* New York: Cambridge University Press. Retrieved from What Is Climate Change?

IPCC. (2022). IPCC WGII Sixth Assessment Report Chapter 4: Water. In Intergovernmental Panel on Climate Change, *Climate Change 2022: Impact, Adaptation and Vulnerability.*

IPCC. (2022). IPCC WGII Sixth Assessment Report Summary for Policymakers. In Intergovernmental Panel on Climate Change, *Climate Change 2022: Impact, Adaptation and Vulnerability.*

Islam, Z. (2011). *A Review on Physically Based Hydrologic Modeling.* doi:10.13140/2.1.4544.5924

Jajarmizadeh, M., Harun, S., & Salarpour, M. (2012). A Review on Theoretical Consideration and Types of Models in Hydrology. *Journal of Environmental Science and Technology, 5*, 249-261.

Kilicarslan, B., Yucel, İ., Pilatin, H., Düzenli, E., & Yilmaz, M. (2021). Improving WRF-Hydro runoff simulations of heavy floods through the sea surface temperature fields with higher spatio-temporal resolution. *Hydrological Processes, 35*(9). doi:10.1002/hyp.14338

Kumar, K., Kumar, K., & Rakhecha, P. (1987). Comparison of Penman and Thornthwaite Methods of Estimating Potential Evapotranspiration for Indian Conditions. *Theoretical and Applied ClimatoIogy, 38*, 140-146. doi:10.1007/BF00868097

Madsen, H. (2000). Automatic calibration of a conceptual rainfall–runoff model using multiple objectives. *Journal of Hydrology 235 (2000)*, 276-288.

Mendez, M., & Calvo-Valverde, L. (2016). Development of the HBV-TEC hydrological model. *12th International Conference on Hydroinformatics, HIC 2016, Procedia Engineering 154* (s. 1116-1123). Elsevier. doi:10.1016/j.proeng.2016.07.521

Moriasi, D., Arnold, J., Van Liew, M., Bingner, R., Harmel, R., & Veith, T. (2007). Model Evaluation Guidelines for Systematic Quantification of Accuracy in Watershed Simulations. *American Society of Agricultural and Biological Engineers, 50*(3), 885-900. doi:10.13031/2013.23153

Moriasi, D., Gitau, M., Pai, N., & Daggupati, P. (2015). HYDROLOGIC AND WATER QUALITY MODELS: PERFORMANCE MEASURES AND EVALUATION CRITERIA. *Transactions of the ASABE (American Society of Agricultural and Biological Engineers), 58*(6), 1763-1785. doi:10.13031/trans.58.10715

Moss, R., Edmonds, J., Hibbard, K., Manning, M., Rose, S., & Vuuren, D. (2010). The next generation of scenarios for climate change research and assessment. *Nature, 463*(7282), 747-756. doi:10.1038/nature08823

Nash, J., & Sutcliffe, J. (1970). River Flow Forecasting through Conceptual Model. Part 1—A Discussion of Principles. *Journal of Hydrology, 10*, 282-290.

NOAA. (2022, March 21). *Climate.gov*. Retrieved from Climate Change: Atmospheric Carbon Dioxide: https://www.climate.gov/news-features/understanding-climate/climate-change-atmospheric-carbon-dioxide

NOAA. (2022, March 21). *Global Monitoring Laboratory*. Retrieved from Trends in Atmospheric Carbon Dioxide: https://gml.noaa.gov/ccgg/trends/

NOAA. (2022, March 21). *NOAA National Centers for Environmental Information*. Retrieved from Global Climate Report - Annual 2021: https://www.ncdc.noaa.gov/sotc/global/202113

NOAA. (2022, March 20). *NOAA National Centers for Environmental Information*. Retrieved from Climate at a Glance: Global Time Series: https://www.ncdc.noaa.gov/cag/global/time-series

OECD. (2013). *Water and Climate Change Adaptation: Policies to Navigate Uncharted Waters, OECD Studies on Water.* OECD Publishing.

Oruç, S. (2018). *Climate change and futureproofing infrastructure: Etimesgut, Ankara case study (Doctoral dissertation).* Ankara: Middle East Technical University.

Ouatiki, H., Boudhar, A., Ouhinou, A., Beljadid, A., Leblanc, M., & Chehbouni, A. (2020). Sensitivity and Interdependency Analysis of the HBV Conceptual Model Parameters in a Semi-Arid Mountainous Watershed. *Water 2020, 12, 2440*. doi:10.3390/w12092440

Oudin, L., Michel, C., & Anctil, F. (2005). Which potential evapotranspiration input for a lumped rainfall-runoff model? Part 1—Can rainfall-runoff

models effectively handle detailed potential evapotranspiration inputs? *Journal of Hydrology, 303*, 275–289. doi:10.1016/j.jhydrol.2004.08.025

Ozkul, S. (2009). Assessment of climate change effects in Aegean river basins: the case of Gediz and Buyuk Menderes Basins. *Climatic Change, 97*, 253-283. doi:10.1007/s10584-009-9589-z

Pechlivanidis, I., Jackson, B., Mcintyre, N., & Wheater, H. (2011). Catchment scale hydrological modelling: A review of model types, calibration approaches and uncertainty analysis methods in the context of recent developments in technology and applications. *Global NEST International Journal, 13*(3), 193-214.

Peel, M., Finlayson, B., & McMahon, T. (2007). Updated world map of the Koppen-Geiger climate classification. *Hydrology and Earth System Sciences*, 1633-1644.

Piani, C., Haerter, J., & Coppola, E. (2010). Statistical bias correction for daily precipitation in Regional Climate Models over Europe. *Theoretical and Applied Climatology, v.99*, 187-192.

Portela, M. (2019). Effect of the Evapotranspiration of Thornthwaite and of Penman-Monteith in the Estimation of Monthly Streamflows Based on a Monthly Water Balance Model. In K. Ghosh, & S. Mukhopadhyay (Eds.), *Current Practice in Fluvial Geomorphology - Dynamics and Diversity.* IntechOpen. doi:10.5772/intechopen.88441

Riahi, K., Rao, S., Krey, V., Cho, C., Chirkov, V., Fischer, G., . . . Rafaj, P. (2011). RCP 8.5—A scenario of comparatively high greenhouse gas emissions. *Climatic Change, 109*(1), 33–57. doi:10.1007/s10584-011-0149-y

Roudier, P., Ducharne, A., & Feyen, L. (2014). Climate change impacts on runoff in West Africa: A review. *Hydrology and Earth System Sciences, 18*(7), 2789–2801. doi:10.5194/hess-18-2789-2014

Schwalm, C., Glendon, S., & Duffy, P. (2020). RCP8.5 tracks cumulative CO2 emissions. *Proceedings of the National Academy of Sciences of the United States of America, 117*(33), 19656-19657. doi:10.1073/pnas.2007117117

Seibert, J. (2000). Multi-criteria calibration of a conceptual runoff model using a genetic algorithm. *Hydrology and Earth System Sciences, 4*(2), 215-224.

Seibert, J. (2005). *HBV light version 2 User's Manual.* Stockholm: Stockholm University.

Seibert, J., & Vis, M. J. (2012). Teaching hydrological modeling with a user-friendly catchment-runoff-model software package. *Hydrology and Earth System Sciences, 16*, 3315-3325. doi:10.5194/hess-16-3315-2012

Sen, O., Unal, A., Bozkurt, D., & Kindap, T. (2011). Temporal changes in the Euphrates and Tigris discharges and teleconnections. *ENVIRONMENTAL RESEARCH LETTERS, 6*(2).

Shi, X., Qin, T., Nie, H., Weng, B., & He, S. (2019). Changes in Major Global River Discharges Directed into the Ocean. *International Journal of Environmental Research and Public Health*.

Sitterson, J., Knightes, C., Parmar, R., Wolfe, K., Muche, M., & Avant, B. (2017). *An Overview of Rainfall-Runoff Model Types.* U.S. Environmental Protection Agency.

Stagl, J., Mayr, E., Koch, H., Hattermann, F., & Huang, S. (2014). Effects of Climate Change on the Hydrological Cycle in Central and Eastern Europe. In S. Rannow, & M. Neubert (Eds.), *Managing Protected Areas in Central and Eastern Europe Under Climate Change. Advances in Global Change Research* (Vol. 58, pp. 31-43). Dordrecht: Springer. doi:10.1007/978-94-007-7960-0_3

SYGM. (2016). *İKLİM Değişikliğinin Su Kaynaklarına Etkisi Projesi Proje Nihai Raporu.* Ankara: ORMAN VE SU İŞLERİ BAKANLIĞI.

SYGM. (2016). *İKLİM DEĞİŞİKLİĞİNİN SU KAYNAKLARINA ETKİSİ PROJESİ Proje Nihai Raporu EK 17 – Kızılırmak Havzası.*

SYGM. (2019). *Kızılırmak Havzası Taşkın Yönetim Planı.* Ankara: Tarım ve Orman Bakanlığı.

Şorman, A., Şensoy, A., Tekeli, A., Şorman, A., & Akyurek , Z. (2009). Modelling and forecasting snowmelt runoff process using the HBV model in the eastern part of Turkey. *Hydrological Processes, 23*, 1031-1040. doi:10.1002/hyp.7204

Taylor, K., Stouffer, R., & Meehl, G. (2012). An overview of CMIP5 and the experiment design. *Bulletin of the American Meteorological Society, 93*(4), 485–498. doi:10.1175/BAMS-D-11-00094.1

Teutschbein, C. (2013). *Hydrological Modeling for Climate Change Impact Assessment: Transferring Large-Scale Information from Global Climate Models to the Catchment Scale, Doctoral Dissertation.* Stockholm: Stockholm University, Department of Physical Geography and Quaternary Geology.

Thornthwaite, C. (1948). An Approach toward a Rational Classification of Climate. *Geographical Review, 38*(1), 55-94. Retrieved from https://www.jstor.org/stable/210739

Trzaska, S., & Schnarr, E. (2014). *A Review of Downscaling Methods for Climate Change Projections.*

Turkish State Meteorological Service. (2021). *State of the Turkey's Climate in 2020.* Ankara: Ministry of Agriculture and Forestry.

UNFCCC. (2011). *Fact sheet: Climate change science - the status of climate change science today.*

Vautard, R., Kadygrov, N., Iles, C., Boberg, F., Buonomo, E., Bülow, K., . . . Corre, L. (2021). Evaluation of the Large EURO-CORDEX Regional

Climate Model Ensemble. *Journal of Geophysical Research: Atmospheres, 126*. doi:10.1029/2019JD032344

Vis, M., Knight, R., Pool, S., Wolfe, W., & Seibert, J. (2015). Model Calibration Criteria for Estimating Ecological Flow Characteristics. *Water, 7*, 2358-2381. doi:10.3390/w7052358

WMO. (2021). *State of global climate 2021 WMO provisional report.*

Yang, D., Yang, Y., & Xia, J. (2021). Hydrological cycle and water resources in a changing world: A review. *Geography and Sustainability*, 115-122.

Yılmaz, K. K., Vrugt, J. A., Gupta, H. v., & Sorooshian, S. (2010). Model calibration in watershed hydrology. *Advances in Data-based Approaches for Hydrological Modelling and Forecasting*, 53-105.

Yüce, M., & Ercan, B. (2015). Kızılırmak Havzası Yağış-Akış İlişkisinin Belirlenmesi. *4. Su Yapilari Sempozyomu*, (pp. 410-418). Antalya.

Yücel, İ., Güventürk, A., & Şen, Ö. (2015). Climate change impacts on snowmelt runoff for mountainous transboundary basins in eastern Turkey. *INTERNATIONAL JOURNAL OF CLIMATOLOGY*, 215-228.

APPENDICES

A. Correlation Table for GCM/RCM Model Validation

Table 7-1 Daily Correlation Values between the GCM/RCM Model Couples and ERA5-Land Datasets

Model ID	SB 1535 precipitation	SB 1535 temperature	SB 1541 precipitation	SB 1541 temperature	SB 1545 precipitation	SB 1545 temperature	Mean
1	0.062	0.807	0.037	0.800	0.017	0.768	0.415
2	0.058	0.839	0.048	0.844	0.024	0.794	0.434
3	0.052	0.854	0.036	0.837	0.018	0.801	0.433
4	0.049	0.849	0.019	0.833	0.021	0.797	0.428
5	0.020	0.854	0.018	0.859	0.038	0.839	0.438
6	0.049	0.849	0.036	0.843	0.030	0.819	0.438
7	0.038	0.839	0.033	0.836	0.014	0.800	0.427
8	0.045	0.845	0.026	0.841	0.017	0.801	0.429
9	0.043	0.855	0.020	0.849	0.027	0.814	0.435
10	0.061	0.851	0.048	0.841	0.030	0.804	0.439
11	0.034	0.864	0.034	0.856	0.018	0.837	0.440
12	0.031	0.844	0.012	0.834	0.018	0.810	0.425
13	0.017	0.860	0.025	0.857	0.016	0.833	0.435
14	0.019	0.846	0.038	0.841	0.006	0.809	0.426
15	0.079	0.848	0.050	0.839	0.043	0.802	0.443
16	0.058	0.834	0.050	0.839	0.035	0.803	0.436
17	0.062	0.860	0.049	0.857	0.031	0.834	0.449
18	0.060	0.852	0.063	0.851	0.044	0.813	0.447
19	0.034	0.779	0.030	0.783	0.008	0.747	0.397
20	0.056	0.837	0.047	0.833	0.031	0.782	0.431
21	0.061	0.859	0.076	0.845	0.052	0.812	0.451
22	0.043	0.847	0.041	0.827	0.009	0.807	0.429
23	0.047	0.824	0.045	0.810	0.000	0.773	0.416
24	0.068	0.819	0.051	0.813	0.014	0.779	0.424
25	0.044	0.846	0.048	0.847	0.028	0.807	0.437
26	0.007	0.018	0.008	0.008	-0.007	0.015	0.008

Model ID	SB 1535 precipitation	SB 1535 temperature	SB 1541 precipitation	SB 1541 temperature	SB 1545 precipitation	SB 1545 temperature	Mean
27	0.003	0.031	0.005	0.026	0.002	0.032	0.016
28	0.056	0.860	0.048	0.852	0.035	0.825	0.446
29	0.017	0.066	0.009	0.052	0.006	0.051	0.033
30	0.011	0.045	0.010	0.033	0.000	0.038	0.023
31	0.002	-0.001	-0.005	0.003	0.002	0.012	0.002
32	0.067	0.861	0.069	0.847	0.046	0.812	0.451
33	0.010	-0.012	0.011	-0.021	0.006	0.003	-0.001
34	0.010	0.022	0.002	0.036	0.008	0.038	0.019
35	0.004	-0.034	0.004	-0.005	0.009	0.000	-0.004
36	0.001	0.009	0.007	-0.009	0.005	0.000	0.002
37	0.086	0.843	0.065	0.834	0.017	0.791	0.439
38	0.077	0.835	0.060	0.824	0.029	0.784	0.435
39	0.070	0.851	0.046	0.848	0.039	0.815	0.445
40	0.059	0.832	0.047	0.834	0.012	0.792	0.429
41	0.073	0.847	0.057	0.848	0.022	0.809	0.443
42	0.043	0.676	0.035	0.673	0.027	0.634	0.348
43	0.057	0.861	0.059	0.845	0.021	0.826	0.445
44	0.060	0.841	0.050	0.837	0.020	0.809	0.436
45	0.077	0.839	0.056	0.843	0.037	0.793	0.441
46	0.053	0.841	0.050	0.846	0.015	0.803	0.435
47	0.054	0.839	0.056	0.825	0.030	0.792	0.432
48	0.069	0.782	0.047	0.772	0.047	0.729	0.408
49	0.070	0.850	0.049	0.843	0.049	0.806	0.444
50	0.030	0.763	0.023	0.768	0.007	0.725	0.386
51	0.070	0.835	0.050	0.839	0.052	0.790	0.439
52	0.069	0.785	0.067	0.786	0.054	0.739	0.417
53	0.075	0.849	0.050	0.839	0.046	0.793	0.442
54	0.042	0.821	0.052	0.810	0.034	0.779	0.423
55	0.048	0.777	0.050	0.768	0.037	0.740	0.404
56	0.046	0.816	0.059	0.803	0.032	0.757	0.419

B. Interquartile Range of Future Precipitation and Temperature Values

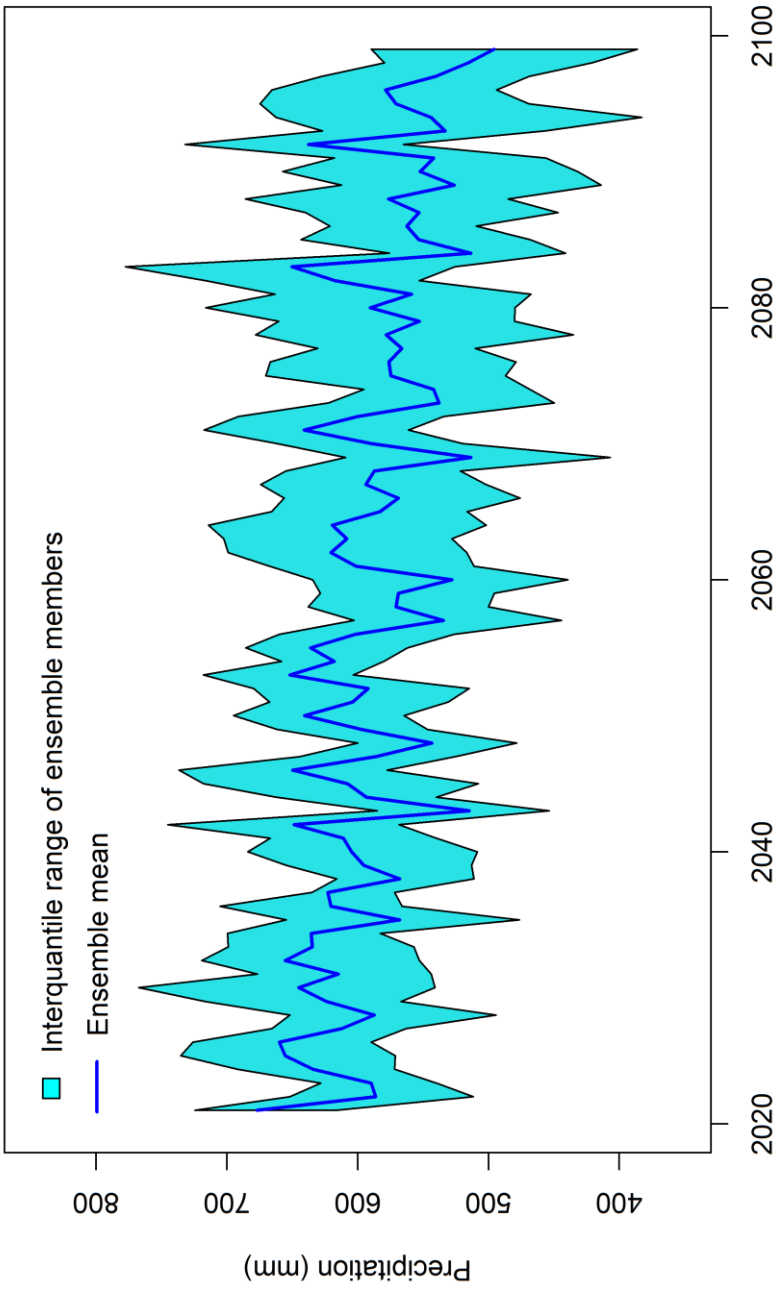

Figure 7-1 Precipitation Trends for SB 1535 (Ensemble mean and Interquartile ranges of 46 models)

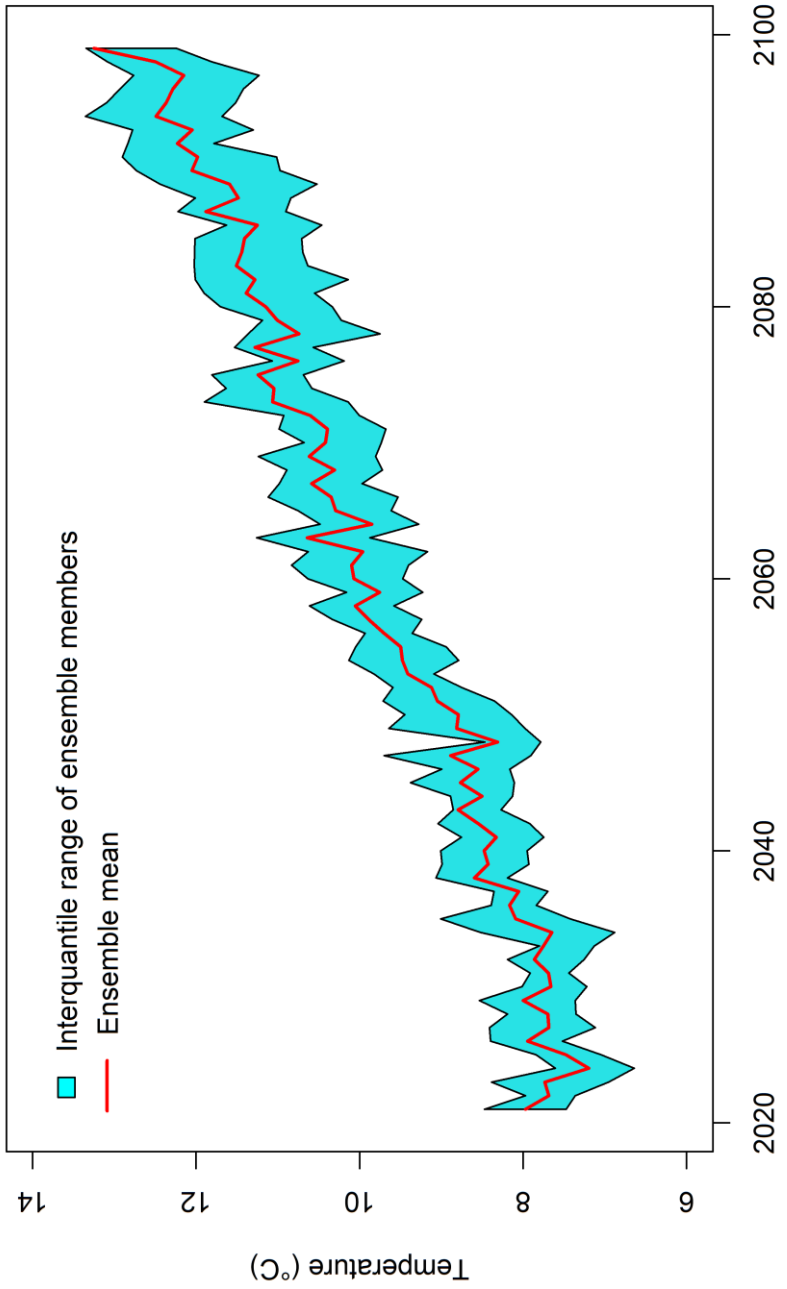

Figure 7-2 Temperature Trends for SB 1535 (Ensemble mean and Interquartile ranges of 46 models)

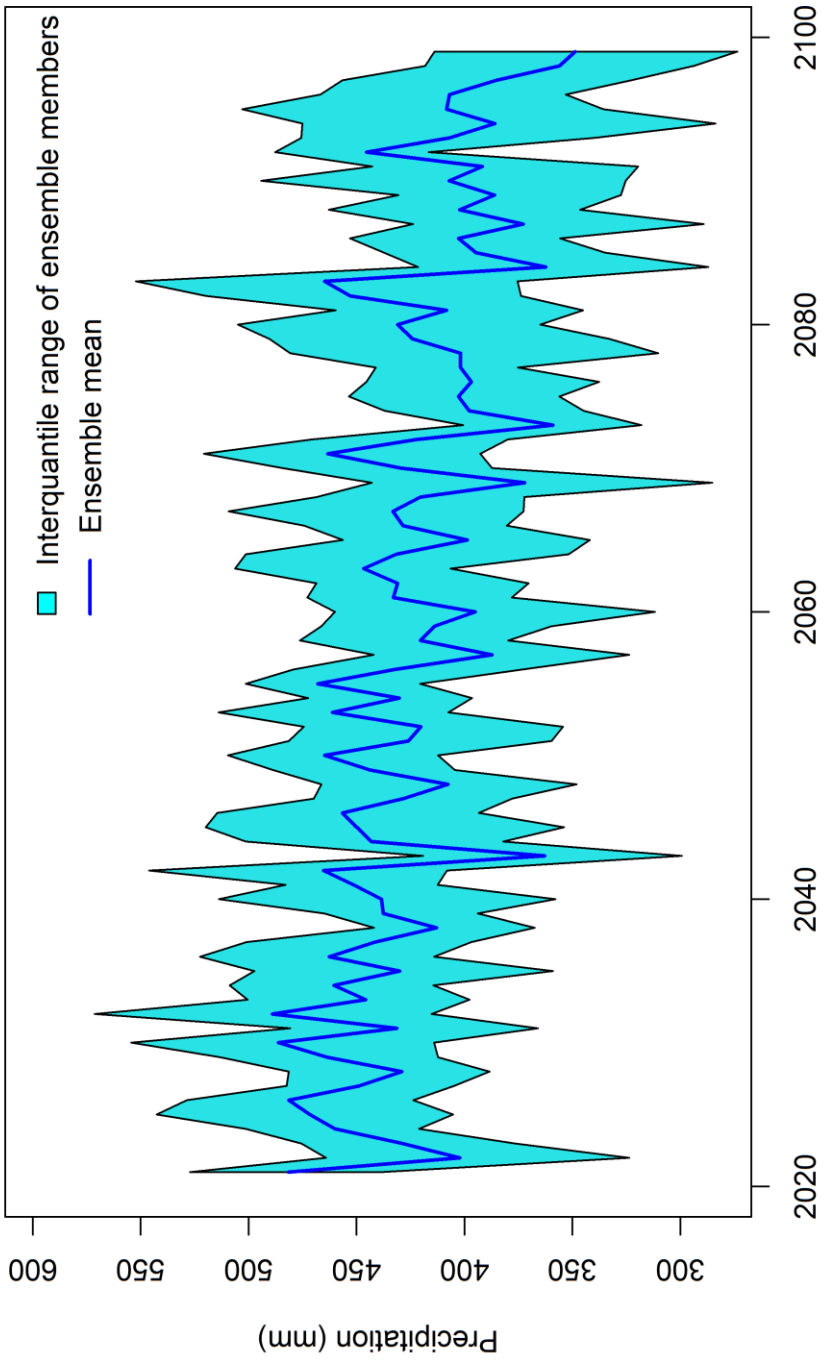

Figure 7-3 Precipitation Trends for SB 1541 (Ensemble mean and Interquartile ranges of 46 models)

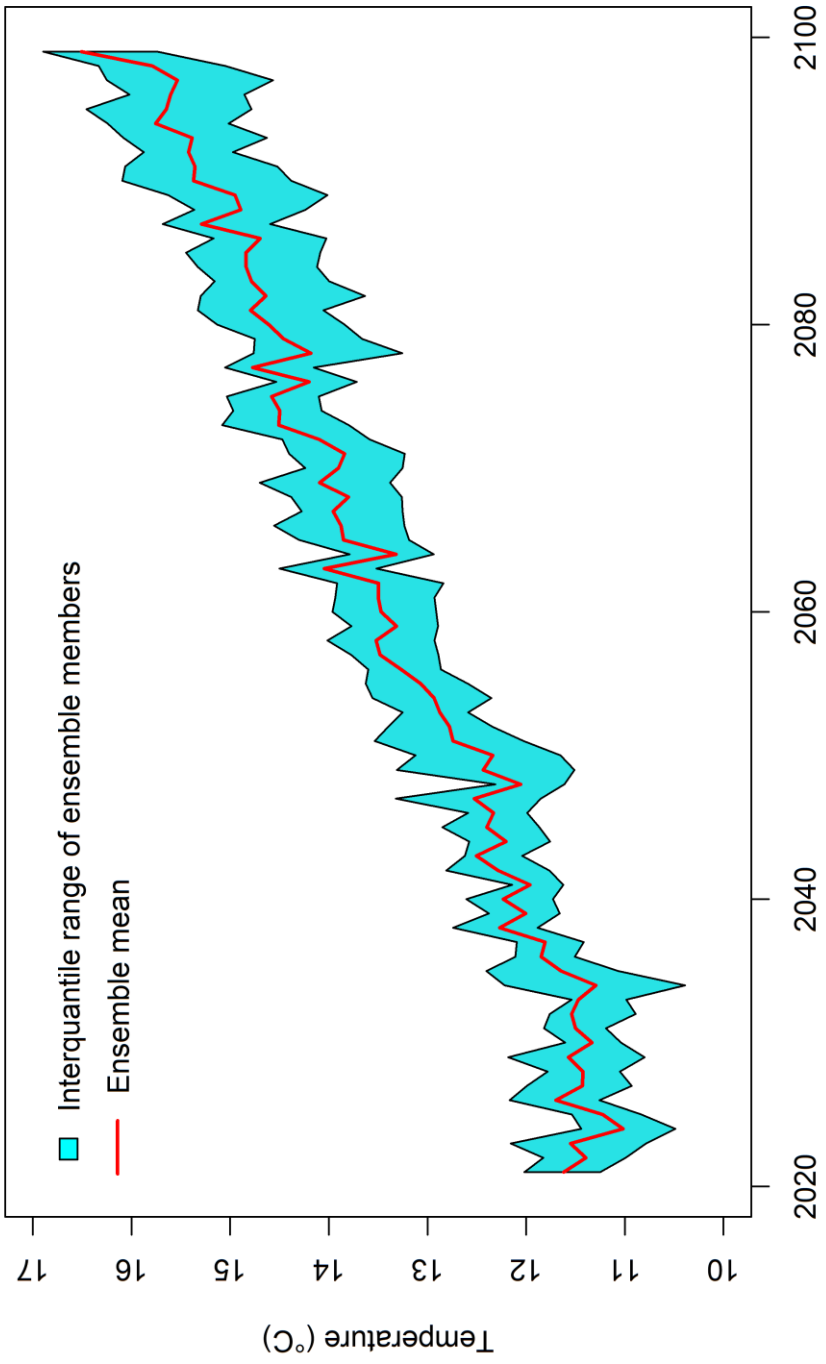

Figure 7-4 Temperature Trends for SB 1541 (Ensemble mean and Interquartile ranges of 46 models)

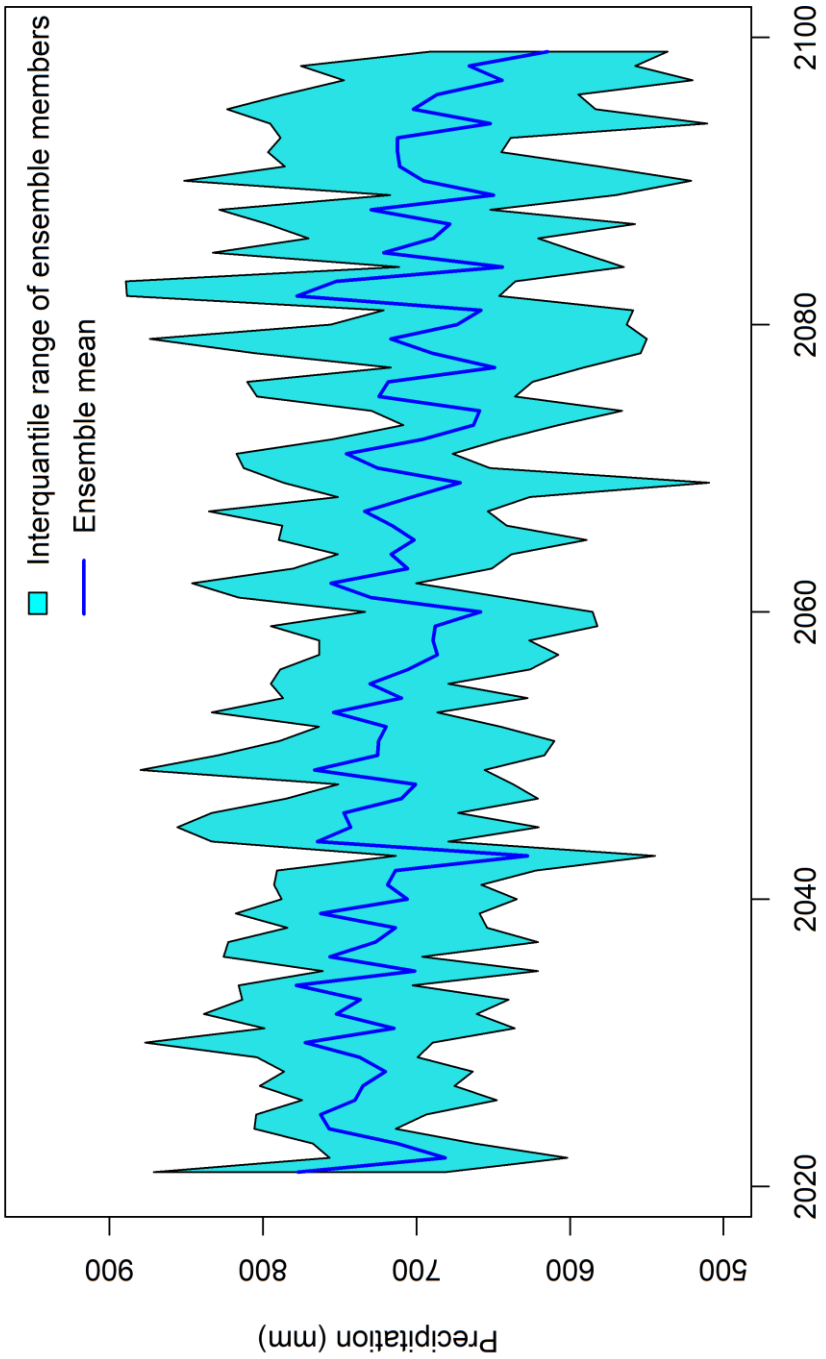

Figure 7-5 Precipitation Trends for SB 1545 (Ensemble mean and Interquartile ranges of 46 models)

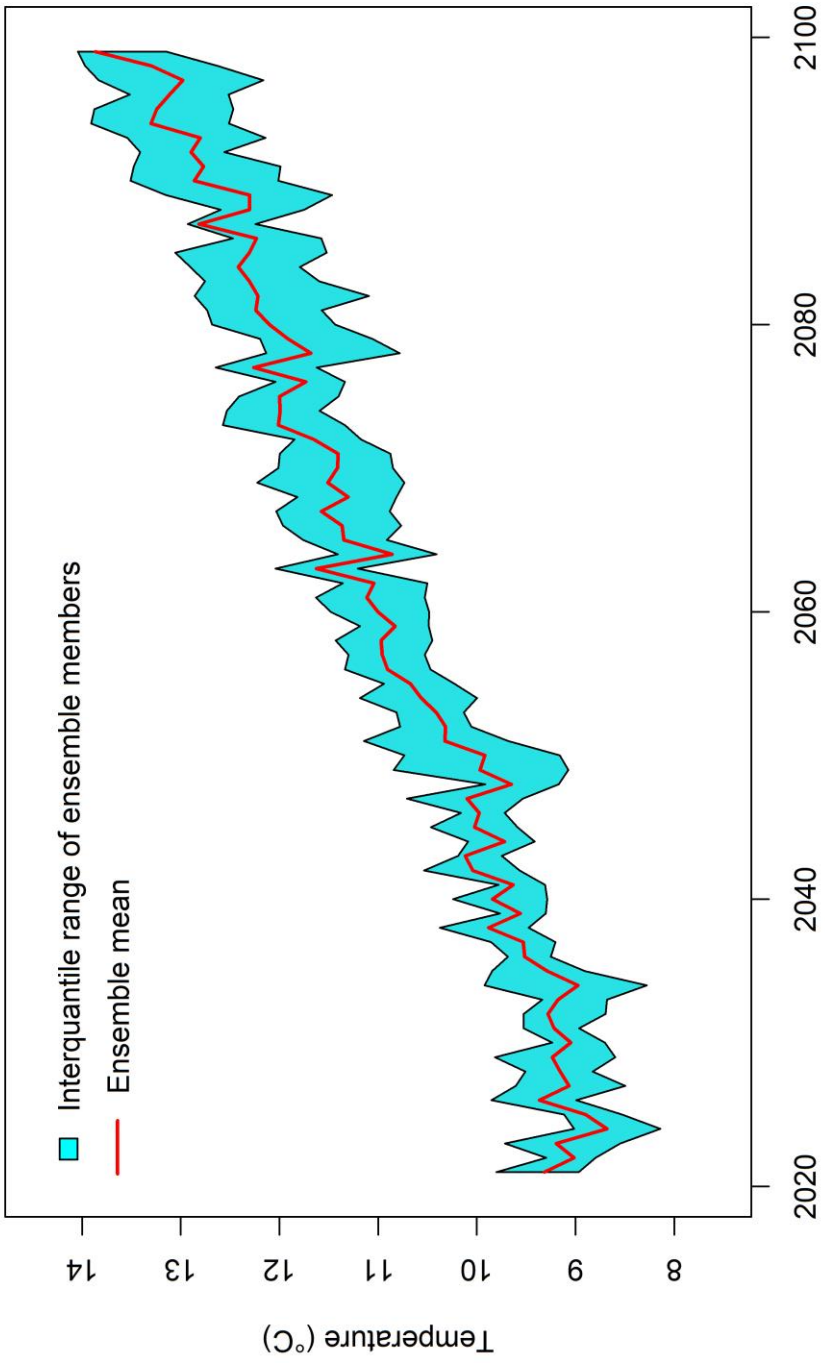

Figure 7-6 Temperature Trends for SB 1545 (Ensemble mean and Interquartile ranges of 46 models)

C. Historical and Future Trend Analysis of Precipitation and Temperature

SB 1535

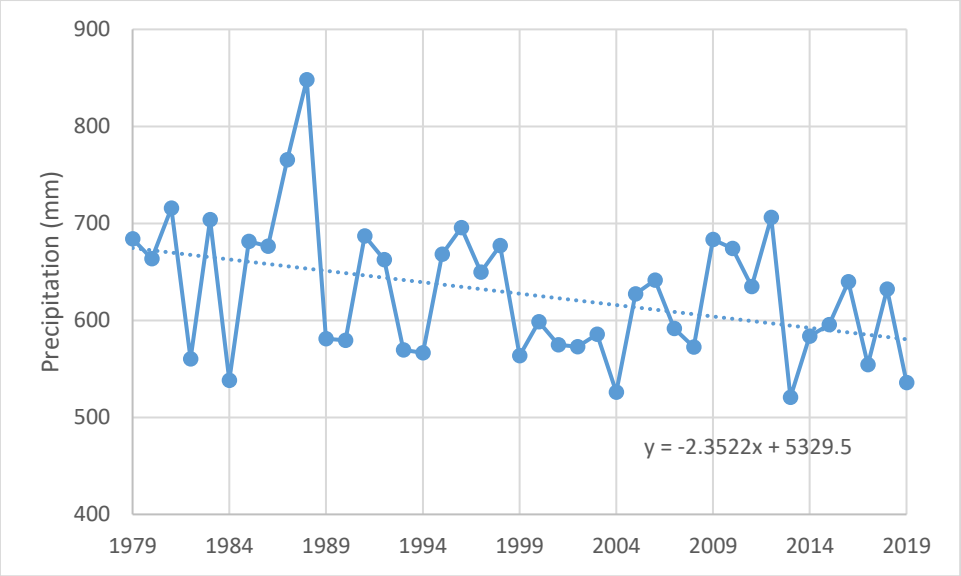

Figure 7-7 Historical Precipitation Analysis of SB 1535

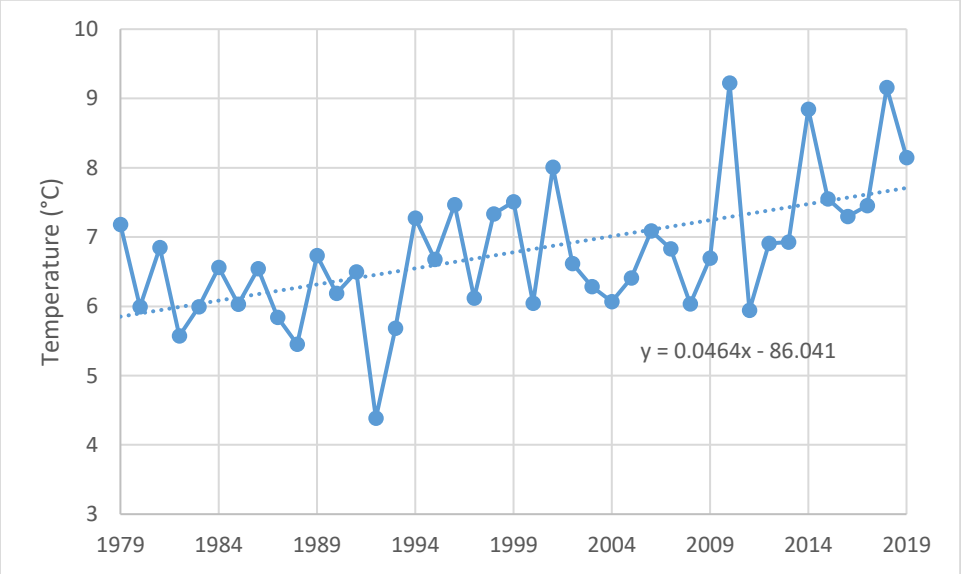

Figure 7-8 Historical Temperature Analysis of SB 1535

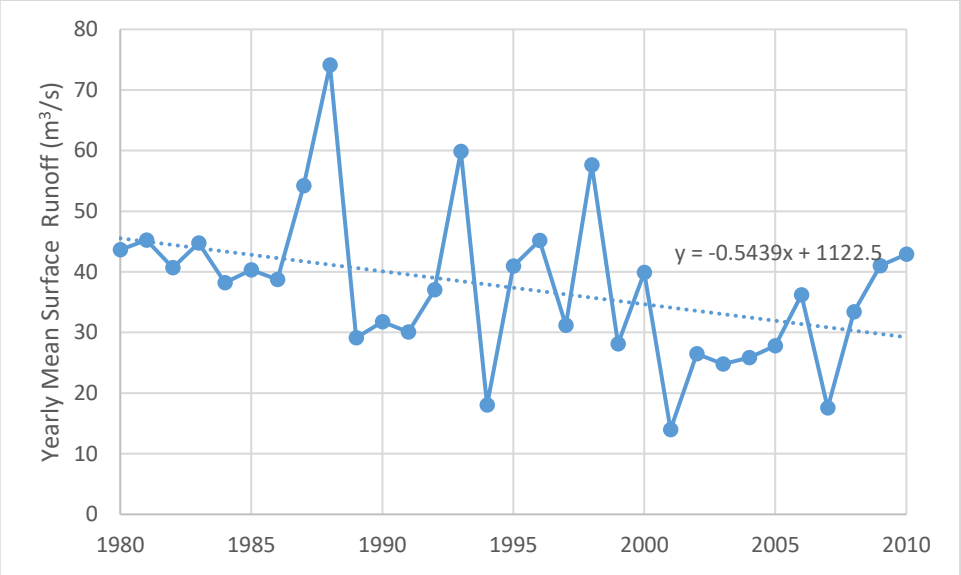

Figure 7-9 Yearly Mean Surface Runoff Analysis of SB 1535

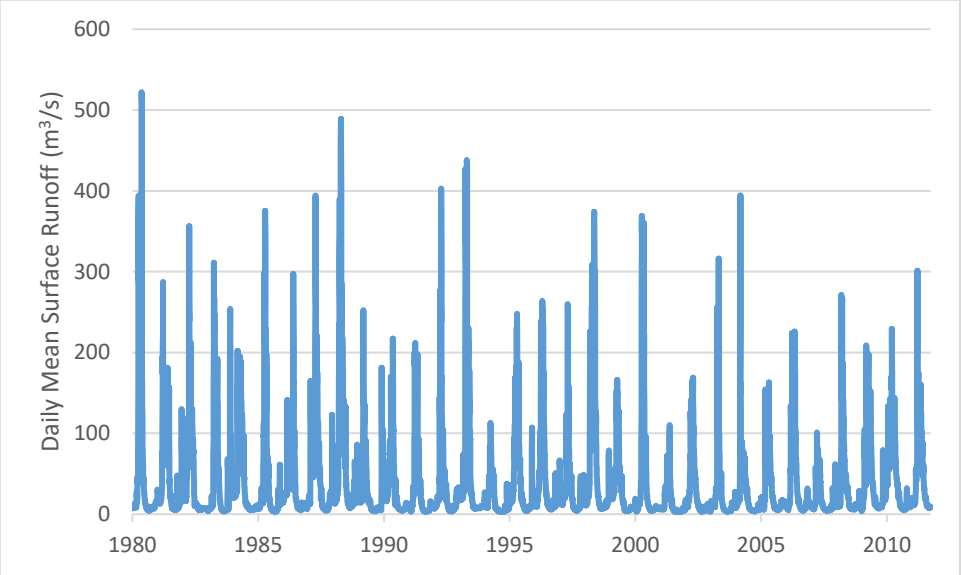

Figure 7-10 Daily Mean Surface Runoff for SB 1535

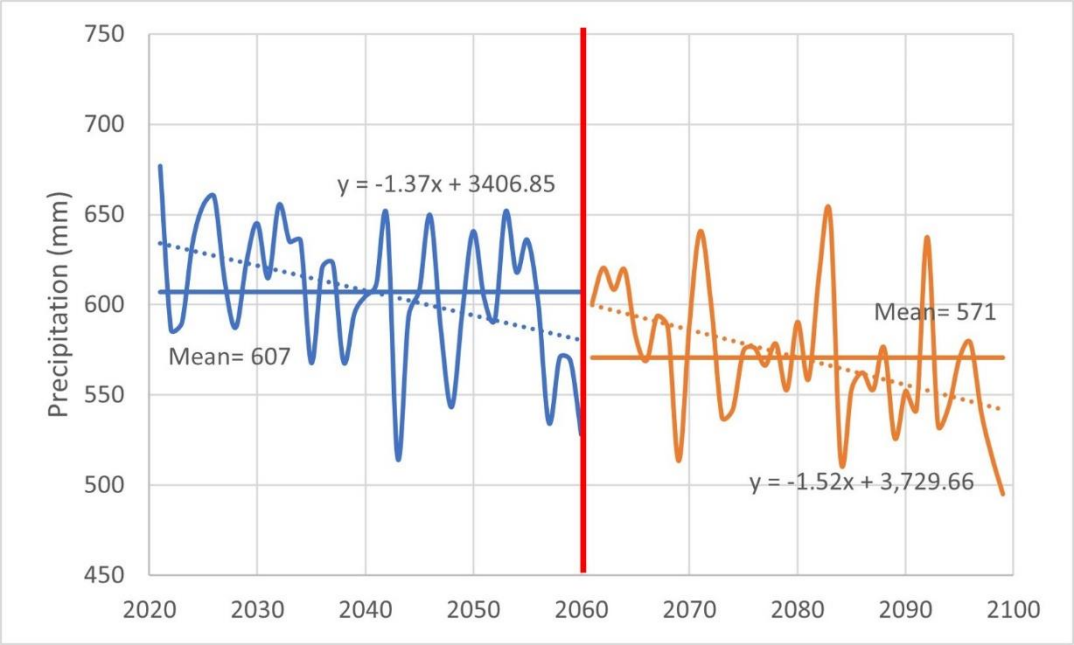

Figure 7-11 Change of future precipitation until 2100 for SB 1535 (Ensemble mean of 46 model)

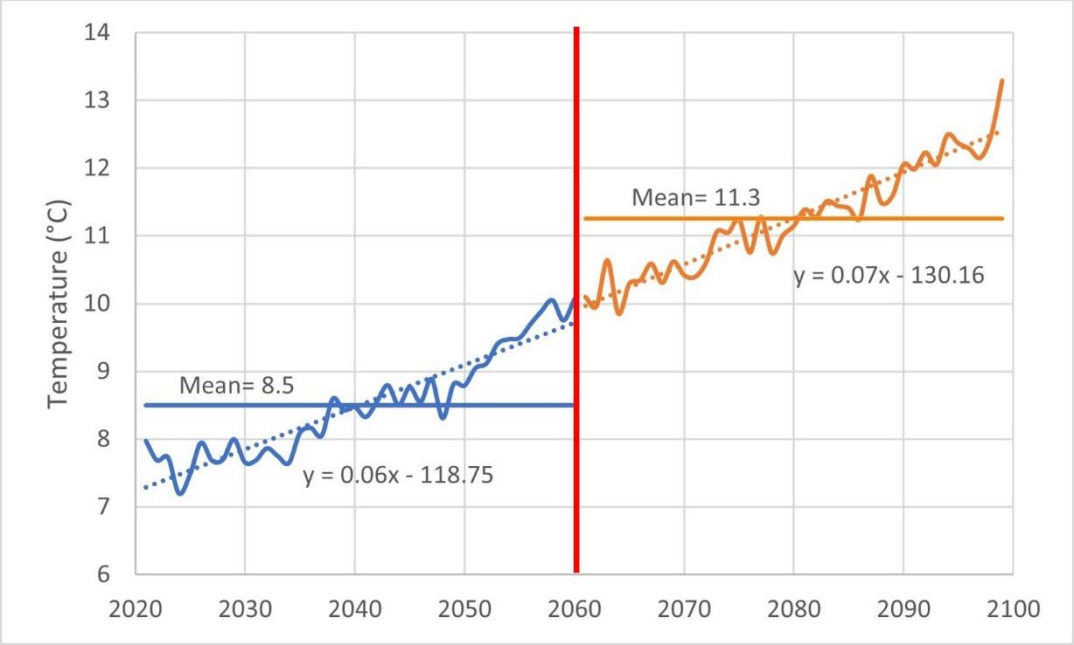

Figure 7-12 Change of future temperature until 2100 for SB 1535 (Ensemble mean of 46 model)

SB 1541

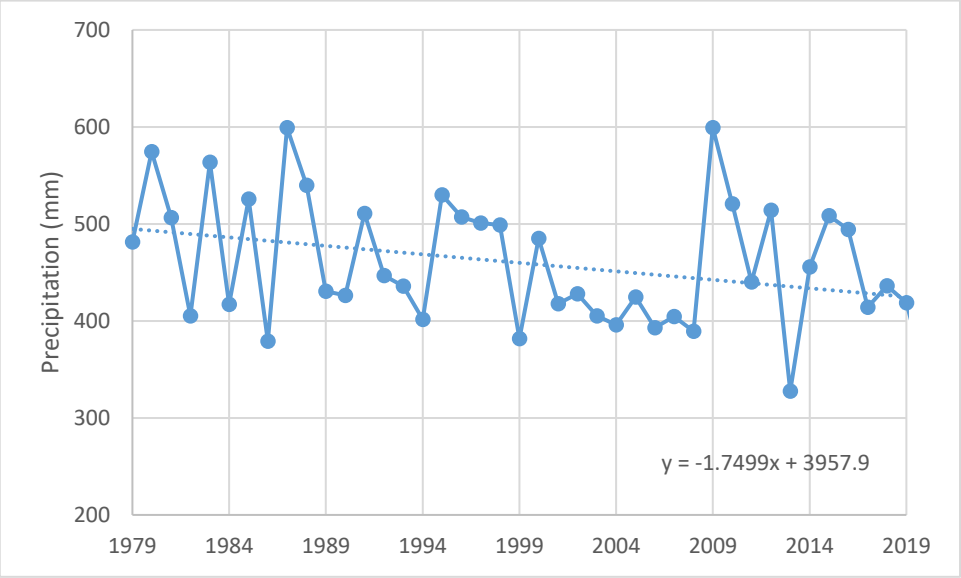

Figure 7-13 Historical Precipitation Analysis of SB 1541

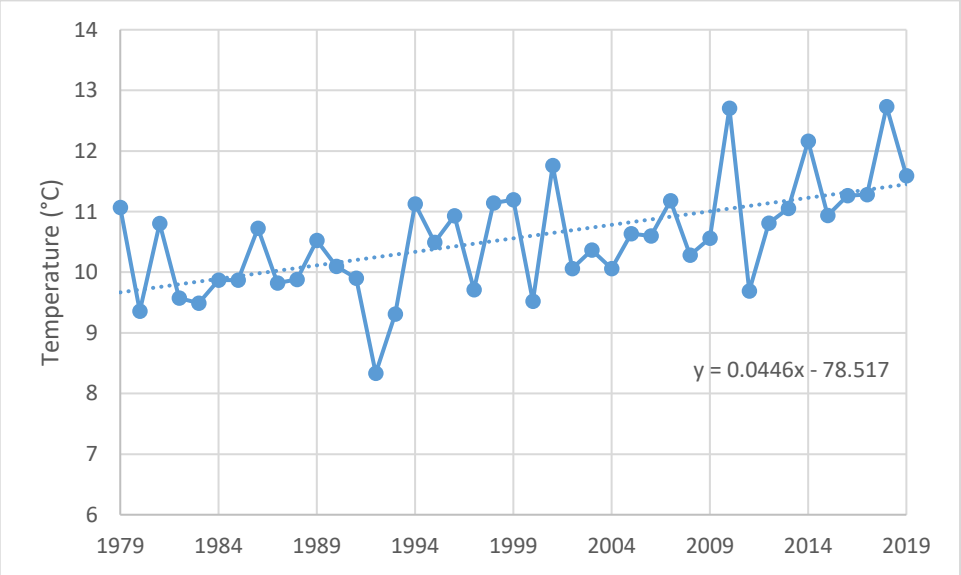

Figure 7-14 Historical Temperature Analysis of SB 1541

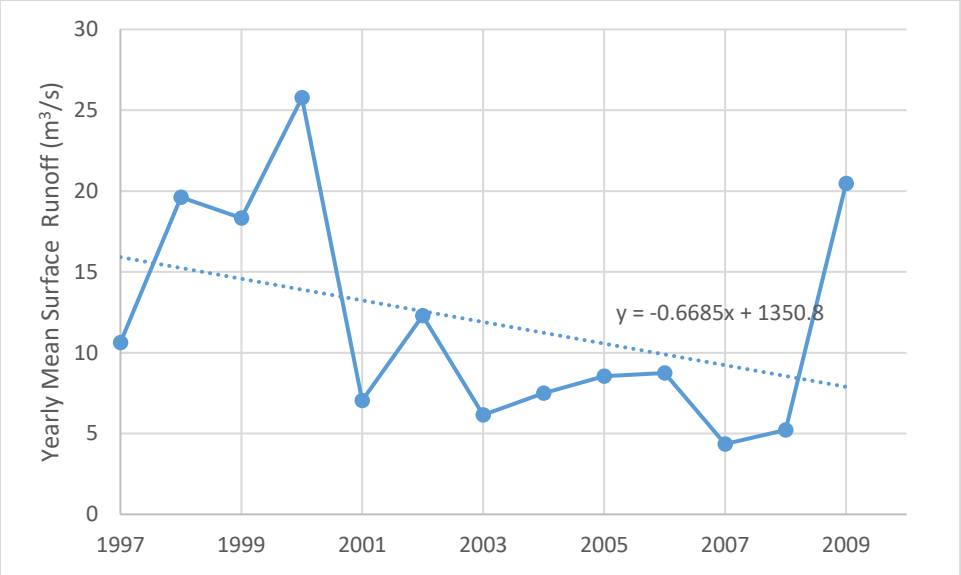

Figure 7-15 Yearly Mean Surface Runoff Analysis of SB 1541

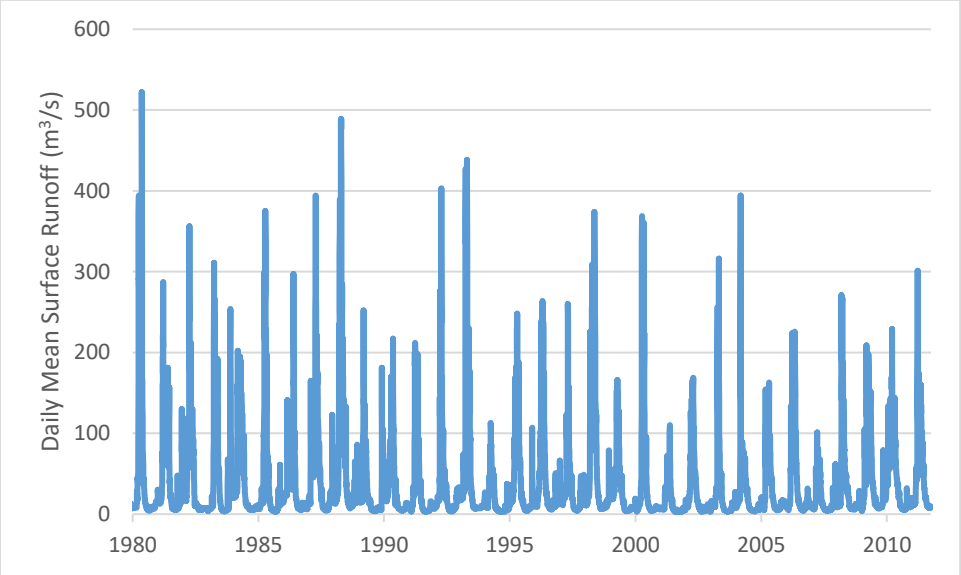

Figure 7-16 Daily Mean Surface Runoff for SB 1541

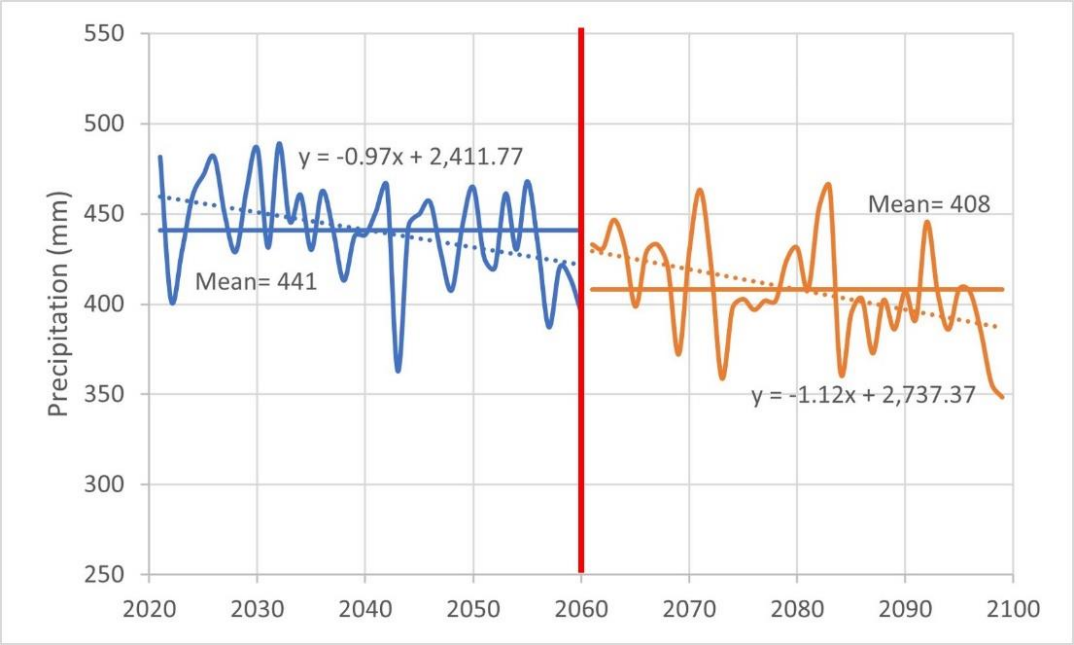

Figure 7-17 Change of future precipitation until 2100 for SB 1541 (Ensemble mean of 46 model)

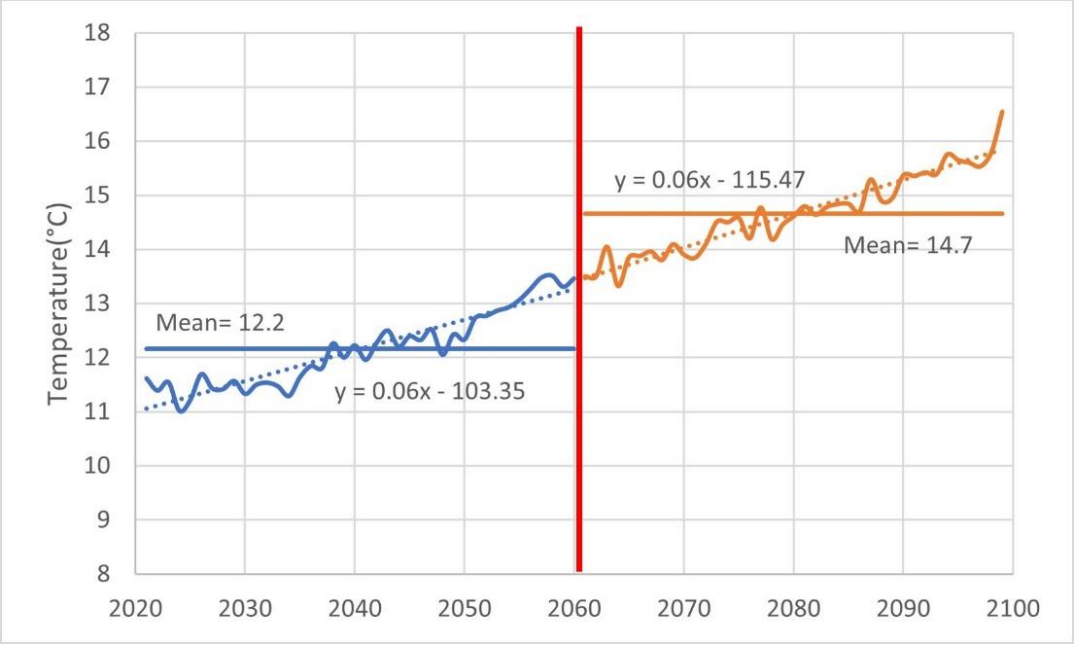

Figure 7-18 Change of future temperature until 2100 for SB 1541 (Ensemble mean of 46 model)

SB 1545

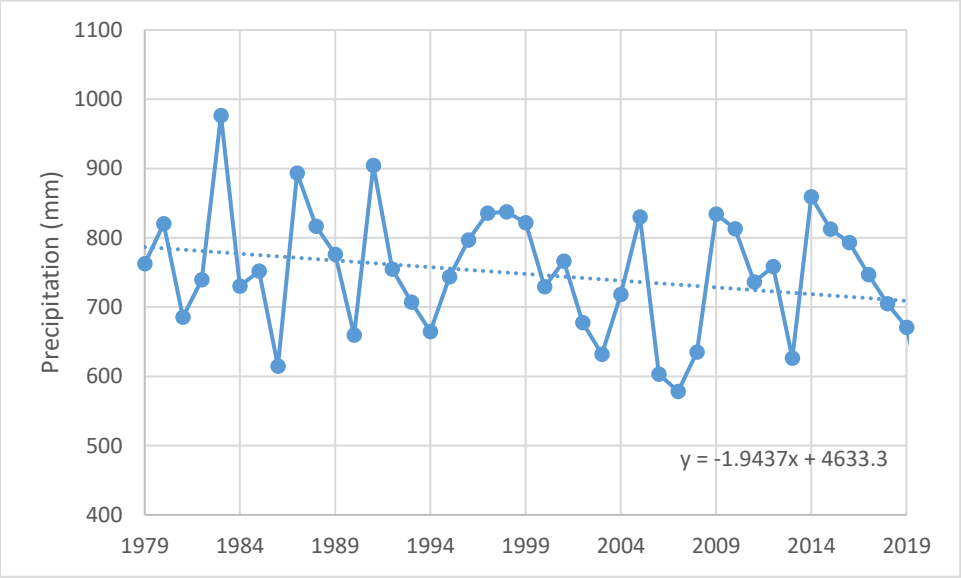

Figure 7-19 Historical Precipitation Analysis of SB 1545

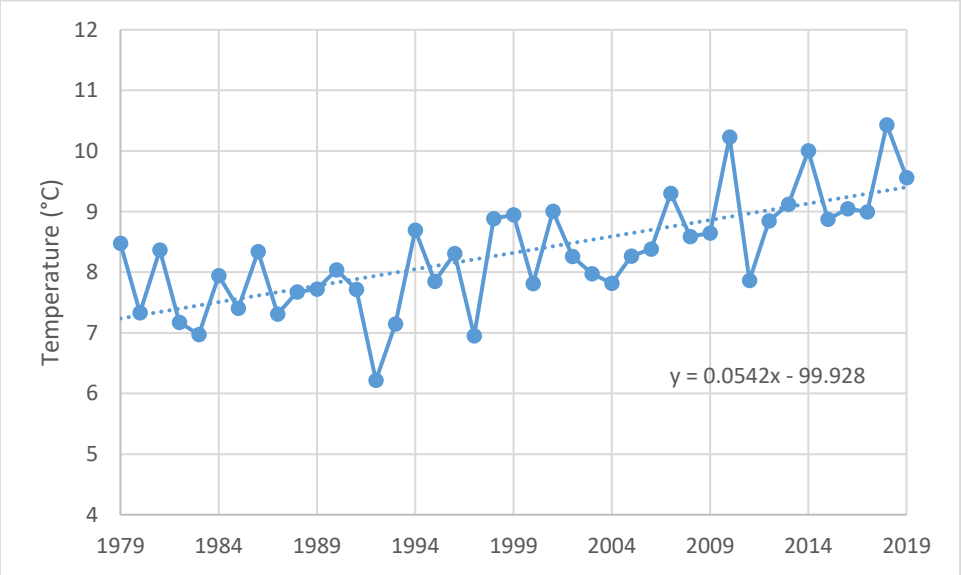

Figure 7-20 Historical Temperature Analysis of SB 1545

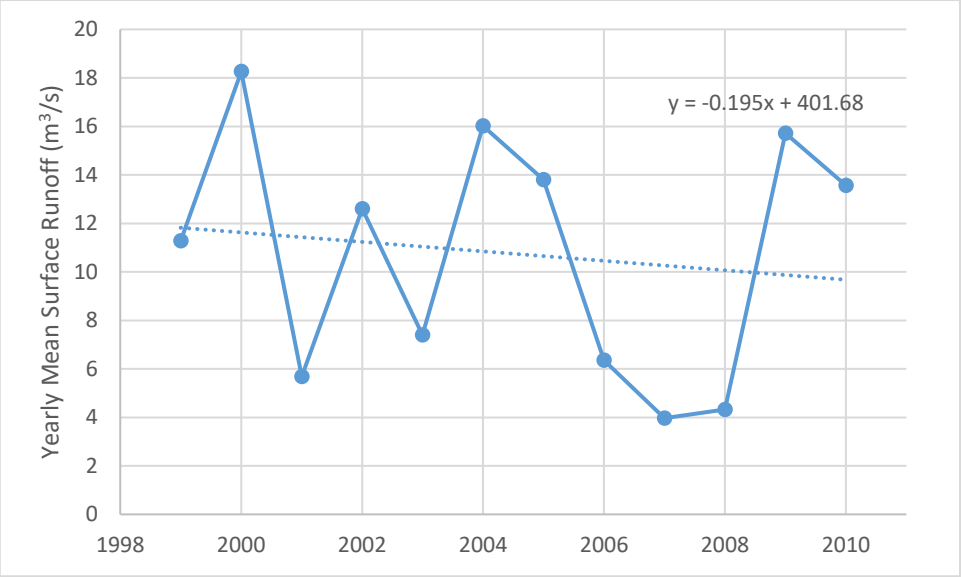

Figure 7-21 Yearly Mean Surface Runoff Analysis of SB 1545

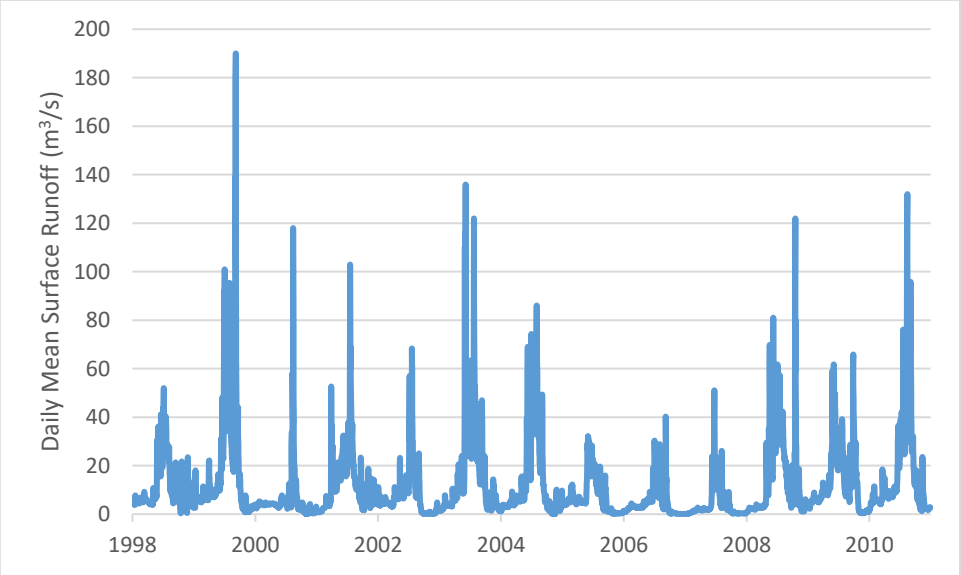

Figure 7-22 Daily Mean Surface Runoff for SB 1545

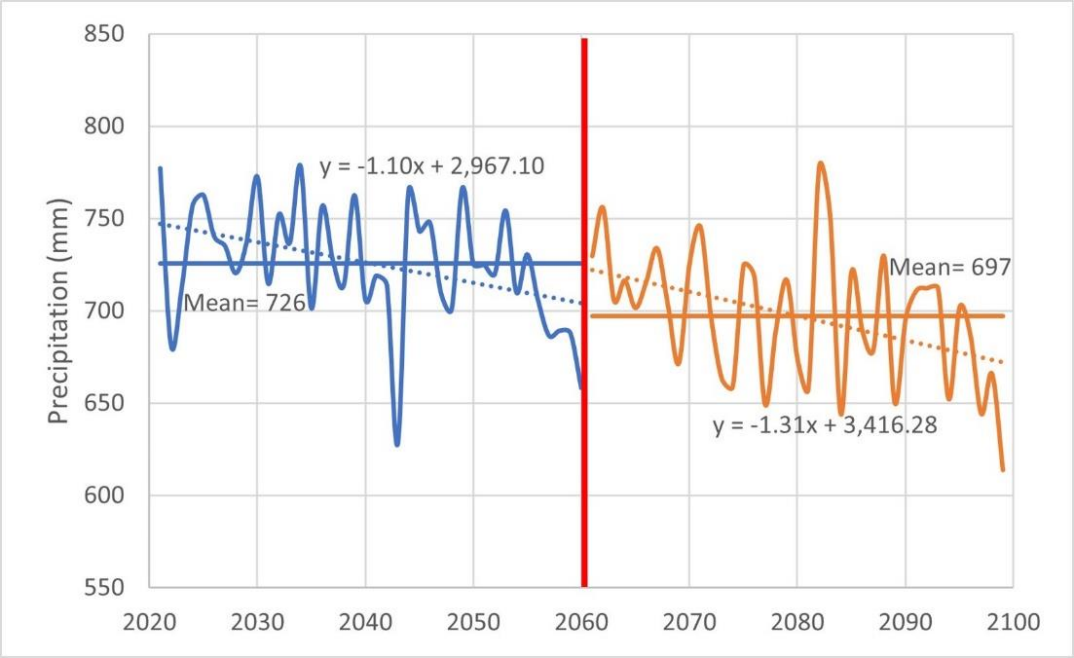

Figure 7-23 Change of future precipitation until 2100 for SB 1545 (Ensemble mean of 46 model)

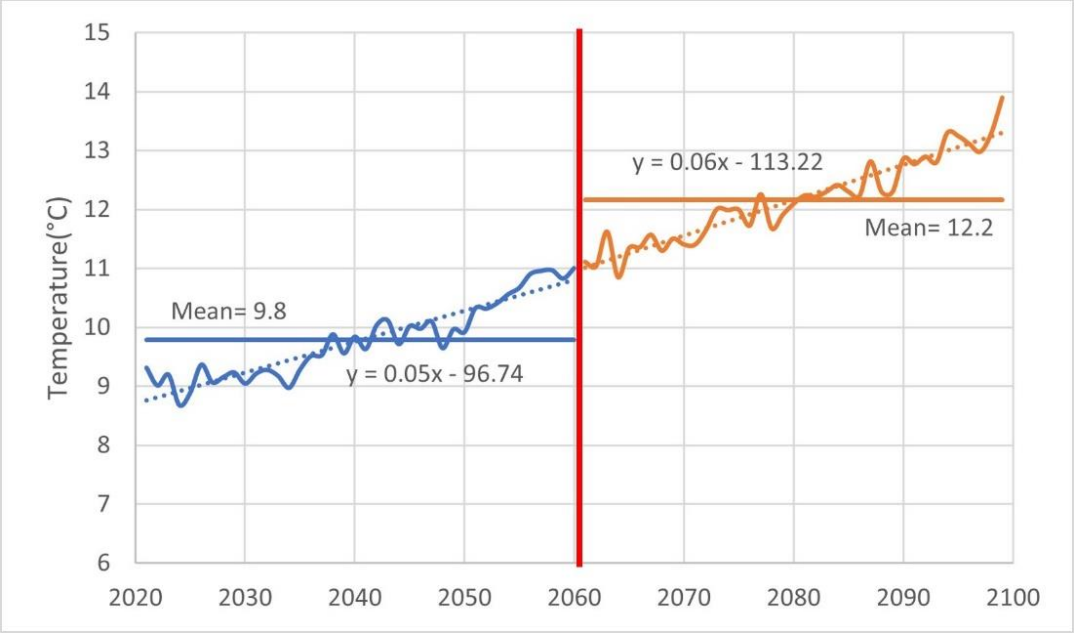

Figure 7-24 Change of future temperature until 2100 for SB 1545 (Ensemble mean of 46 model)

D. Corrected and non-corrected precipitation and temperature

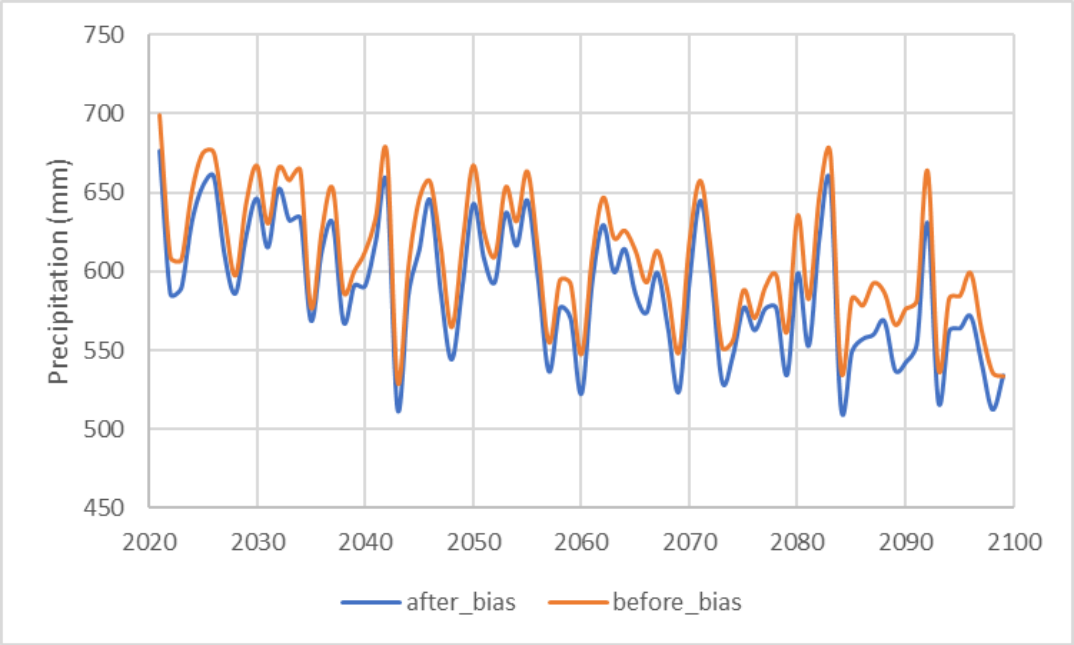

Figure 7-25 Precipitation Graph for SB 1535 (Before and After Bias Correction)

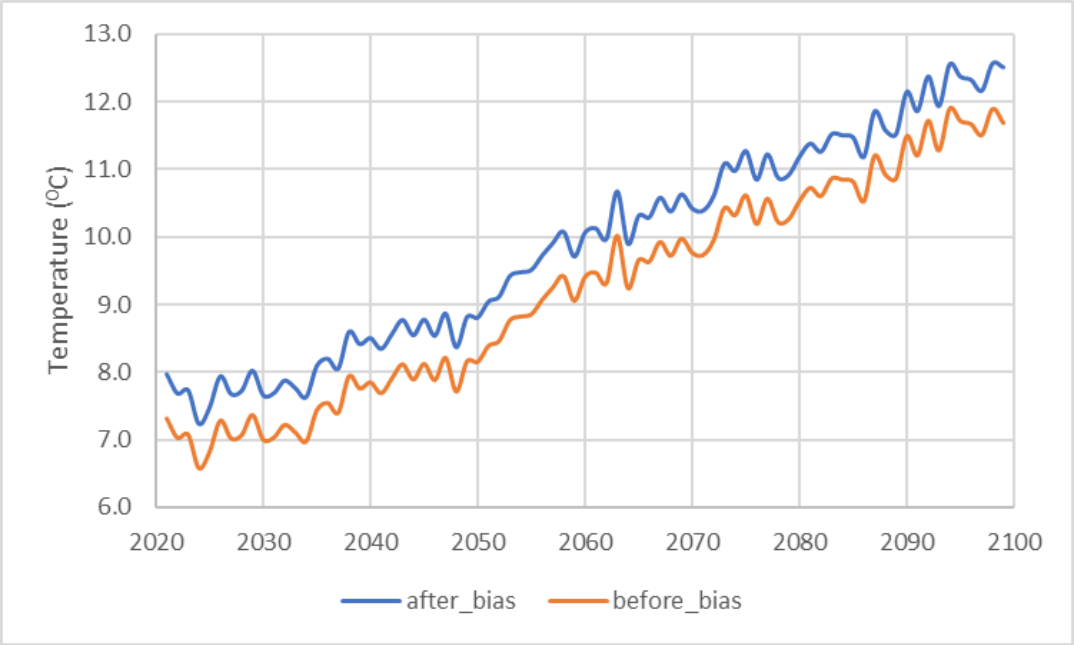

Figure 7-26 Temperature Graph for SB 1535 (Before and After Bias Correction)

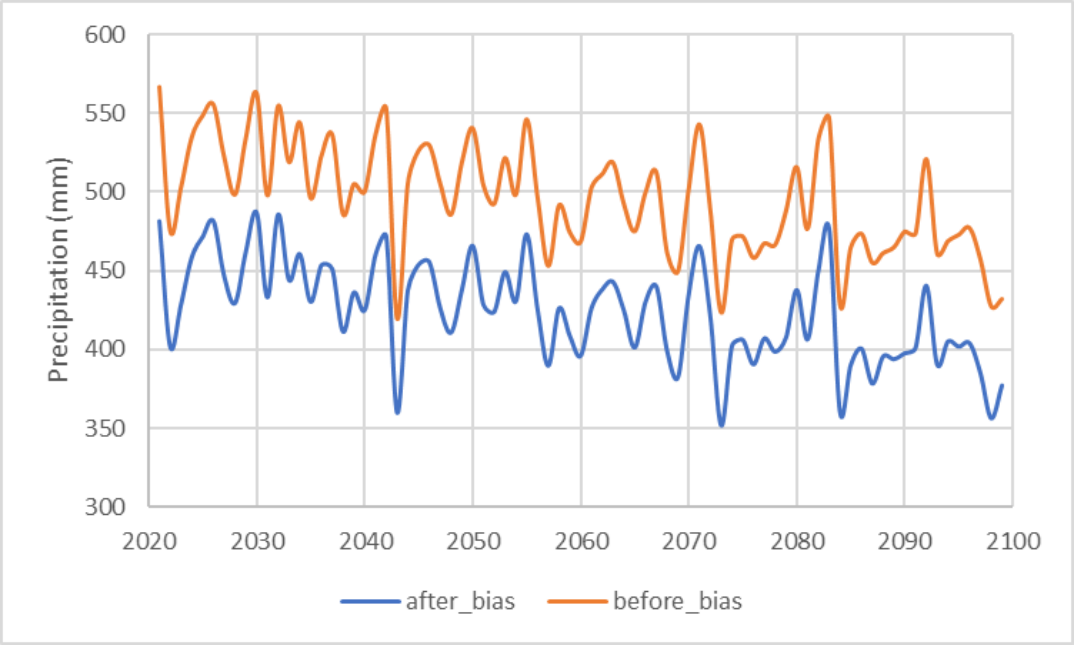

Figure 7-27 Precipitation Graph for SB 1541 (Before and After Bias Correction)

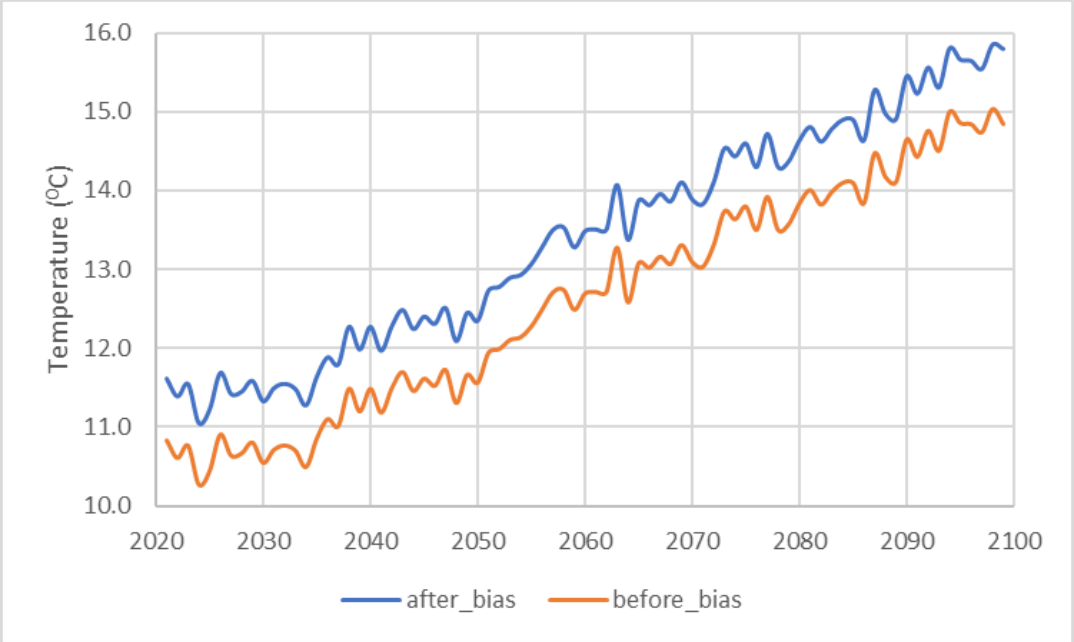

Figure 7-28 Temperature Graph for SB 1541 (Before and After Bias Correction)

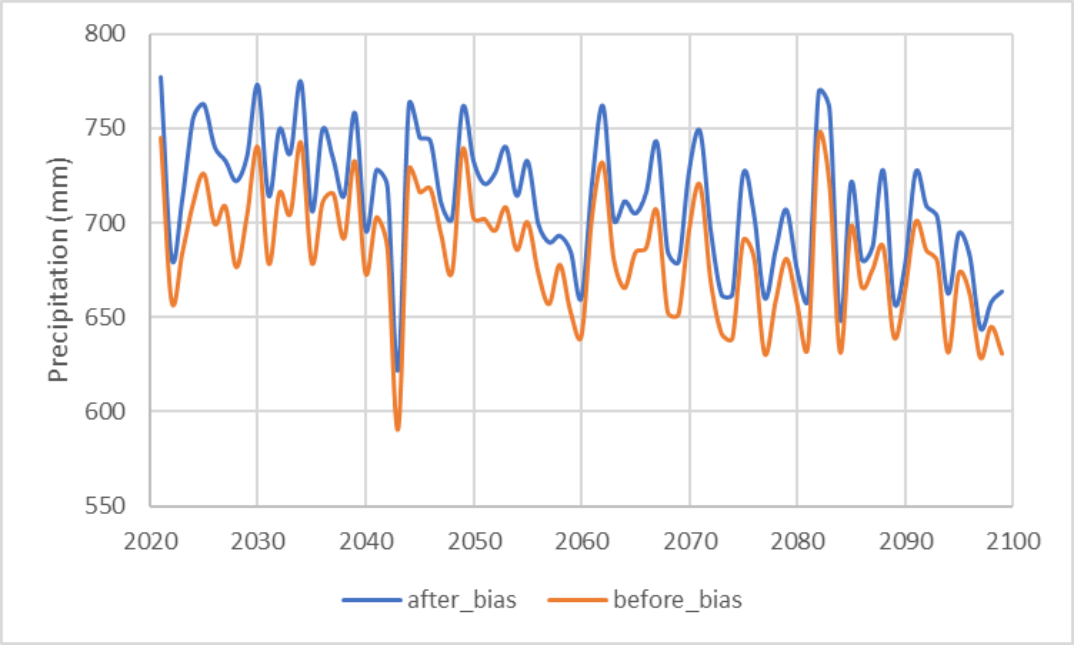

Figure 7-29 Precipitation Graph for SB 1545 (Before and After Bias Correction)

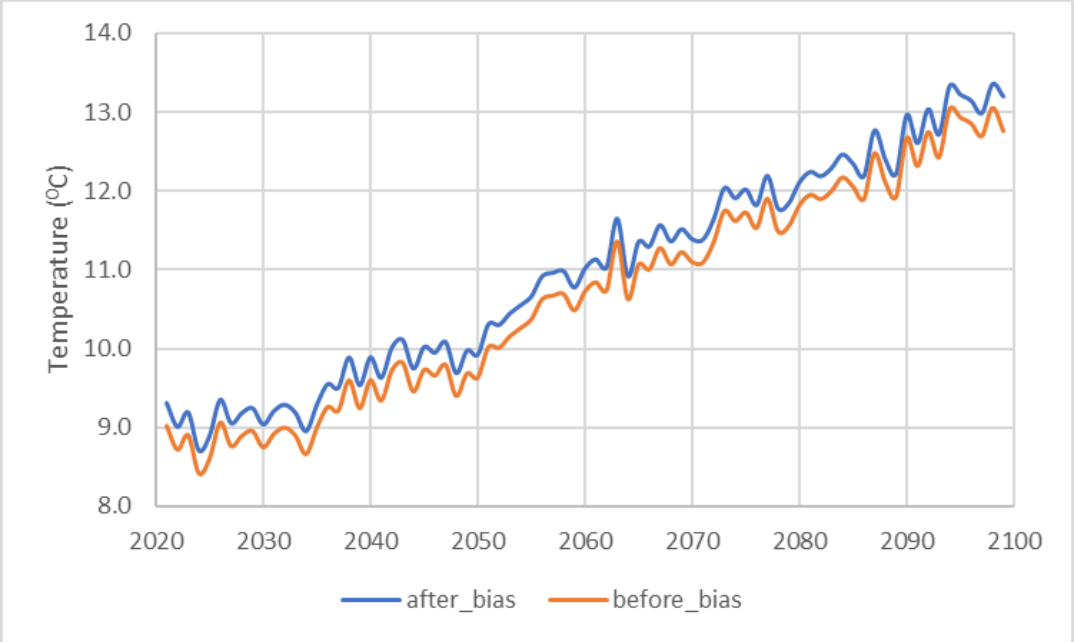

Figure 7-30 Temperature Graph for SB 1545 (Before and After Bias Correction)